ML-TDR-64-173
Part II

HIGH TEMPERATURE PROTECTIVE COATINGS FOR GRAPHITE

TECHNICAL DOCUMENTARY REPORT NO. ML-TDR-64-173, Part II
October 1964

Air Force Materials Laboratory
Research and Technology Division
Air Force Systems Command
Wright-Patterson Air Force Base, Ohio

Project No. 7350, Task No. 735002

(Prepared under Contract AF 33(657)-11253 by Union Carbide Corporation,
Carbon Products Division, Parma, Ohio;
J. M. Criscione, R. A. Mercuri, E. P. Schram,
A. W. Smith, and H. F. Volk, Authors)

HIGH TEMPERATURE PROTECTIVE COATINGS FOR GRAPHITE - PART II

J. M. Criscione, et al

Union Carbide Corporation
Parma, Ohio

October 1964

CLEARINGHOUSE FOR FEDERAL SCIENTIFIC AND TECHNICAL INFORMATION CFSTI
DOCUMENT MANAGEMENT BRANCH 410.11

LIMITATIONS IN REPRODUCTION QUALITY

ACCESSION # AD 608 092

☒ 1. WE REGRET THAT LEGIBILITY OF THIS DOCUMENT IS IN PART UNSATISFACTORY. REPRODUCTION HAS BEEN MADE FROM BEST AVAILABLE COPY.

☐ 2. A PORTION OF THE ORIGINAL DOCUMENT CONTAINS FINE DETAIL WHICH MAY MAKE READING OF PHOTOCOPY DIFFICULT.

☐ 3. THE ORIGINAL DOCUMENT CONTAINS COLOR, BUT DISTRIBUTION COPIES ARE AVAILABLE IN BLACK-AND-WHITE REPRODUCTION ONLY.

☐ 4. THE INITIAL DISTRIBUTION COPIES CONTAIN COLOR WHICH WILL BE SHOWN IN BLACK-AND-WHITE WHEN IT IS NECESSARY TO REPRINT.

☐ 5. LIMITED SUPPLY ON HAND: WHEN EXHAUSTED, DOCUMENT WILL BE AVAILABLE IN MICROFICHE ONLY.

☐ 6. LIMITED SUPPLY ON HAND: WHEN EXHAUSTED DOCUMENT WILL NOT BE AVAILABLE.

☐ 7. DOCUMENT IS AVAILABLE IN MICROFICHE ONLY.

☐ 8. DOCUMENT AVAILABLE ON LOAN FROM CFSTI (TT DOCUMENTS ONLY).

☐ 9.

PROCESSOR: P McLean

TSL-107-10/64

NOTICES

When Government drawings, specifications, or other data are used for any purpose other than in connection with a definitely related Government procurement operation, the United States Government thereby incurs no responsibility nor any obligation whatsoever; and the fact that the Government may have formulated, furnished, or in any way supplied the said drawings, specifications, or other data, is not to be regarded by implication or otherwise as in any manner licensing the holder or any other person or corporation, or conveying any rights or permission to manufacture, use, or sell any patented invention that may in any way be related thereto.

Qualified requesters may obtain copies of this report from the Defense Documentation Center (DDC), (formerly ASTIA), Cameron Station, Bldg. 5, 5010 Duke Street, Alexandria, Virginia, 22314.

This report has been released to the Office of Technical Services, U.S. Department of Commerce, Washington 25, D. C., for sale to the general public.

Copies of this report should not be returned to the Research and Technology Division, Wright-Patterson Air Force Base, Ohio, unless return is required by security considerations, contractual obligations, or notice on a specific document.

FOREWORD

This Summary Technical Report was prepared by Union Carbide Corporation, Carbon Products Division, Research Laboratory, Parma, Ohio 44130, under USAF Contract No. AF 33(657)-11253. This contract was initiated under Project No. 7350, "Refractory Inorganic Non-Metallic Materials," Task No. 735002, "Refractory Inorganic Non-Metalic Materials: Graphitic." The title of the project is "High Temperature Protective Coatings for Graphite." This work is being administered under the direction of the Air Force Materials Laboratory, Research and Technology Division, with Mr. J. D. Latva and Captain W. C. Simmons as project engineers.

This report covers the work conducted from 1 June 1963, to 31 May 1964.

The authors would like to express their thanks to Drs. J. L. Margrave and A. K. Kuriakose for work on the oxidation of iridium, J. W. Nuss for work on chemical reactions, C. E. Lowell for interpretation of X-ray diffraction data, and the aid of J. D. Ruggiero and F. W. Meszaros.

ABSTRACT

A comprehensive program to provide fundamental information concerning various factors controlling the oxidation behavior of protective coating systems for graphite at temperatures up to 2200°C is outlined and described.

Work presented includes: the evaporation of iridium in the presence of oxygen and water vapor to temperatures of 1300°C; the results of studies involving carbon diffusion through iridium; the permeability of iridium, rhodium, ZrO_2, HfO_2, and ThO_2 to oxygen at temperatures of 2000°C; the coating of graphite with iridium, including the carbon iridium eutectic temperature determination; the reactions of iridium and rhodium with ZrB_2, HfB_2, ZrC, HfC, and ThC_2; the kinetics of the carbothermic reduction of ZrO_2, HfO_2, and ThO_2 to temperatures in excess of 2000°C; the chemical reactions of graphite with ZrB_2 and HfB_2; and arc plasma tests of iridium-coated graphite.

The diffusivity, permeability, and kinetic data are presented in the form of mathematical expressions. A mechanism for the diffusion of oxygen through the refractory oxides based on ion vacancy transport is presented. The chemical kinetics for the carbothermic reductions of the oxides are described by linear rate laws for the initial 50 per cent of the reaction.

The experimental results are also discussed as to their practical implications to oxidation protective coatings.

This technical documentary report has been reviewed and is approved.

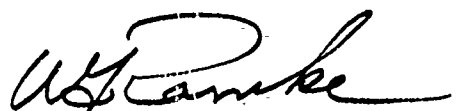

W. G. RAMKE
Chief, Ceramics and Graphite Branch
Air Force Materials Laboratory
Research and Technology Division

TABLE OF CONTENTS

ILLUSTRATIONS

ILLUSTRATIONS (Cont'd)

ILLUSTRATIONS (Cont'd)

ILLUSTRATIONS (Cont'd)

TABLES

I. INTRODUCTION

At high temperatures, where its physical properties are exceptional, graphite oxidizes quite readily and forms gaseous oxides which afford no protection against further attack. The successful use of graphite in high temperature oxidizing atmospheres depends, therefore, on the control or prevention of oxidation reactions. A direct solution to the problem is the introduction of a stable barrier layer between the graphite and the oxidizing environment.

A review of the existing information on oxidation protective coatings for graphite[1] has revealed that much effort has been devoted to controlling the oxidation of graphite by the use of surface coatings, impregnants, and oxidation retardants. In the past, technical approaches to the problem have involved detailed studies of methods of applying coatings to various graphite substrates and a somewhat qualitative means of testing the coating. The most satisfactory coating for graphite by this approach is silicon carbide, which protects graphite for substantial periods to about 1650°C. No systematic effort to determine the principles leading to improved coating systems for graphite has been put forth previously.

Since a permanent protective coating on a material must be thermochemically and mechanically compatible with both its substrate and the hostile atmosphere, oxidation-resistant coatings for graphite must prevent the diffusion of oxygen and carbon and be chemically stable with respect to both oxygen and carbon. The volatility of the coatings must be low, particularly in environments of reduced pressures and high temperatures. Physically, the coatings should be uniform and nonporous, should have thermal expansion coefficients compatible with the substrates, and should be sufficiently tough to resist erosion by impinging gases. Additional considerations include properties such as thermal shock resistance, possible self-healing mechanisms, chemical inertness to water vapor, and heat transfer.

Manuscript released by the authors August 1964 for publication as an RTD Technical Documentary Report.

II. SUMMARY

1.0 Research Results

The program effort to date has shown that iridium is an outstanding material with high potential as a single layer coating for the oxidation protection of graphite. It has been demonstrated that (1) iridium is virtually impervious to oxygen at temperatures up to 2200°C, (2) iridium does not react with graphite even at temperatures in excess of 2000°C, and (3) molten iridium wets graphite and forms an adherent coating which exhibits excellent thermal shock resistance in the temperature range 25° to 2200°C. This information and the known thermodynamic data on the iridium-oxygen system suggest that a thin iridium coating (2.0 mils) should adequately protect a graphite surface at temperatures in excess of 2000°C and at reduced oxygen pressures (10^{-3} torr) for one hour or longer.

Theoretical calculations of the rate of ablation of iridium in air at hypersonic flight conditions were carried out using existing vapor pressure data, the Langmuir evaporation formula, and the Scala-Vidale equations for the transport of evaporating species. Calculations were performed for surface temperatures of 1400°C and 2000°C at an altitude of 66,000 feet, nose cone radius of one foot, and flight speeds of Mach 10 and Mach 20. The ablation rate in all cases is calculated to be less than 1 mil/hour.

A 0.005-inch thick coating of iridium submitted to an oxidation test in an arc plasma provided complete protection for the graphite substrate at 2000°C. At this temperature, the ablation rate of iridium was 5.4 mils/hr. in an air pressure of one atmosphere and 0.5 mils/hr. in a stagnation pressure of 48 torr.

1.1 Oxidation of Iridium

The rate of oxidation of iridium in the temperature range 1010° to 1300°C as a function of temperature, oxygen pressure, and total gas flow rate was determined using a quartz spring thermal gravimetric balance. These studies are in agreement with previous workers in this field and are preliminary to extending this investigation to higher temperatures. The expression $K_1 = 4.1 \times 10^{-4} P$, describes the reaction kinetics at 1180°C, where K_1 is the linear rate constant in mg cm^{-2} min^{-1}, and P is the oxygen partial pressure in torr.

The oxidation of iridium exhibits a strong temperature dependence, as evidenced by an activation energy of 80 ± 5 kcal/mole up to about 1100°C and a lower activation energy of 7.5 ± 1 kcal/mole in the 1100° to 1300°C range. A preliminary study of the iridium-water vapor system showed that water vapor has no pronounced effect on the oxidation of iridium at 1160°C. Various efforts to study the sublimation of IrO_2 by mass spectrometric methods have failed to identify the high temperature volatile species of iridium oxide.

1.2 Permeability Studies

The permeability of a 14-mil thick iridium sample to oxygen was determined for the temperature range 1075° to 2200°C. Using 150 torr of oxygen, the permeability was found to be less than 1×10^{-13} g cm^{-2} sec^{-1}. This extremely low permeability may be attributed to the low solubility of oxygen in iridium.

The permeability of rhodium to 50 torr of oxygen was measured in a similar manner over the range 1290° to 1510°C. The permeability constant, $P \times l$, is given by

$$P \times l = 3.63 \times 10^{2}\, e^{-116,600/RT} \text{ g cm}^{-1} \text{ sec}^{-1}.$$

The permeability of carbon through iridium was determined by coating an iridium membrane with carbon on one side, sweeping with oxygen on the other side, and measuring the resultant carbon dioxide. The permeability constant of carbon to iridium for the temperature range 1300° to 1900°C is expressed by

$$P \times l = 2.75 \times 10^{-4}\, e^{-56,400/RT} \text{ g cm}^{-1} \text{ sec}^{-1}.$$

The permeability of calcia stabilized zirconia to oxygen was determined in the temperature range 1120° to 2060°C at 25 torr oxygen pressure. The permeability constant is

$$P \times l = 7.85 \times 10^{-2}\, e^{-55,700/RT} \text{ g cm}^{-1} \text{ sec}^{-1}.$$

Steady-state permeabilities determined at 1275°C in the pressure range 3 to 90 torr showed a slight variation with oxygen pressure, the dependence being proportional to the pressure of oxygen to the one-fourth power $(P_{O_2})^{1/4}$. The permeability values obtained in this work are lower than would be expected from normal self-diffusion coefficients. A mechanism of diffusion based on oxygen vacancy and electron hole migration is presented. The temperature dependence of the diffusivity for the 1120° to 1590°C temperature range is given by the expression

$$D = 1.85 \times 10^{2}\, e^{-57,600/RT} \text{ cm}^{2} \text{ sec}^{-1}.$$

The pressure dependence and mechanism of diffusion for calcia stabilized hafnia are the same as for zirconia. The permeability constant and the diffusivity were determined over the temperature range 1220° to 1640°C using 25 torr of oxygen. They are given by

$$P \times \ell = 2.02 \times 10^{-1} e^{-58,500/RT} \text{ g cm}^{-1} \text{ sec}^{-1}$$

and

$$D = 2.18 \times 10^{1} e^{-55,700/RT} \text{ cm}^{2} \text{ sec}^{-1} .$$

The permeability of thoria to oxygen showed a variable pressure dependence. The permeability constant obtained using 25 torr of oxygen over the temperature range 1140° to 1930°C is given by

$$P \times \ell = 4.68 \times 10^{-3} e^{-46,100/RT} \text{ g cm}^{-1} \text{ sec}^{-1}$$

1.3 Chemical Reaction Studies

The carbothermic reduction kinetics of HfO_2(I), HfO_2 + 5 per cent Y_2O_3(II), ZrO_2(III), BeO(IV), and ThO_2(V) were investigated in the temperature range 1700° to 2200°C. The rate laws, expressed in mmoles CO/mmole metal oxide per minute, were found to be

$$1.5 \text{ exp. } -7100/RT \text{ (I)},$$

$$2.0 \times 10^{4} \text{ exp. } -48,000/RT \text{ (II)},$$

$$1.8 \times 10^{6} \text{ exp. } -70,500/RT \text{ (III), and}$$

$$1.4 \times 10^{3} \text{ exp. } -36,000/RT \text{ (V)}.$$

The rate law for BeO was not determined because the reaction involved, in addition to reduction of the oxide, dissociation of Be_2C to yield Be and C and subsequent oxidation of Be by CO.

The stated linear rate laws for materials I, II, and III apply only during the first 50 per cent of reaction; after that time the reduction rate follows a parabolic function. The rate law for V was found to be linear until the reaction was 80 per cent complete. Reproducibility of the rate data on compound I was poor. The scatter in the rate data was minimized by utilizing phase stabilized hafnia. Minimum reaction temperatures, defined as the temperature where the CO pressure became noticeable (i.e., a few torr), were found to be 1730°C(I), 1780°C(II), 2110°C(III), 1300°C(IV), and 1640°C(V).

The chemical reaction of hafnium and zirconium carbide with iridium and rhodium in the temperature range 1200° to 2200°C is summarized

by the equation

$$RC + 3X = RX_3 + C$$

where R = Hf or Zr, and X = Ir or Rh. The reaction product RX_3 is obtained independent of the molar ratios of reactants or temperature of the reaction. Only the reaction between iridium and zirconium carbide showed the formation of a liquid phase and this occurred at temperatures in excess of 2100°C.

The reaction of iridium with thorium dicarbide investigated in the temperature range 1950° to 2200°C is summarized by the equation

$$2Ir + ThC_2 \rightarrow ThIr_2 + C.$$

Melting occurred only when this reaction was carried out at 2200°C.

A vigorous reaction takes place when either zirconium diboride or hafnium diboride is heated with iridium or rhodium at temperatures in excess of 1000°C. The minimum reaction temperatures were determined by differential thermal analysis methods and were found to range from 1160° to 1230°C depending on the diboride and platinum metals used as reactants. Treatment of all four systems Ir + HfB_2, Ir + ZrB_2, Rh + HfB_2, and Rh + ZrB_2 in vacuo at 1430°C resulted in an extremely dense product. The products in these reactions have been identified as platinum metal-rich cubic phases after examination by X-ray diffraction and metallographic methods.

The chemical stability of zirconium diboride and hafnium diboride with graphite has been investigated in the temperature range 1970° to 2420°C and 1875° to 2500°C, respectively. Both of the borides were found to be stable at these temperatures and agree with findings of several other investigators.

1.4 Mechanical Compatibility Studies

A very strong adherent bond may be formed by allowing molten iridium to wet the surface of a graphite substrate. The bonding of the iridium coating results from a dissolution of graphite in the molten iridium (~ 2200°C) with subsequent reprecipitation of the graphite upon solidification of the metal. The graphite crystallites form an interlocking network with the iridium and graphite substrate.

An investigation of the iridium-carbon eutectic temperature reveals melting at 2110 ± 25°C. Although this figure is about 190°C below the previously accepted value, it is still high enough to continue consideration of iridium as a candidate for graphite coatings.

A slurry dip method of applying iridium coatings on graphite has been developed which produces coatings exhibiting excellent adherence and thermal shock resistance. Samples were subjected to repeated rapid heat cycling from room temperature to 2000°C without cracking. A metallographic

examination of the iridium coatings applied by the slurry dip method revealed the presence of pores and pinholes. Dense, nonporous, adherent layers of Ir on graphite were obtained by a metal cladding method, by electrodeposition, and by vapor plating. The cladded coatings developed some cracks which may be due to the 20 per cent difference in thermal expansion between iridium and the substrate. Since the CTE of graphite can be varied, this problem can be overcome by development of a graphite with a CTE of approximately 7×10^{-6} cm/cm/°C.

Electrodeposition experiments have demonstrated that a dense iridium deposit can be plated directly onto graphite. However, the electrolytic method is probably not suitable as a single means of applying a coating to graphite since the fused salt penetrates into the pores of the graphite substrate. Therefore, the substrate should first be coated by some other means, for example, by vapor deposition, before being immersed in the electrolytic bath.

Iridium vapor deposition was achieved from various iridium carbonyl compounds. Iridium dodeca-carbonyl $Ir_4(CO)_{12}$ itself was found to be the least suitable carrier material because of its low vapor pressure and low thermal decomposition temperature. Good deposits were obtained using a more volatile iridium compound, which appears to be an intermediate of the high pressure synthesis of $Ir_4(CO)_{12}$. The iridium chlorocarbonyls $Ir(CO)_2Cl_2$ and $Ir(CO_3)Cl$ are also promising starting materials. Vapor deposition from iridium trichloride $IrCl_3$ was investigated briefly with encouraging results. However, perfection of the $IrCl_3$ method would require a detailed investigation of the thermodynamics and kinetics of the iridium-chlorine system.

2.0 Practical Implications

The practical implication section is presented mainly to stimulate the application of program findings. The interpretations and implications may in some cases be somewhat tenuous; however, they may motivate others to use the information here for the solution of coatings problems in general.

2.1 Iridium as a Barrier to Oxygen

Iridium is virtually impermeable to oxygen to its melting point of 2450°C and, thus, should be considered an excellent barrier to oxygen. Its use as a protective coating will be limited to those temperatures at which iridium interacts with the substrate material and the rate of chemical corrosion of the metal in an oxidizing atmosphere.

2.2 Iridium on Graphite

The use of a coating of iridium on graphite would be limited to operational temperatures of 2110 ± 25°C, the eutectic temperature determined by this research. Iridium does not form any carbides and the permeability of carbon through iridium should not result in a loss of

adherence of the coating since the permeability of this metal to carbon is less than 10^{-7} g cm^{-2} sec^{-1} at 2110°C. For example, a graphite sphere 10 cm in radius and a density of 1.7 g/cm^3 would lose 0.15 per cent per day, whereas the loss of iridium by the formation of IrO_3 proceeds at a faster rate at 2110°C. Tests of an iridium-coated graphite rod in an arc plasma at 2000°C in one atmosphere air pressure resulted in complete protection of the substrate and a coating recession rate of 5.4 mils/hour. The weight of an iridium coating would be 0.1165 lb. (avoirdupois) per square foot per mil thickness. The materials cost per mil thickness of iridium per square foot of coating is calculated to be 126 dollars at the current price of 74 dollars per troy ounce of the metal powder.

2.3 Iridium on Refractory Metals

Molybdenum, columbium, tantalum, and tungsten have been considered for leading edges, attachments, and structural members for reentry spacecraft. During reentry, leading edges encounter temperatures in the range from 1650° to 1950°C under oxidizing conditions which require protection for the refractory metals.

The success with iridium on graphite suggests that the same metal coating might offer the solution to the important problem of protection of the refractory metals. The compatibility of iridium with the refractory metal must be carefully scrutinized since interdiffusion and reaction between coating and substrate will (1) reduce the coating thickness, (2) may alter the protective nature of the coating, and (3) may affect the properties of the substrate.

Passmore et al.[2] have screened various materials as barriers to solid state diffusion in refractory metals at 1700°C. Iridium was recommended as a good diffusion barrier on tungsten, tantalum, and molybdenum. The couple iridium-niobium was not investigated. The minimum melting temperatures for the binary systems of iridium with these refractory metals are high; tungsten 2305°C; molybdenum 2080°C; tantalum 1948°C; and niobium 1840°C. The coefficient of thermal expansion of iridium closely matches that of molybdenum and tantalum. The mismatch is small relative to niobium and larger with respect to tungsten.

2.4 Vaporization and Oxidation Data—Iridium

Evaporation of iridium is negligible at temperatures up to 2100°C. The maximum rate (e.g., evaporation into vacuum) was calculated from vapor pressure data using the Langmuir formula. The results are shown in Table 1.

TABLE 1

EVAPORATION RATE OF IRIDIUM

Temperature °C	Rate in mils/hr.
1900	5.3×10^{-3}
2000	2.4×10^{-2}
2100	9.5×10^{-2}
2200	0.35
2300	1.14

The behavior of iridium in an oxidizing environment is of greater interest. The weight loss of iridium per cm^2 of surface represents a certain thickness of the metal which can be calculated from the expression

$$R = \frac{K}{d} \times \frac{390 \text{ mils } cm^2}{1 \text{ } cm^3}$$

$$= 17.4 \times 10^{-3} K$$

where R = the recession rate in mils/min.

K = linear rate constant $mg/cm^2/min.$

d = density of iridium 22.42 g/cm^3.

The linear rate constant determined from the oxidation of iridium allows one to estimate the recession rate of an iridium coating. For example, at 1300°C, a linear rate of 0.451 $mg/cm^2/min.$ was observed at one atmosphere oxygen pressure. This quantity represents a recession rate of

$$R = 17.4 \times 10^{-3} \times 0.451 = 7.8 \times 10^{-3} \text{ mils/min.}$$

The possibility of a change in mechanism of oxidation at higher temperatures should caution one not to extrapolate the limited existing data much beyond the 1300°C temperatures studied thus far; it is planned to extend the temperature range of this investigation beyond 2000°C.

2.5 Permeability Data

Permeability data provide a basis for assessing the merit of various coating materials for the protection of the substrate. For estimating the rate of corrosion of a graphite substrate, it is assumed that all of the oxygen that penetrates the coating reacts with the carbon to form carbon monoxide which may diffuse away through the pores of the carbon. The depletion of

carbon from the graphite coating interface can result in loss of adherence of the coating.

A sample of the mathematical treatment of the corrosion rate of graphite, based on oxygen transport through a coating with a permeability constant of 10^{-17} g cm^{-1} sec^{-1}, is shown in Table 2. Figure 1 represents a

TABLE 2

CALCULATIONS OF THE CORROSION RATE OF GRAPHITE BASED ON OXYGEN TRANSPORT THROUGH COATING

$$\text{Corrosion Rate} = \frac{K(P\ell')}{\ell} \text{ mils/hour} \qquad (1)$$

where for a graphite substrate

$$K = 2.18 \times 10^8 \left(\frac{\text{cm mil}^2 \text{ sec}}{\text{g } O_2 \times \text{hr.}}\right)$$

$(P\ell')$ = permeability constant $\left(\frac{\text{g } O_2}{\text{cm sec}}\right)$

ℓ = coating thickness (mils).
K is obtained in the following manner:

Since $C + \frac{1}{2}O_2 \rightarrow CO$, (a)

$12 \text{ g C} \cong 16 \text{ g } O_2$. (b)

The density of C = 1.88 g/cm^3.
The diffusing oxygen is related to the carbon corrosion by combining a and b and using the proper conversion factors consistent with obtaining corrosion rate of carbon in mils per hour.

$$K = \frac{12 \text{ g C}}{16 \text{ g } O_2} \times \frac{1 \text{ cm}^3}{1.88 \text{ g C}} \times \frac{3600 \text{ sec}}{1 \text{ hr.}} \times \frac{(3.9 \times 10^2 \text{ mil})^2}{1 \text{ cm}^2}$$

$$K = 2.18 \times 10^8 \ \frac{\text{cm mil}^2 \text{ sec}}{\text{g } O_2 \text{ hr.}}$$

Using equation (1), the corrosion rate for a 10-mil coating when $(P\ell')$ = 1×10^{-7} g O_2/cm sec is calculated.

$$\text{Corrosion Rate} = 2.18 \times 10^8 \ \frac{\text{cm mil}^2 \text{ sec}}{\text{g } O_2 \text{ hr.}} \times 1 \times 10^{-7} \ \frac{\text{g } O_2}{\text{cm sec}} \times \frac{1}{10 \text{ mil}}$$

$$= 2.18 \ \frac{\text{mils}}{\text{hour}} .$$

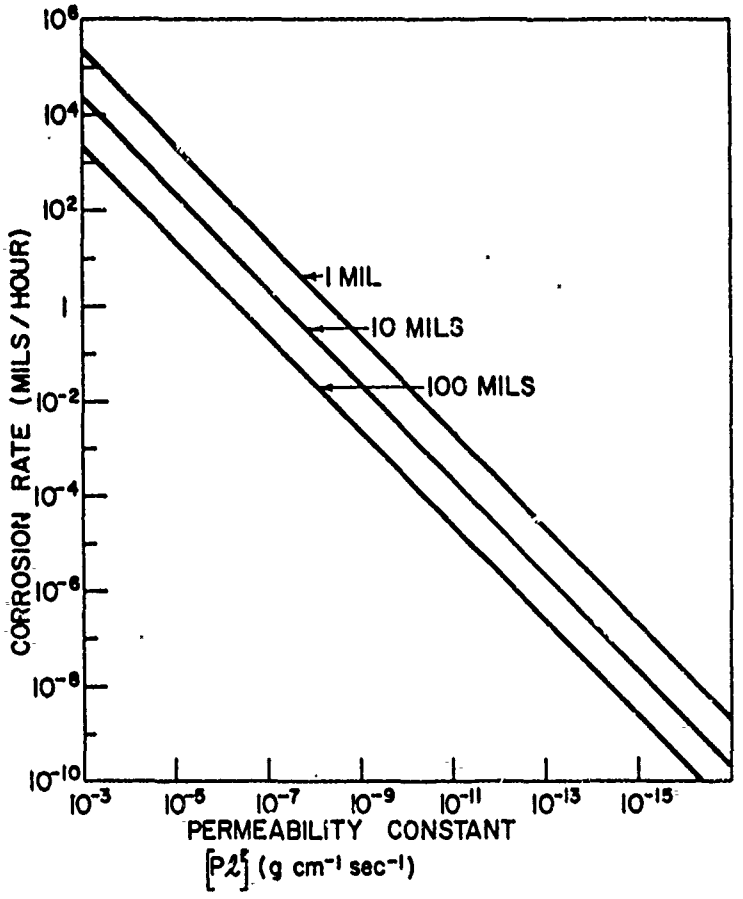

Figure 1. Corrosion Rate of Graphite vs. Permeability Constant for Several Coating Thicknesses

plot of the corrosion rate as a function of the permeability factor. The corrosion rate is plotted against the permeability constant (permeability times thickness) for various coating thicknesses. The permeability constant represents a property of the material which is independent of geometry; whereas, the permeability itself will vary with the thickness of a given material.

One may speculate that coatings which will only permit corrosion rates of 1 mil/hour or less should provide good oxygen barriers for short time protection. As seen in Figure 1, coatings with a ($P\ell'$) factor of $< 1 \times 10^{-9}$ g cm^{-1} sec^{-1} should perform adequately as barriers to oxygen. Those with a ($P\ell'$) factor $> 1 \times 10^{-7}$ g cm^{-1} sec^{-1} would very likely lead to loss of adherence of the coating, and those exhibiting permeability factors between 10^{-9} and 10^{-8} g cm^{-1} sec^{-1} should be viewed with caution.

Table 3 represents a summary of the practical application of permeability data to a graphite substrate with a 10-mil coating in the presence of 25 torr oxygen pressure. Assuming that only 1-mil corrosion

TABLE 3

PRACTICAL APPLICATION OF PERMEABILITY DATA FOR EVALUATING OXIDATION PROTECTIVE COATINGS ON GRAPHITE

T (°C)	Pℓ (gm/cm. Sec)	Materials	Graphite Corrosion Rate*	
			mils/hr.	mins/mil
1600	$<3\times10^{-15}$	O thru Ir	$<5.6\times10^{-8}$	3.4×10^{9}
1800	$<3\times10^{-15}$	"	$<5.6\times10^{-8}$	3.4×10^{9}
2000	$<3\times10^{-15}$	"	$<5.6\times10^{-8}$	3.4×10^{9}
2200	$<3\times10^{-15}$	"	$<5.6\times10^{-8}$	3.4×10^{9}
1600	1.1×10^{-11}	O thru Rh	2.3×10^{-4}	2.6×10^{5}
1800	2.2×10^{-10}	"	5.0×10^{-3}	1.2×10^{4}
1600	2.8×10^{-8}	O thru ZrO_2	7.1×10^{-1}	84
1800	1.2×10^{-7}	"	2.8	24
2000	4.0×10^{-7}	"	10	6
2200	1.0×10^{-6}	"	25	2.4
1600	3.6×10^{-8}	O thru HfO_2	8.3×10^{-1}	72
1800	1.6×10^{-7}	"	4.0	15
2000	5.6×10^{-7}	"	14	4.2
2200	1.5×10^{-6}	"	38	1.8
1600	2.1×10^{-8}	O thru ThO_2	5.0×10^{-1}	120
1800	7.1×10^{-8}	"	1.9	30
2000	1.9×10^{-7}	"	4.9	12
2200	4.2×10^{-7}	"	11	5.4

*Based on the oxygen permeation through a 10-mil coating and an oxygen pressure of 25 torr.

of the substrate would lead to loss of adherence, only iridium would offer long duration protection (3.4×10^9 min) before loss of adherence at 2200°C. On the other hand, rhodium just below its melting point of 1955°C should adhere for 12,000 minutes. In addition, zirconia will adhere for 2.4 minutes, hafnia for 1.8 minutes, and thoria for 5.4 minutes at 2200°C in an oxygen pressure of 25 torr. For extended use periods, oxidation protective coatings of these latter materials would require an intermediate layer of a more oxidation-resistant material to further protect the graphite.

2.6 Chemical Reaction Data

The data for the kinetics of reactions between the oxides and graphite provide another means of evaluating these materials as single layer coatings. The chemical kinetics of the carbothermic reduction of hafnia, thoria, and zirconia were found to be quite rapid when reactants were present as

intimately mixed powders with over 50 per cent of the initial reaction obeying linear rate laws.

The rapidity of the reactions has been described by a calculation (see Table 4) of the reaction rate of a zirconia coating assuming the bulk

TABLE 4

CALCULATION OF THE REACTION RATE OF ZIRCONIA ON GRAPHITE AT 2000°C

Considering a volume of ZrO_2, 1 cm x 1 cm x 1 cm, a density of 5.56 g cm^3, and a molecular weight of 123.2 g, one obtains $\frac{45 \text{ mmoles } ZrO_2}{1 \text{ cm}^3 \ ZrO_2}$.

Since $\frac{dCO}{dt} = 0.30 \frac{\text{mmoles CO}}{\text{min. mmole } ZrO_2}$, the total CO evolved from the 1 cm^3 ZrO_2 is found by,

$$\frac{0.30 \text{ mmoles CO}}{\text{min. mmole } ZrO_2} \times \frac{45 \text{ mmoles } ZrO_2}{1 \text{ cm}^3 \ ZrO_2} = \frac{13.5 \text{ mmoles CO}}{\text{min. cm}^3 \ ZrO_2}$$

From the reaction stoichiometry $ZrO_2 + 3C = ZrC + 2CO$
13.5 mmoles CO $\cong$ 6.75 mmoles ZrO_2 reacted.

$$\therefore \frac{6.75 \text{ mmoles } ZrO_2}{\text{min cm}^3 \ ZrO_2} \times \frac{123.2 \text{ mg } ZrO_2}{1 \text{ mmole } ZrO_2} \times \frac{1 \text{ cm}^3 \ ZrO_2}{5.56 \times 10^3 \text{ mg } ZrO_2} = \frac{0.1496}{\text{min.}}$$

0.1496 min^{-1} = 6.68 min. = time for reaction of 1 cm^3 ZrO_2. A 1-mil thickness of ZrO_2, equivalent to 1 cm^2 x 2.54 x 10^{-3} cm, would react in 1.7 x 10^{-2} min. or 1.02 seconds.

Thus, at 2000°C, a one-mil layer of ZrO_2 will react with graphite in approximately one second.

oxide coating reacts with graphite at the same rate as the powdered materials. This assumption imposes a more severe situation in that the reaction between bulk phases may be expected to obey a parabolic rate law rather than the linear behavior found for the powders. Table 5 summarizes the calculated reaction rates for several oxides studied to date. In the absence of a solid state diffusion controlled process, one second or less would be required for complete reaction of a 1-mil thick coating of these refractory oxides on graphite; whereas, the formation of the carbide could provide a diffusion barrier which inhibits further reaction, a pressure build-up of carbon monoxide at the coating-substrate interface could lead to cracking or spalling of the coating. The reaction kinetics of these oxides with graphite will be studied further using the reactants in bulk form to investigate the interfacial behavior under conditions which duplicate an actual coated substrate. This work will also define the need for an intermediate layer.

TABLE 5

REACTION RATE OF REFRACTORY OXIDES ON GRAPHITE

Oxides	Reaction Rate sec/mil
HfO_2 (yttria stabilized)	0.72
HfO_2	0.96
ThO_2	0.72
ZrO_2	1.02

The interaction of hafnium carbide, zirconium carbide, thorium carbide, hafnium diboride, and zirconium diboride with iridium and rhodium at low temperatures (< 1200 °C), excludes their further consideration as intermediate layer materials in a multilayer coating system with these platinum metals. However, the reaction products themselves present some interesting prospects for coating systems. Although the platinum metal borides exhibited melting at temperatures as low as 1450°C, the other intermetallic compounds, $HfIr_3$, $HfRh_3$, $ZrRh_3$, and $ThIr_3$, were still solid at temperatures in excess of 2000°C. These materials may well be considered as candidates for single layer coatings or components of multilayer coatings for the protection of graphite or refractory metals against oxidation at high temperatures.

In view of their chemical stability in the presence of graphite, zirconium diboride and hafnium diboride still show promise as intermediate layer materials in contact with graphite. Further studies such as an investigation of the mechanical compatibility and permeability to carbon of these materials will be necessary to evaluate completely the stability with respect to graphite.

2.7 Mechanical Compatibility Data

It has been demonstrated that a strong adherent bond can be formed by dip-coating graphite in a slurry of iridium and subsequently fusing the metal on the substrate. This method of applying the coating is particularly suited to a graphite substrate since the metal and graphite form a eutectic composition which upon cooling results in the reprecipitation of graphite and the formation of an interlocking network of graphite and iridium. Iridium does not form a carbide at temperatures up to 2100°C. If protection for more than a few minutes is required, the usefulness of an iridium coating on graphite is probably limited by the formation of the eutectic melt to temperatures below 2110°C. However, since the diffusion of carbon in iridium is slow, short time (up to one minute) overheating to temperatures in excess of 2200°C may be permissible under static conditions.

The methods of applying an iridium coating need to be investigated further. The slurry dip and sintering procedure has the advantage of producing a strongly adherent and shock resistant coating. However, even multiple application of slurry dip coatings have not yet resulted in an iridium layer which is entirely free of pinholes.

The electro-deposition method produces very dense iridium coatings, but the problem of salt penetration into the graphite substrate has not yet been overcome. Plating from an aqueous solution appears to be one way of solving this problem. The possible influence of the columnar structure of electro-deposited iridium on the coating properties also needs further study. Electroplating appears to be an ideal method for coating nonporous materials (e.g., metals) with iridium.

At this time, vapor-plating appears to be the most promising method for obtaining satisfactory iridium coatings on graphite, as demonstrated by the limited work carried out so far. Further work to synthesize more volatile iridium compounds and to find the optimum plating conditions is needed.

III. PROGRAM MANAGEMENT

Official award of Contract No. AF 33(657)-11253 was made on 1 June 1963, to the National Carbon Company (renamed the Carbon Products Division of Union Carbide Corporation on 1 September 1963). Union Carbide as Prime Contractor of this program is to provide a detailed description of all major parameters controlling the oxidation behavior of selected protective coating systems for graphite at temperatures as high as 2200°C. The research is being carried out as a group effort with Dr. E. Epremian as Principal Investigator, and Dr. J. M. Criscione serving as Technical Coordinator.

The research on all tasks, except tasks A1-1, A3-1, and A3-2 will be performed by Carbon Products Division personnel.

The following research tasks have been subcontracted to Dr. J. L. Margrave at Rice University, Houston, Texas, beginning January 1, 1964:

A1-1, "The Vaporization of Iridium and Rhodium in the Presence of Water Vapor";

A3-1, "The Vapor Pressure of Compound Oxides"; and

A3-2, "The Vaporization of Compound Oxides in the Presence of Water Vapor."

Mr. J. D. Latva and Capt. W. C. Simmons are serving as Project Engineers for the Air Force Materials Laboratory, Research and Technology Division.

IV. TECHNICAL BACKGROUND

Materials which may be stable in the presence of oxygen for extended time periods at temperatures in excess of the present 1700°C limitation of silicon-based coatings may be divided into three groups on the basis of existing thermochemical and experimental data; these are the platinum metals, the single refractory oxides and the compound refractory oxides. A critical review of the existing information pertinent to these materials as oxidation protective coatings has been reported previously[1] and serves as the technical background for this program.

On the basis of reference (1), the materials listed in Table 6 have been selected as prime candidates for oxidation protective coatings for graphite.

TABLE 6

SELECTED COATING MATERIALS

Oxygen Barrier			Intermediate Layers	
Platinum Metals	Single Oxides	Compound Oxides	Carbides	Borides
Iridium	ThO_2	$ThO_2 \cdot ZrO_2$	ZrC	ZrB_2
Rhodium	HfO_2	$SrO \cdot ZrO_2$	HfC	HfB_2
	ZrO_2	$BaO \cdot ZrO_2$	ThC_2	
	BeO	$3BeO \cdot 2ZrO_2$		
		$CaO \cdot ZrO_2$		
		$ZrO_2 \cdot SiO_2$		
		$HfO_2 \cdot SiO_2$		

V. RESEARCH PROGRAM

1.0 Outline

The major research areas of the program are concerned with investigations at very high temperature of the following five systems:

A. Selected platinum metals, oxides, and mixed oxides in contact with oxygen.

B. Selected platinum metals, oxides, and mixed oxides in contact with graphite.

C. Selected refractory metals, carbides, or borides in contact with the materials of Group A. These studies are needed because, in some cases, a reaction barrier (a layer between the outer coating and the graphite) will be necessary.

D. Selected refractory metals, carbides, or borides in contact with graphite. These studies will determine the stability of the barrier materials of Group C with respect to graphite.

E. Selected multiple systems based on the results of A, C, and D. The data obtained from A, C, and D will logically lead to potential multiple-coating systems. The studies under Group E will supply experimental data concerning the high temperature behavior of these combined systems.

2.0 Discussion

The proposed program, which will extend over a period of three years, is shown diagrammatically in Figure 2. The letter designation at the left side of each block refers to the area of investigation outlined above. The diagram shows the contemplated sequence of tasks designed to supply information for evaluating single- and multi-layer coatings for the oxidation protection of graphite.

A. Platinum Metals, Oxides, and Mixed Oxides in Contact With Oxygen and Water Vapor

A1-0 Platinum Metals (Iridium and Rhodium)

A1-1 Vaporization Studies

The vapor pressure and evaporation rate of both iridium and rhodium will be determined as functions of oxygen and water vapor pressure to temperatures in excess of 2000°C. Experiments in this area will be designed to encompass possible coating applications in oxygen and water vapor environments extending from a reduced pressure of 10^{-3} mm Hg to one atmosphere.

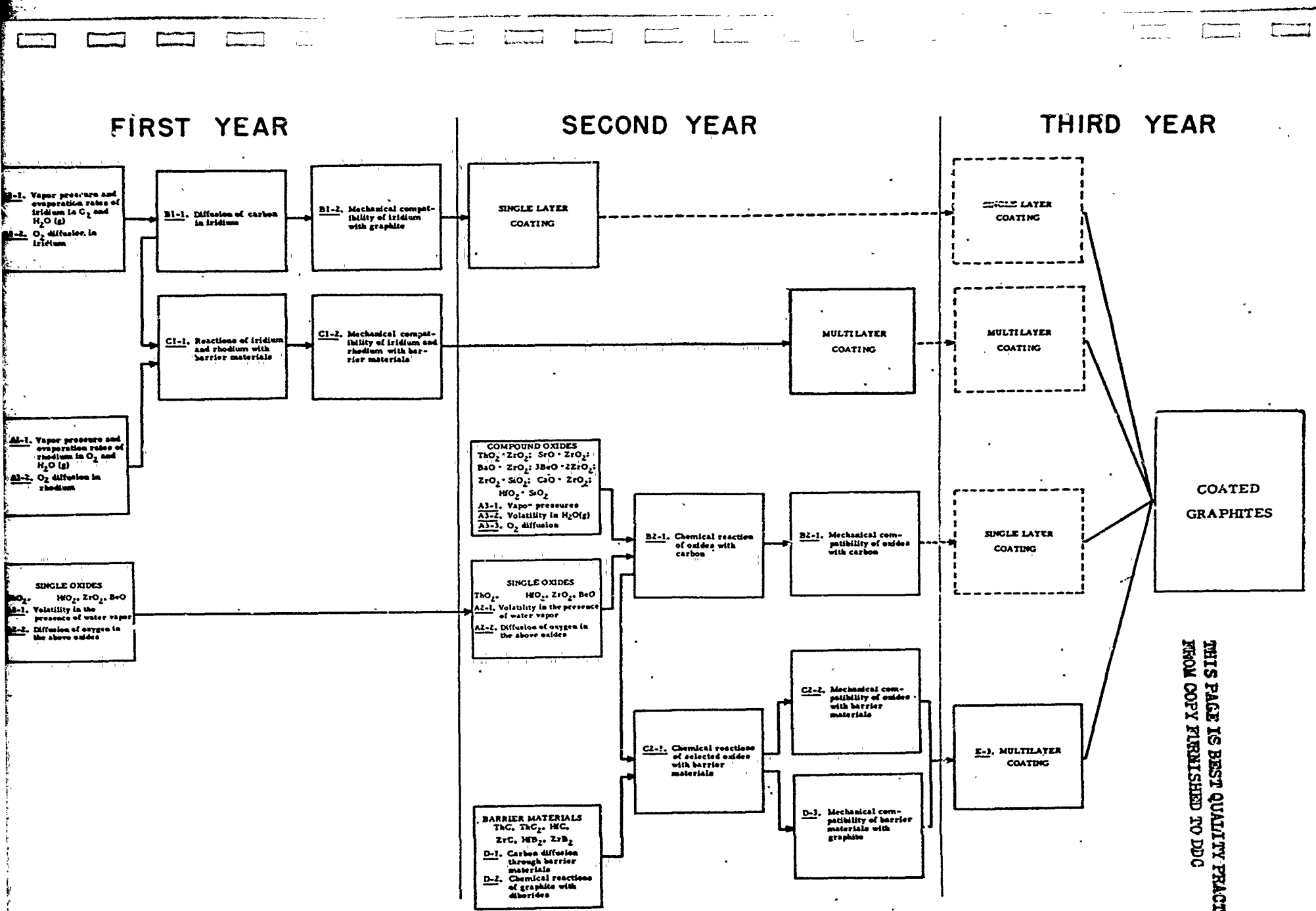

Figure 2. Research Program—Oxidation Protective Coatings for Graphite

A1-2 Oxygen Diffusion Studies

The diffusion of oxygen through iridium and rhodium will influence their behavior as oxidation protective coatings. This research effort, therefore, will be concerned with an investigation of the diffusion of oxygen through iridium and rhodium at high temperatures (>2000°C). Since diffusion rates are strongly dependent on microstructure, porosity, and impurity content, the influence of these factors will also be investigated.

A2-0 Simple Refractory Oxides

On the basis of the available literature, the refractory oxides, thoria (ThO_2), hafnia (HfO_2), beryllia (BeO), and zirconia (ZrO_2), have been selected as the most promising for high temperature oxidation protection.

A2-1 Vaporization Studies

The volatility of these oxides has already been extensively investigated over the pertinent temperature range. The object of this research task is to measure the volatility of these compounds in the presence of water vapor to temperatures in excess of 2000°C.

A2-2 Oxygen Diffusion Studies

The object of this investigation is to measure the diffusion rate of oxygen through the selected refractory oxides. The dependency of the diffusion on microstructure, porosity, and composition will also be investigated.

A3-0 Compound Refractory Oxides

Among the high melting compound oxides, zirconium and/or hafnium silicate and the calcium, strontium, barium, and thorium zirconates will be considered as potential oxidation barriers.

A3-1, A3-2 Vaporization Studies

No experimental data exist on the volatility of these compounds in the temperature range of interest. Therefore, the absolute vapor pressure of several compound oxides will be determined to temperatures in excess of 2000°C. On those compounds which appear promising, the volatility will be determined as functions of oxygen and water vapor pressures.

A3-3 Oxygen Diffusion Studies

As with the simple refractory oxides, information on the diffusion of oxygen through the compound oxides is necessary to evaluate these materials as oxygen barriers. This task will be concerned with the investigation of the diffusion of oxygen through the compound oxides listed in Table 6.

B. Interactions of Prospective Coating Materials With Graphite

B1-0 Iridium in Contact With Graphite

B1-1 Carbon Diffusion Studies

Of the two selected platinum metals, iridium and rhodium, only iridium has a metal-carbon eutectic sufficiently high to permit its use as a coating in direct contact with graphite at temperatures of about 2000°C. Because of its lower metal-carbon eutectic (below 1800°C), rhodium will be considered only as the external component of a multilayer coating. The purpose of this phase of the program is to measure the diffusion of carbon through iridium over an appropriate temperature range up to 2200°C.

B1-2 Mechanical Compatibility Studies

The data obtained from the studies outlined above should establish to what extent iridium might function as a single layer coating system for the oxidation protection of graphite at temperatures in excess of 2000°C. The object of task B1-2 is to investigate the factors controlling the mechanical compatibility of iridium with the graphite substrate as a function of temperature, including the coefficient of thermal expansion, porosity, and degree of surface roughness of the graphite substrate. Completion of the A1 and B1 series of research tasks will provide the basic information needed for a logical, well-conceived coating development effort utilizing iridium as a single layer oxidation protective coating for graphite.

B1-3 Oxides and Mixed Oxides in Contact With Graphite

Even though the oxides ThO_2, HfO_2, BeO, and ZrO_2 are thermodynamically unstable with respect to carbon at 2000°C, the reaction rates may be low enough to justify an investigation of the factors controlling these rates. The purpose of task B1-3 is to measure the reaction kinetics in these cases and determine the factors, such as carbon diffusion, controlling the rates.

Should the time-temperature behavior appear favorable, the parameters affecting the mechanical compatibility of the coating and the substrate will be investigated. Completion of the A2, A3, and B2 series of tasks will supply the necessary background information for evaluating oxides as single layer oxidation protective coatings for graphite at temperatures in excess of 2000°C.

C. Refractory Metals, Carbides, or Borides in Contact With Materials of Section A

An intermediate layer will be necessary to establish those promising oxidation-resistant materials which are not chemically stable in the presence of graphite. On the basis of their low volatilities, high melting points, and high metal-carbon eutectics, HfC, ZrC, ThC, ThC_2, HfB_2, and ZrB_2 have been selected as promising intermediate layers.

C1-0 Interaction of the Platinum Metals With Selected Barrier Materials

C1-1 Reactions of Iridium and Rhodium With Barrier Materials

The chemical reactions of both iridium and rhodium with the selected intermediate layers (barrier materials) at temperatures in excess of 2000°C will be investigated in this research task. These investigations will include identification of the reaction products and the temperatures and structural dependencies of the reactions.

C1-2 Mechanical Compatibility of Iridium and Rhodium With Barrier Materials

This task will investigate the factors influencing the mechanical compatibility of these metals and the barrier materials. The information gained from the series of tasks A1 and C1 will be used to evaluate multilayer coatings utilizing iridium and rhodium as the exterior layers.

C2-0 Interaction of Selected Oxides and Mixed Oxides With Barrier Materials

C2-1 Chemical Reactions

This task will be concerned with the chemical compatibility of the carbides and borides with the oxide layers. The interactions among the coating layers may result in the formation of volatiles at the interface. The kinetics and pressure dependency of these reactions will be investigated at appropriate temperatures (up to 2200°C).

C2-2 Mechanical Compatibility of Oxides With Barrier Materials

The object of this task is to study the mechanical compatibility of the carbides and borides with the oxide layers. The information gained will be utilized to evaluate the mechanical stability of the outer layer with respect to the intermediate layer of the multilayer coatings.

D. Refractory Metals, Carbides, or Borides in Contact With Graphite

The intermediate layer coating must be compatible with both the oxide outer layer and the graphite substrate. The following tasks will supply the necessary information for evaluating the stability of the intermediate layer with respect to graphite.

D1. Carbon Diffusion Studies

This task will be concerned with the diffusion of carbon through the selected carbide and boride barrier materials to temperatures in excess of 2000°C. The influence of microstructure will be considered.

D2. Chemical Reactions of Diborides With Graphite

The interactions of both zirconium diboride and hafnium diboride with graphite will be investigated. This task will also be concerned with the application of dense boride coatings on graphite.

D3. Mechanical Compatibility Studies

The purpose of this task is to study the mechanical compatibility of the various selected boride and carbide barrier materials with graphite. Tasks A2, C2, and D will supply the necessary background information pertinent to developing a multilayer coating system.

E. Interaction of Multilayer Systems

The investigations carried out in tasks A through D will provide an extensive body of information on the high temperature behavior of binary coating systems. An analysis of this information will indicate certain combinations of materials for further consideration as multilayer coating systems. We will investigate several of these multilayer systems where sufficient potential is demonstrated.

Since the previous studies will have supplied much information on the behavior of the binary systems (oxidation protective coating and barrier layer; graphite and barrier layer), the investigations of the present section will be concerned with the possible interactions resulting from the use of ternary systems and with the more detailed analyses of the multilayer behavior. The effects of the diffusion of oxygen through the barrier to the graphite substrate will be determined. In addition, the observed operational behavior of the ternary systems will be correlated with the vaporization, chemical reactivity, and diffusion data obtained from the previous studies on binary systems.

The information gained from the entire program will serve as a sound background for the interpretation and understanding of the mechanisms controlling the oxidation behavior of protective coatings on graphite. It will furnish a basis for predicting methods of modifying and improving both simple and complex coatings to achieve extended-time oxidation protection of structural graphites to temperatures approaching 2200°C.

VI. OXIDATION OF IRIDIUM AT HIGH TEMPERATURES

TASK A1-1

Although the platinum metals group are used for several high temperature applications, data on the thermochemical and kinetic behaviors of these metals under various environments are far from complete. Some oxides of these elements are volatile, the solid oxides are unstable at high temperatures, and the metal oxidation mechanisms are still uncertain. Several kinetic studies have been done on platinum[3, 4, 5, 6], and there have been a few investigations reported on the oxidation kinetics of other platinum metals, including iridium[7, 8, 9]. Krier and Jaffee[7] measured weight losses of Ir in air at 1000°, 1200°, and 1400°C which followed a linear reaction rate and calculated an activation energy of 16 kcal/mole for the process in slowly moving air.

This report deals with a detailed account of the oxidation rates of iridium in pure oxygen, oxygen-helium, in the temperature range 1010° to 1300°C under various oxygen partial pressures and gas flow rates.

Experimental

Iridium foil of 0.002 inch thickness was used for the oxidation experiments. The reactions were carried out in a vertical, 1 inch I.D. Vycor or Mullite combustion tube, about 2 feet long, heated inside a Kanthal wire wound furnace as shown in Figure 3. Rectangular pieces of 0.002 inch thick iridium foil with a surface area of 2.5 cm^2 were suspended from a quartz spring balance by means of a quartz fiber into the hot zone of the furnace. Prior to each run the surfaces of the specimen were cleaned, first with acetone, then distilled water, and subsequently dried in air. In a typical experiment, helium gas was allowed to flow over the suspended iridium sheet which was being brought to temperature. After the specimen had reached temperature equilibrium (about half-an-hour), the system was rapidly flushed with a very high flow rate of pure oxygen (99.8 per cent). After the oxygen flow rate was controlled, the zero reading of the cathetometer was taken. For runs in O_2-He mixtures, oxygen was also injected into the helium stream at zero time. A 15-foot length of $^1/_4$ inch copper tube was used to properly mix the reactant gases.

The change in extension of the quartz spring was measured with a high precision cathetometer at suitable time intervals, and each reaction was run until sufficient readings were taken to establish the kinetics of the process. The temperature was measured with a calibrated Pt versus Pt-10 per cent Rh thermocouple and was maintained within ± 2°C. The oxidation rate constants were obtained from plots of the weight losses/cm^2 versus time and the values were reproducible to within 10 per cent. It should be mentioned that the zero times in these runs do not necessarily coincide with the actual onset of the reaction because of the technique used. This uncertainty, however, does not affect the rate constants.

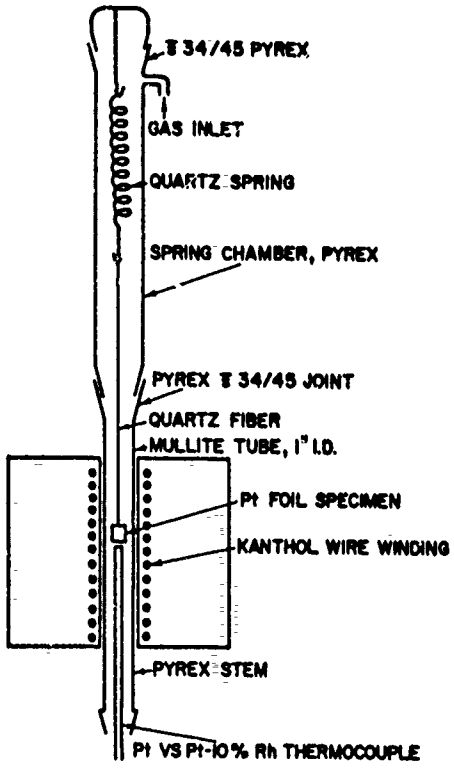

Figure 3. The Oxidation Furnace and Accessories

Results and Discussion

As expected and in agreement with Krier and Jaffee[7], the oxidation of iridium obeyed a linear rate law under all the experimental conditions. Several parameters affecting the oxidation rate were investigated.

a. The Effect of Oxygen Flow Rate

Since the oxidation products of iridium at high temperatures are volatile, the rate of oxidation depends on the gas flow rate in the system. The oxygen flow velocity was varied between 4.8 and 2193 ml/min/cm^2 at 1060°C and between 7.2 and 928 ml/min/cm^2 at 1162°C where the cm^2 represents the cross sectional area of the reaction chamber. The flow rates and the respective rate constants are presented in Table 7 and the nature of the dependence of the rate constant on the flow rate is illustrated in Figure 4. It is clear that the oxidation rate of iridium increases with increasing oxygen flow rate, as expected. It should be mentioned that at 1060°C, with the low flow rates of 4.8 and 48 ml/min/cm^2, the iridium foil surfaces were black due to the incomplete volatilization of the oxide or due to the back reflection of the oxide from the walls; but at higher flow rates at 1060°C and at all flow rates

at 1162°C, the surfaces were clean showing complete volatilization of the oxide. Since no other values are found in the literature on the effect of gas flow rate on the oxidation of iridium, a comparative study is not possible.

TABLE 7

THE EFFECT OF OXYGEN FLOW RATE
ON THE OXIDATION OF IRIDIUM

Temperature °C	Initial Surface area cm^2	Flow Rate $ml/min/cm^2$	Total Oxidation time/min.	Total Weight loss, mg	Linear Rate Constant $mg/cm^2/min$
1060	3.00*	4.8	60	12.50	0.070
1060	3.00	48	64	19.35	0.104
1060	2.25	210	60	20.05	0.152
1060	2.25*	210	32	11.70	0.156
1060	2.25*	928	64	30.00	0.201
1162	2.00	7.2	32	8.35	0.130
1162	2.00*	48	20	14.75	0.372
1162	2.41	178	10	13.25	0.552
1162	2.41*	336	20	33.00	0.694
1162	2.00*	928	18	28.25	0.801

Oxygen Pressure = 1 Atmosphere
* Sample Reused

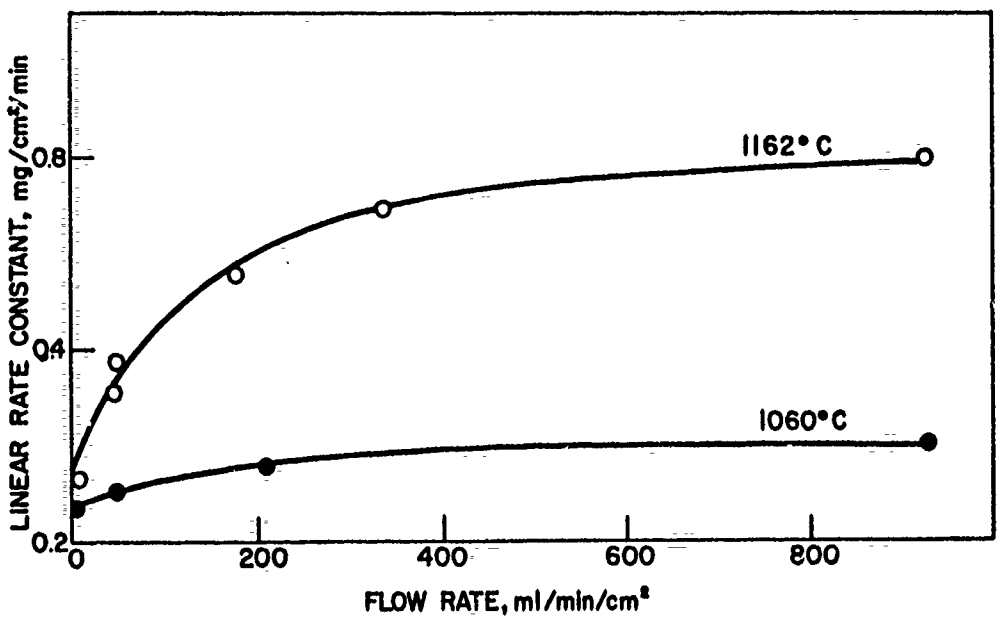

Figure 4. The Effect of Oxygen Flow Rate on Oxidation Rate of Iridium Foil. Oxygen Pressure = 1 Atmosphere.

b. The Effect of Oxygen Partial Pressure

By mixing the oxygen with helium at a constant total flow rate of 48 ml/min/cm^2, various oxygen partial pressures were effected. The rate constants obtained at 1181°C are shown in Table 8. Figure 5 is a plot of the rate constants against oxygen partial pressure and the linearity of the plot indicates that the rate of oxidation of iridium is directly proportional to the oxygen partial pressure, up to 1 atmosphere. The expression $k_l = 4.1 \times 10^{-4} P$ was derived for the dependence of the iridium oxidation rate of the oxygen partial pressure at 1181°C, where k_l is the linear rate constant in $mg/cm^2/min$, of the reaction and P the oxygen partial pressure in torr. According to the transpiration studies by Alcock and Hooper[10], Cordfunke and Meyer[11], and Schäfer and Heitland[12] under equilibrium conditions, the reaction should have a 3/2 order dependence on the oxygen pressure. However, at comparatively fast oxygen flow rates, as in the present case, where equilibrium is not established, a direct comparison of the pressure dependencies is not appropriate.

TABLE 8

THE EFFECT OF OXYGEN PARTIAL PRESSURE AT 1181°C
TOTAL FLOW RATE = 48 ML/MIN/CM^2

P_{O_2} Torr	Initial Surface Area cm^2	Reaction Time min.	Total Wt. loss mg	Linear Rate Constant $mg/cm^2/min$
76	2.25	40	2.60	0.029
152	2.25*	40	4.55	0.048
296	2.18*	30	7.85	0.115
380	2.25*	32	10.62	0.146
456	2.18*	24	12.05	0.236
654	2.25	20	11.60	0.272
760	2.18	28	20.00	0.320

* Sample Reused

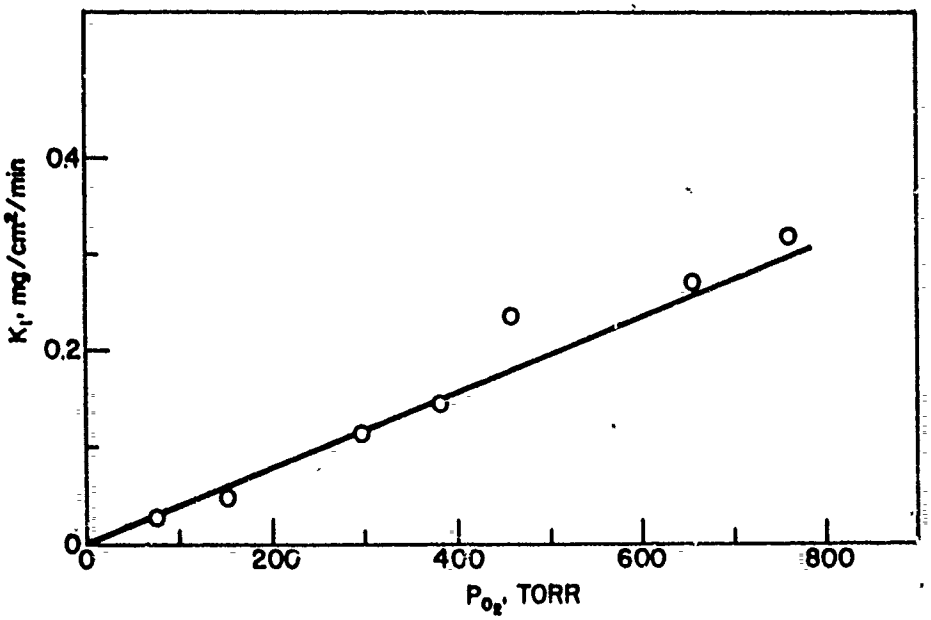

Figure 5. The Effect of Oxygen Partial Pressure on the Oxidation Rate of Iridium. Temperature = 1181°C. Flow Rate = 48 ml/min/cm^2.

c. The Influence of Temperature

The effect of temperature on the oxidation rate of iridium foil between 1010° and 1300°C was investigated in pure oxygen at a pressure of 1 atmosphere, and an oxygen flow velocity of 48 ml/min/cm^2, down the combustion tube. The linear rate constants calculated are given in Table 9. An Arrhenius plot of the data (Figure 6) shows a strong temperature dependence of the reaction, characterized by an activation energy of 80 ± 5 kcal/mole up to about 1100°C, and a lower activation energy of only 7.5 ± 1 kcal/mole in the 1100° to 1300°C range. The apparent high activation energy in the low temperature range may be partly due to the incomplete volatilization of the oxide formed on the surface and a chemisorption controlled reaction. Specimens oxidized at 1010°, 1050°, and 1060°C were black; whereas, at higher temperatures the surface was void of any discoloration. The black color on the iridium is indicative of the presence of an oxide layer which is probably caused by either incomplete volatilization or back reflection of the oxide from the hot walls of the reaction chamber.

TABLE 9

LINEAR RATE CONSTANTS FOR THE OXIDATION OF IRIDIUM AT VARIOUS TEMPERATURES AT 1 ATMOSPHERE OXYGEN PRESSURE

Temperature °C	Initial Surface area cm^2	Reaction Time min.	Total Wt. loss mg	Linear Rate Constant $mg/cm^2/min$
1010	2.50*	90	7.20	0.034
1050	2.48*	60	9.60	0.066
1060	3.00	64	19.35	0.104
1070	2.50	30	8.10	0.108
1100	2.63	48	25.70	0.206
1114	2.46	40	30.00	0.327
1153	2.60	20	18.00	0.379
1156	2.48	10	9.25	0.378
1174	2.14	20	16.25	0.372
1175	2.14*	24	18.00	0.364
1181	2.18	28	20.00	0.321
1264	2.14*	36	31.00	0.438
1301	2.46	32	32.70	0.451

Flow Rate = 48 $ml/min/cm^2$
* Sample Reused

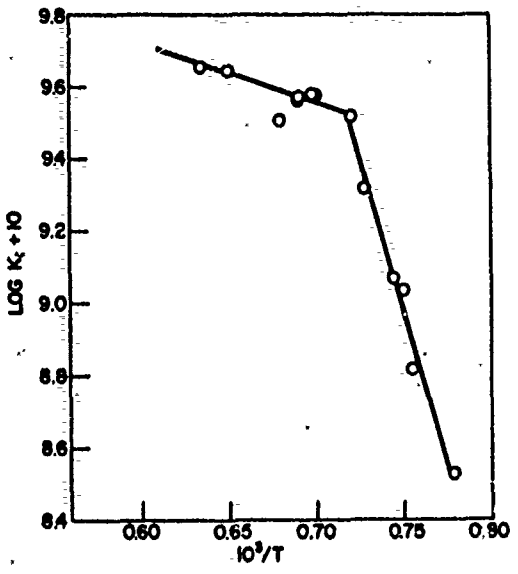

Figure 6. Arrhenius Plot for the Oxidation of Iridium
O_2 Pressure = 1 Atmosphere
O_2 Flow Rate = 48 $ml/min/cm^2$.

The only available rate data in the literature on the oxidation of iridium are that of Krier and Jaffee[7] which were reported for the temperature range 1000° to 1400°C. Since their measurements were carried out under different experimental conditions, the two sets of rate constants as such cannot be compared. However, an approximate extrapolation of the oxidation rates at a partial oxygen pressure of 152 torr in the temperature range 1100° to 1300°C from this investigation shows that the rate constants are higher by a factor of two than the findings of Krier and Jaffee who ran their experiments in an atmosphere of air (152 torr oxygen). On the other hand, a similar comparison of the data at 1000°C shows that our values are 50 per cent lower than those of Krier and Jaffee. Unlike the observations in this investigation at 1000°C, Krier and Jaffee did not observe a black layer on the iridium surface. The differences in appearance of the metal after low temperature oxidation could be due to the difference in gas flow rates, which were 62 ml/min/cm^2 in case of the Krier and Jaffee studies and 48 ml/min/cm^2 in the present experiments. Apparent discrepancies between the two independent investigations cannot be rationalized or the results compared since the rate of oxidation varies with many factors such as the relative sizes of the specimens, the furnace[13], the mounting of the sample inside the furnace, the total pressure in the system[7], the chemical composition of the gas stream[14, 15, 16], the temperature, the oxygen partial pressure, and the flow rates.

Differences in the observed activation energies in the two studies may be attributed to the variation in these experimental conditions. Since Krier and Jaffee report the activation energy of 16 kcal/mole from three experiments at 1000°, 1200°, and 1400°C in air, it is difficult to say if anything happens in between these temperatures. Since IrO_2 has an equilibrium dissociation pressure of 1 atmosphere at about 1100°C[11, 17] there might be some change in the mechanism of the oxidation of iridium around this temperature.

The calculated activation energy of 80 kcal below 1100°C in our investigation may be only apparent due to the presence of small quantities of oxide on the surface. That a change in the activation energy takes place at 1100°C in 1 atmosphere oxygen does not seem to be a mere coincidence in view of the dissociation pressure of IrO_2. The activation energy between 1100° and 1330°C is only about 7.5 kcal/mole which is quite reasonable for a gas diffusion controlled reaction.

d. Presence of Water Vapor in the Oxygen

Reactions at 1160°C with dry oxygen and oxygen bubbled through water at room temperature ($P_{H_2O} \approx 18$ torr) yielded rate constants of 0.38 and 0.33 mg/cm^2/min respectively, at a flow rate of 48 ml/min/cm^2 which indicates that water vapor in the oxygen does not have any pronounced effect on the oxidation rate of iridium at 1160°C. Helium bubbled through water did not cause any measurable reaction at the same temperature. It is further planned to extend these studies to temperatures in excess of 2000°C.

e. The Oxidation Products of Iridium and Reaction Mechanisms

Cordfunke and Meyer have demonstrated that the solid reaction product in the oxidation of iridium which normally deposits on the cooler parts of the cumbustion tube is IrO_2 and Ir[11]. X-ray analysis of the oxidation products of Ir during the present investigation also indicated only IrO_2 with a small amount of Ir. Since IrO_2 is unstable at high temperatures, the high volatility of Ir in oxygen at elevated temperatures suggested the possible existence of some stable oxide species in the gaseous state. Transpiration studies by Alcock and Hooper[10], Cordfunke and Meyer[11], and Schäfer and Heitland[12] indicate that the volatile oxide of iridium is either Ir_2O_3 or IrO_3. But apart from this indirect evidence, there is no proof for the existence of either of these species in the gas phase. According to Wöhler and Witzmann[18] IrO_3 is highly unstable and exists at low temperatures only in the presence of alkali.

In this laboratory various efforts have been made to study the sublimation of IrO_2 by mass spectrometric methods, using an Ingrahm type and a Bendix "time of flight" mass spectrometer.

The experiments are summarized in Table 10. Eight experiments have thus far been carried out in an attempt to identify the high temperature volatile species of iridium oxide. No iridium oxide has been detected in these studies. An Ingrahm type mass spectrometer was used in experiments 1 through 4 to detect the volatile species.

TABLE 10

SUMMARY OF MASS SPECTROMETER EXPERIMENTS ON IRIDIUM OXIDE

Experiment Number	Type of Mass Spectrometer	Material Heated	Temperature °C	Container Material
1	Ingrahm Type	$IrO_{2(s)}$	770 to 1760	Ta Knudsen Cell
2	"	"	845 to 1650	ZrO_2 lined
3	"	Ir, RhO_2	770 to 1525	ThO_2 lined
4	"	Ir, Fe_2O_3	864 to 1620	ThO_2 lined
5	Bendix time of flight	$IrO_{2(s)}$	1050	Vycor Tube
6	"	IrO_2, Na_2O_2	1100	Ta Knudsen Cell
7	"	IrO_2, CuO	1100	Ta Knudsen Cell
8	"	Ir, O_2	1000 to 1800	Pyrex GlassBulb

In the first study, a sample of $IrO_{2(s)}$ was heated in a tantalum Knudsen cell and the mass spectrum was scanned up to mass 400 in the temperature range 770° to 1760°C. At temperatures of 1500°C and higher some TaO + and Ta+ were observed, indicating reaction of the iridium oxide with the tantalum cell. In the second study, the IrO_2 was contained in a ZrO_2 lined tantalum crucible and the experiment was carried out in the temperature range 845° to 1650°C. The third experiment was carried out by heating a mixture of RhO_2 and iridium in a thoria lined tantalum Knudsen cell in the temperature range 770° to 1525°C to study the reaction,

$$RhO_{2(y)} + Ir_{(s \text{ or } g)} \rightleftharpoons RhO_{(g)} + \left[IrO_{(g)} \text{ or } IrO_{2(g)}\right].$$

The fourth experiment was similar to the third, however, Fe_2O_3 was substituted for the RhO_2 and the mass spectrum was scanned at 864° to 1620°C.

The Bendix "time of flight" mass spectrometer was used in experiments 5 through 8. In the fifth experiment, $IrO_{2(s)}$ was heated in a Vycor tube with a small leak into the ion source up to 1050°C. The sixth experiment involved heating a mixture of $IrO_{2(s)}$ with Na_2O_2 up to 1100°C in a tantalum Knudsen cell while CuO was used in place of Na_2O_2 in the seventh experiment.

In the eighth experiment, an iridium filament was sealed inside a Pyrex glass bulb with a molecular leak into the ion source. It was heated by low voltage a.c. in a low partial pressure of oxygen (10 to 15 torr) at various temperatures from 1000° to 1800°C (uncorrected). There was a black deposit over the surface of the bulb and at the molecular leak.

Although the transpiration work authors[10, 11, 12] claim that IrO_2 or Ir_2O_3 is the volatile species in the oxidation of iridium, we feel that these be considered with some degree of reservation until the actual vapor species are identified by some suitable means. It is planned to carry out more elaborate experiments in the mass spectrometer in order to characterize the volatile iridium oxides, if any, with the belief that so far we have not been able to get any appreciable amount of it into the mass spectrometer ion source.

From the low activation energy of 7.5 kcal/mole from 1100° to 1300°C, for the oxidation of iridium we may say with some certainty that the rate determining step in the reaction is the diffusion of oxygen across the outcoming gaseous iridium oxide or vice versa. The first order dependence of oxygen pressure in the system suggested that IrO_2 may be the volatile species, similar to the case of the oxidation of platinum[19] at high temperatures.

VII. PERMEABILITY OF COATING MATERIALS

TASKS A1-2, A2-2, and B1-1

Introduction

The ability of a given material to serve as a coating to protect graphite from oxidation at high temperatures depends on a number of factors. The permeability of the material to either carbon or oxygen determines the limits of protection for an adherent, nonreactive, nonporous coating. In the following sections, the permeability of zirconia, hafnia, and thoria to oxygen, the permeability of iridium and rhodium to oxygen and of iridium to carbon is reported and discussed in terms of other diffusion measurements in the literature and of the ability of these materials to protect graphite from oxidation.

The rate of permeation through a barrier may be limited either by reactions at the surfaces or by diffusion through the barrier.[20] However, if the barrier is thick enough, diffusion will determine the rate of permeation. Reactions at the surface will be in equilibrium and serve to establish the concentration of the diffusing substance at the interfaces.

The steady state rate of mass transport through a membrane is given in Equation 1 by Fick's first law[21].

$$P = D \frac{dc}{dx} \quad , \tag{1}$$

where P = the permeability,
D = the diffusivity, and
$\frac{dc}{dx}$ = the concentration gradient.

Assuming that the diffusivity is independent of concentration, Equation 1 can be written as

$$P = D\left(\frac{C_1 - C_2}{\ell}\right) \tag{2}$$

where C_1 and C_2 are the concentrations immediately below the two surfaces and ℓ is the thickness of the membrane. If the rate determining step is diffusion within the solid and not transport across the boundaries, C_1 and C_2 are the concentrations in equilibrium with each external phase.

The diffusivity, D, can be obtained from the time dependence of the permeation after one surface is exposed to the diffusing substance. This requires consideration of the concentration gradient which will occur prior to reaching steady state permeation. The buildup of the diffusing substance passing through a membrane is obtained by solving Fick's second law

$$\frac{dc}{dt} = D\left(\frac{d^2c}{dx^2}\right) \quad . \tag{3}$$

Barrer[21] gives a solution for the case where

$C = C_1$ at $x = 0$ for all t,
$C = C_2$ at $x = \ell$ for all t,

and

$C = C_0$ for $0 < x < \ell$ at $t = 0$.

This solution at $x = 0$ is

$$\frac{dc}{dx} = \frac{C_2 - C_1}{\ell} + \frac{2}{\ell} \sum_1^{\infty} \left[(C_2 \cos n\pi - C_1)\, e^{-\frac{Dn^2\pi^2 t}{\ell^2}} \right] + \frac{4C_0}{\ell} \sum_{m=0}^{\infty} e^{-\frac{D(2m+1)^2\pi^2 t}{\ell^2}} \quad . \qquad (4)$$

If the total amount of matter diffused through the membrane is plotted against time, after an initial period a straight line is obtained. Extrapolating this line back to zero amount gives an "induction time" L,

$$L = \frac{1}{C_2 - C_1} \left[\frac{C_2 \ell^2}{6D} + \frac{C_1 \ell^2}{3D} - \frac{C_0 \ell^2}{2D} \right] \quad . \qquad (5)$$

For the case where $C_0 = 0$ and $C_1 \ll C_2$,

$$L = \frac{\ell^2}{6D} \quad . \qquad (6)$$

Thus, by measuring the time dependence of the permeation, not only the permeability but also the diffusivity and the concentration of the diffusing material may be obtained. This method has been used in studying the permeability of alumina to oxygen.[22]

Experimental

Two classes of materials were studied: the platinum metals (iridium and rhodium) and the refractory oxides (zirconia, hafnia, and thoria).

The iridium and rhodium samples were three or four inch long tubes closed at one end. The open ends were welded to stainless steel tubes about five inches long which fitted into standard Swagelok fittings with Teflon ferrules. The rhodium samples and one iridium sample were enclosed in a water cooled Pyrex jacket (quartz was used for the higher temperatures) to form the diffusion cell shown in Figure 7. The other iridium sample was not enclosed in the water cooled jacket; its outside was exposed to air and the inside was monitored for oxygen with the Omegatron mass spectrometer. Since the water jacket was left off this iridium sample, the stainless steel tube was cooled by forced air to prevent oxygen from diffusing through this portion of the system and to prevent any oxygen that diffused through the iridium from reacting with the carbon in the stainless steel to produce carbon dioxide.

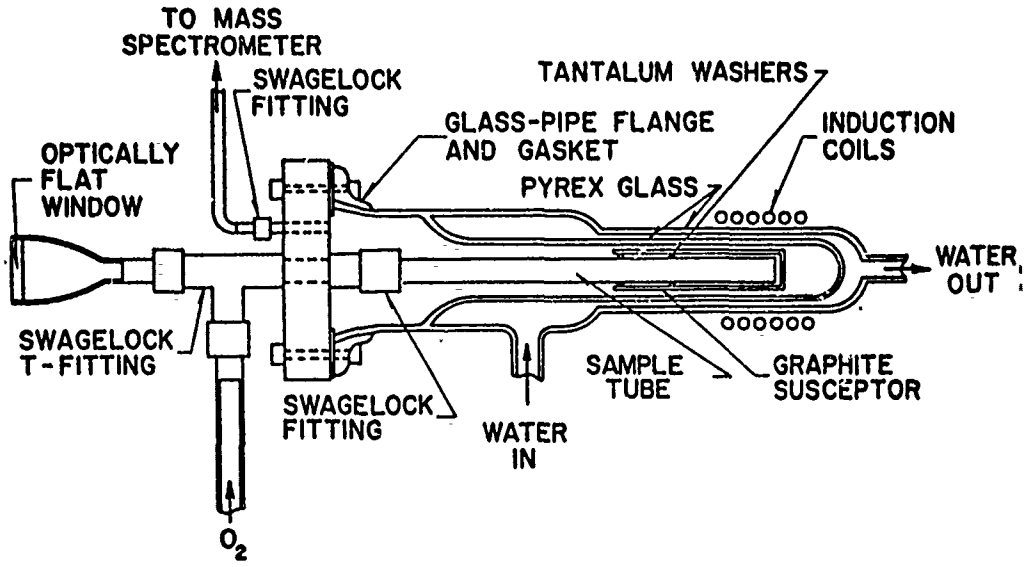

Figure 7. Diffusion Cell

A 25 KW, 400 KC induction heater was used to heat the iridium and rhodium samples directly. Since the outside of the sample could not be sighted with a pyrometer due to the presence of the water jacket and the evaporation of metal on the glass walls of the diffusion cell, it was necessary to sight down the inside of the sample and to consider the apparent emissivity of shallow cavities. Using the correction for shallow cavities,[23] one may calculate that for a substance with an emissivity of 0.33 (which is the best value for iridium),[24] the apparent emissivity sighting down a hole with a 2:1 depth to diameter ratio is 0.86. However, this correction is for a matt surface, whereas the surface of the iridium tube was smooth; therefore, the temperature correction used is the average of that for a smooth and a diffuse reflecting surface (apparent emissivity of 0.53). An error of ± 0.1 in the assumed emissivity corresponds to an error of approximately ± 25°C at 1300°C and of ± 50 °C at 2000°C. A micro-optical pyrometer that can be read to ± 2°C was used for the measurement of the brightness temperature.

The oxide samples (zirconia, hafnia, and thoria) were also in the form of tubes closed at one end. The experimental setup was the same as that for the iridium and rhodium samples except that no intermediate stainless steel tube was used and a graphite susceptor was fitted over the closed end of the tube since it could not be heated directly with the induction heater. The sample and susceptor were then enclosed within the Pyrex jacket (see Figure 7). An iridium coating was placed on the graphite susceptor to reduce its emissivity. Temperatures 200°C higher than those obtained with the uncoated susceptor could be reached by the use of this coating. Tantalum washers, drilled with small holes to permit gas flow, were used to hold the susceptor in place for all of the oxides except thoria. In the case of thoria, one set of experiments was performed using Lucalox washers and another set was performed using tantalum washers.

For the oxides, the length of the hot zone was greater than four times the diameter of the tube so black body conditions were assumed in measuring the temperature. A difficulty was met in determining the extent of the hot zone and the role played by the intermediate temperature zone. From observations of the susceptor, the length of the hot zone at nearly constant temperature was estimated. This was varied from one-half inch to one inch long. Within one-fourth inch after this, the temperature decreased by about 100°C. This temperature change decreased the permeability by about an order of magnitude. The fact that the same permeabilities were obtained when the length of the hot zone was varied indicates that the presence of an intermediate temperature zone did not appreciably effect the results.

The vacuum system used in these studies was an ultrahigh vacuum system including an Omegatron mass spectrometer originally used for adsorption studies.[25] The jacket of the cell was installed with a rubber gasket limiting the vacuum to the 10^{-7} to 10^{-6} torr region. A schematic drawing of the system is shown in Figure 8. Except for one series of iridium studies and the carbon diffusion studies, the permeability of the samples to oxygen was obtained by letting a constant pressure of oxygen into the inside of the sample tube and measuring the gas flow out of the diffusion cell into vacuum system I (see Figure 8). For quantitative results the pressure of an ion gauge in vacuum system I was calibrated in terms of gas flow. This was done by connecting a gas reservoir of known volume through a leak valve to vacuum system I and measuring the pressure decrease in the reservoir as a function of time. Calibrations were carried out using both carbon monoxide and oxygen. The measured flow rates were compared with those calculated from the theory of free molecular flow[27] and excellent agreement was obtained.

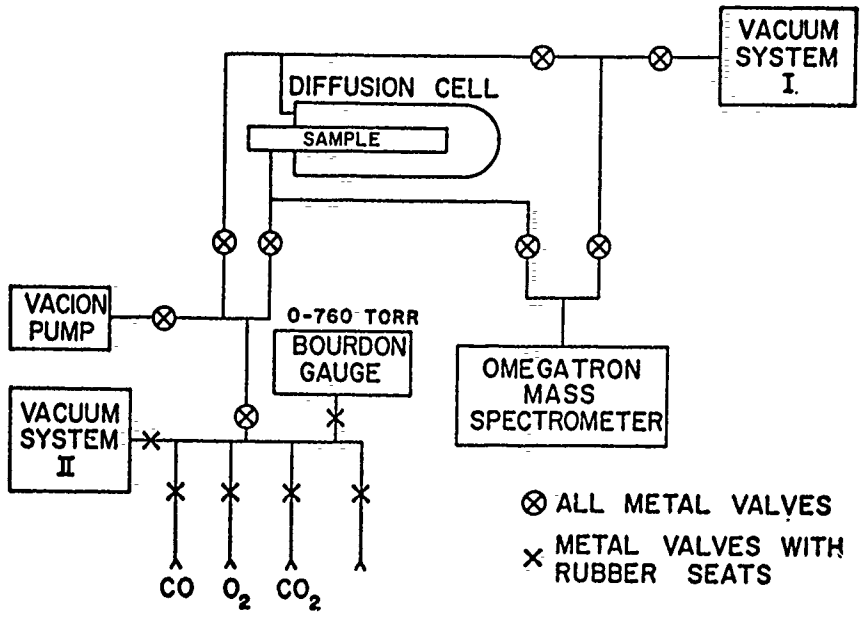

Figure 8. Schematic Drawing of Vacuum System

One per cent or less of the gas flow was allowed to leak into the mass spectrometer to obtain a knowledge of the gas composition. The oxygen permeating through the rhodium reacted with the carbon present in the hot stainless steel to give a gas which was composed of carbon dioxide and oxygen. In the case of the oxides, the oxygen which diffused through the sample immediately reacted with the hot graphite susceptor to form a gas which was better than 99 per cent carbon monoxide with only a trace of carbon dioxide and water present. Due to the presence of the hot graphite susceptor, the gas was essentially all carbon monoxide even without oxygen permeation.

For the study of carbon permeability, the outside end of the cup was painted with carbon (aquadag) and oxygen was allowed to flow into and out of the inside of the cup to react with carbon diffusing through the iridium. The reaction product, carbon dioxide, was then detected with the mass spectrometer.

The porosity of the samples was frequently checked by the use of argon. All of the results reported here were on samples which showed no detectable argon permeation.

As a check on the performance of this system, the permeability of a silver tube to oxygen was measured and the results (see Table 11) were compared with those of Johnson and Larose.[26] The agreement is satisfactory considering the general dependence of permeability on sample history.

TABLE 11

PERMEABILITY OF SILVER TO OXYGEN

	This Work	Johnson and Larose[26]
550°C	0.6×10^{-8}	1.0×10^{-8}
600°C	1.3×10^{-8}	2.2×10^{-8}

* P_{O_2} = 159 torr

ℓ = 0.09 cm (wall thickness of tube)

Specimens

The specimens used were of the purest material available in the form of impervious tubes. The iridium and rhodium were purchased from Engelhard Industries while the zirconia, hafnia, and thoria were purchased from the Zirconium Corporation of America. Spectrographic analysis of all the specimens were performed before and after heating. In all cases, the number and amounts of impurities were either the same or less after the high temperature studies were made. Sections of the specimens were also subjected to metallographic examination.

1. Iridium

Two samples of iridium were used. They were made from a 0.015 inch sheet welded by the vendor into tubes with one end closed. The tubes were one-half inch in diameter and three and four inches long, respectively. The end of the second specimen was made from a 0.010 inch sheet in order to determine the effect of thickness on the measurements.

No purity specifications were received from the vendor; however, the results of a spectroscopic analysis, performed at this Laboratory, on the first specimen are given in Table 12.

TABLE 12

SPECTROSCOPIC ANALYSIS OF IRIDIUM SPECIMEN

Element	Per Cent
Pt	0.01 to 0.1
Rh	"
Ru	"
Pd	"
Ni	"
Fe	"
Co	"
Cu	"
Ti	"
Si	"
Al	"
Mg	less than 0.01
Mn	less than 0.01

After the first time the iridium cup was heated to 1800°C, large grains of iridium appeared. These soon grew to a size of about 1 mm, and then stopped growing. The iridium did not develop porosity although after many runs, a break in the weld developed when the sample was heated in air, presumably due to the end bowing in. The appearance of the iridium heated to 2000°C in air is interesting as is seen in Figure 9. The top end of the tube shown in this photograph was at 2050°C and the bottom of the tube at a temperature <1000°C. The high temperature oxidation caused the iridium to be highly polished as can be seen from the light reflection. Below this area is a dark ring and a light ring in both of which etching and faceting of iridium crystallites can be seen. Below the light area is a narrow dark ring which is presumedly an IrO_2 layer marking the maximum temperature stability of IrO_2. Below this the oxide layer becomes thin and some faceting can be seen. The bottom area has a matt appearance characteristic of the unheated tube. Apparently in the highest temperature region the oxidation rate is limited by diffusion through the gas so that the iridium is removed evenly. At lower temperatures the oxidation is preferential on certain places leading to etching and faceting.

Figure 9. Photograph of Iridium Tube Heated to 2000°C in Air (top at 2050°C, bottom at less than 1000°C)

The photomicrographs of the hot zone and cold zone iridium cross sections are shown in Figure 10 with a magnification of 150X. (The hot zone is the section on the sample which had been heated and the cold zone is the section on the sample which had not been heated.) The photomicrographs clearly show larger grains in the portion of the sample that was heated. The hot zone cross section is smaller than the cold zone cross section because the hot zone on this particular sample had been heated in air for approximately two days and some of the iridium reacted with the oxygen in the air to form the volatile oxide presumably IrO_3 from the investigations of others[10,11,12].

Cold Zone

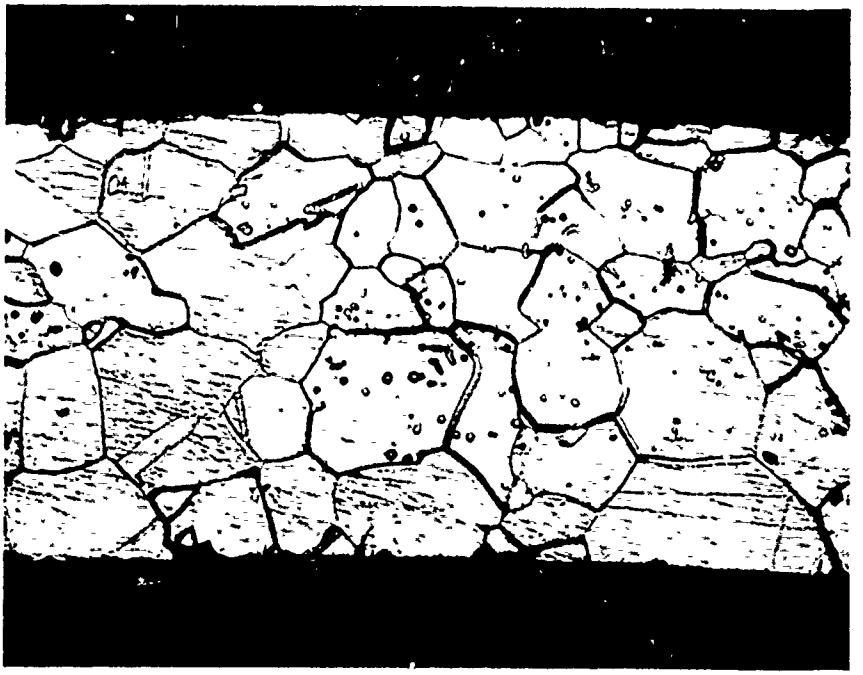

Hot Zone

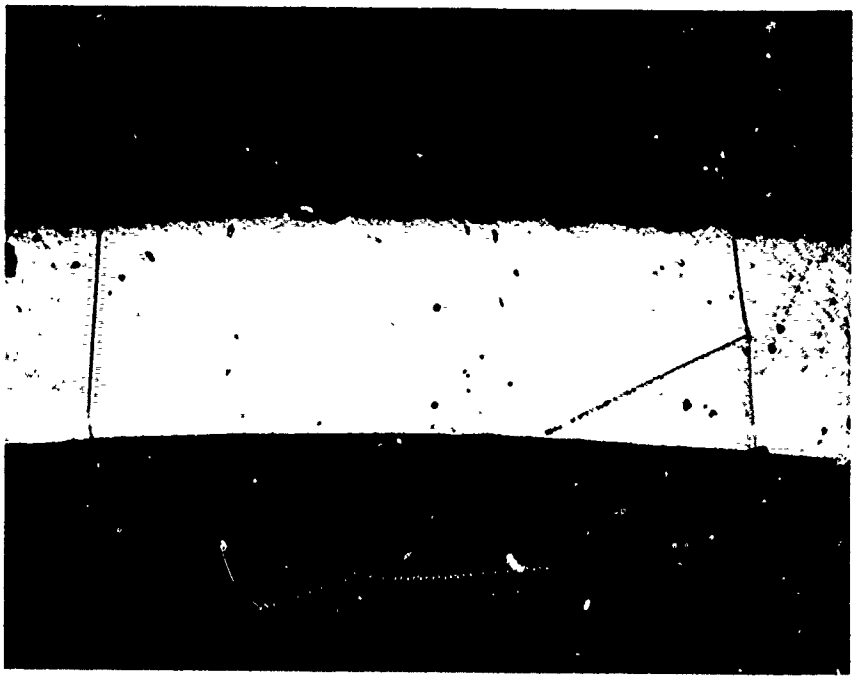

Figure 10. Photomicrographs of Cross Section of Iridium Sample (top of each photograph shows edge of oxidized surface). (150 X)

2. Rhodium

Two rhodium samples were used. Both specimens were made from a 0.015 inch sheet in the same way that the iridium samples were. The length of the samples was three and four inches, respectively, with a diameter of one-half inch. The first sample became porous during the first series of runs and no further work could be done on this sample. Rhodium has a characteristic of becoming porous after it has been exposed to oxygen at elevated temperatures. In fact, the second sample had to be rewelded several times.

The results of a spectroscopic analysis, performed at this Laboratory, on the first rhodium sample are given in Table 13.

TABLE 13

SPECTROSCOPIC ANALYSIS
OF RHODIUM SPECIMEN

Element	Per Cent
Pt	0.01 to 0.1
Pd	"
Au	"
Ni	"
Cu	"
Fe	"
Co	"
Al	"
Ti	"
Si	"
Mg	less than 0.01
Mn	less than 0.01

After the second rhodium sample had been heated to 1510°C in vacuum, grains ~ 1 mm in size became visible; however, it exhibited less faceting than the iridium did.

As can be seen in Figure 11, the photomicrographs of the hot zone and cold zone rhodium cross sections with a magnification of 150X show larger grains after the sample had been heated.

Cold Zone

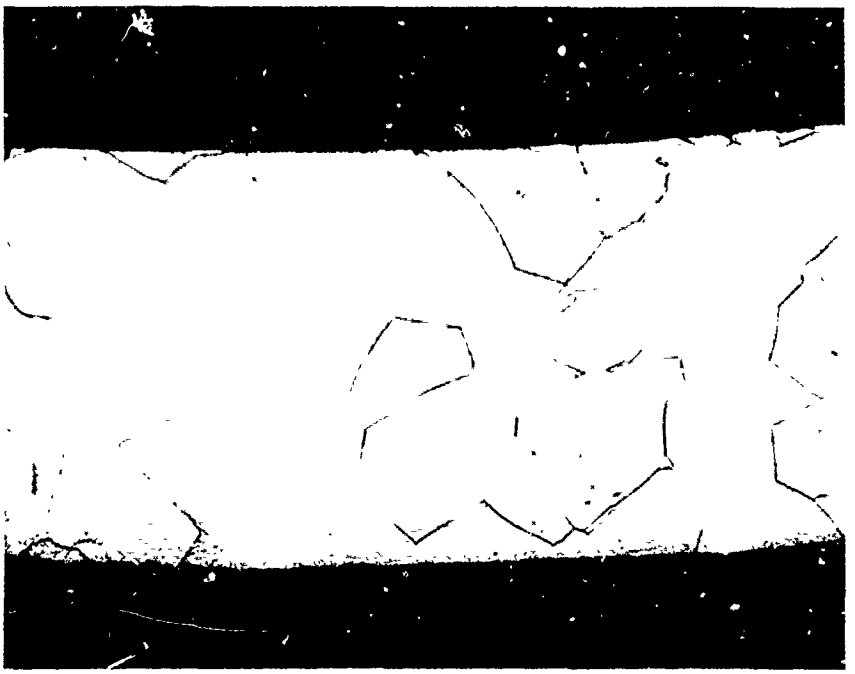

Hot Zone

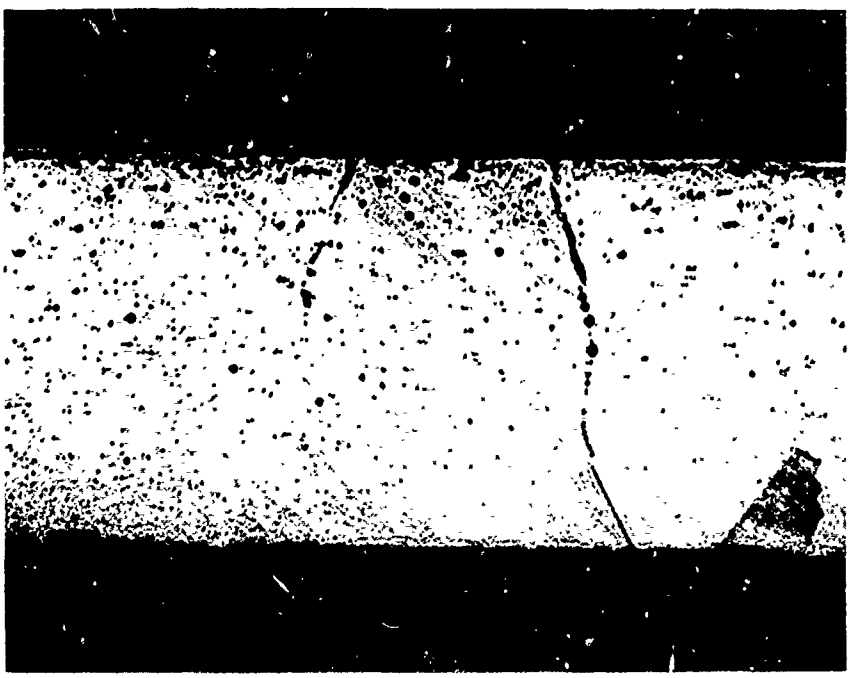

Figure 11. Photomicrographs of Cross Sections of Rhodium Sample (top of each photograph shows edge of oxidized surface). (150 X)

3. Zirconia

For this part of the study, a 4 per cent lime stabilized, slip cast, $8\frac{1}{2}$ inches long x $\frac{3}{8}$ inch O. D. x $\frac{9}{32}$ inch I. D., impervious zirconia tube was used. The manufacturer's chemical analysis of the zirconia sample is given in Table 14 and the spectrographic analysis performed at this Laboratory is given in Table 15. Its density was 5.4 gm/cm^3 with about a 5 per cent porosity.

TABLE 14

MANUFACTURER'S ANALYSIS OF ZIRCONIA, IMPURITIES

Compound	Per Cent
CaO	4.0
HfO_2	1.5
SiO_2	0.5
MgO	0.20
Fe_2O_3	0.10
Al_2O_3	0.17
TiO_2	0.11

TABLE 15

SPECTROGRAPHIC ANALYSIS OF ZIRCONIA SPECIMEN

Element	Per Cent
Ca	greater than 0.1
Hf	0.01 to 0.1
Mg	"
Al	"
Ti	"
Si	"
Fe	"
Cu	"
Mn	"
Cr	less than 0.01

Figure 12 shows the photomicrographs of the hot zone and cold zone zirconia cross sections with a magnification of 150X. A definite grain structure is visible in the cold zone whereas the grain structure is nearly lost in the hot zone. There appears to be a segregation of some material at the grain boundaries in the cold zone, but this has disappeared in the hot zone. Also, the total pore volume appears larger in the hot zone, but the number of pores appears to be the same.

A second sample was also investigated. Although it was impervious initially at room temperature, when it was heated to 1550°C for the first run, it lost its imperviousness even after cooling to room temperature. No further work was done with this sample.

Using X-ray techniques, the crystal structure of the zirconia specimen was determined at this Laboratory. The study was made between 800° and 1800°C and only the cubic structure was detected.

Cold Zone

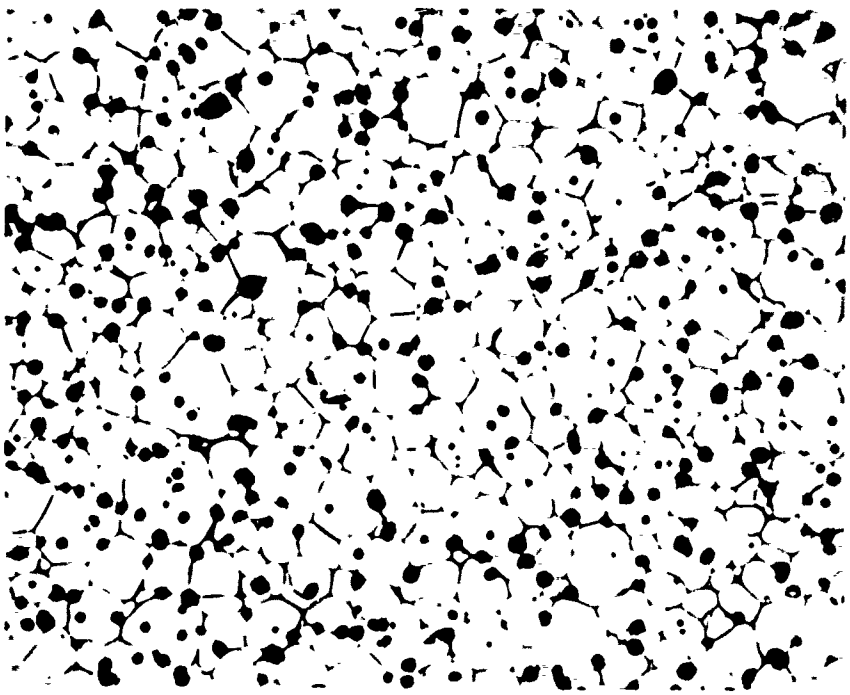

Hot Zone

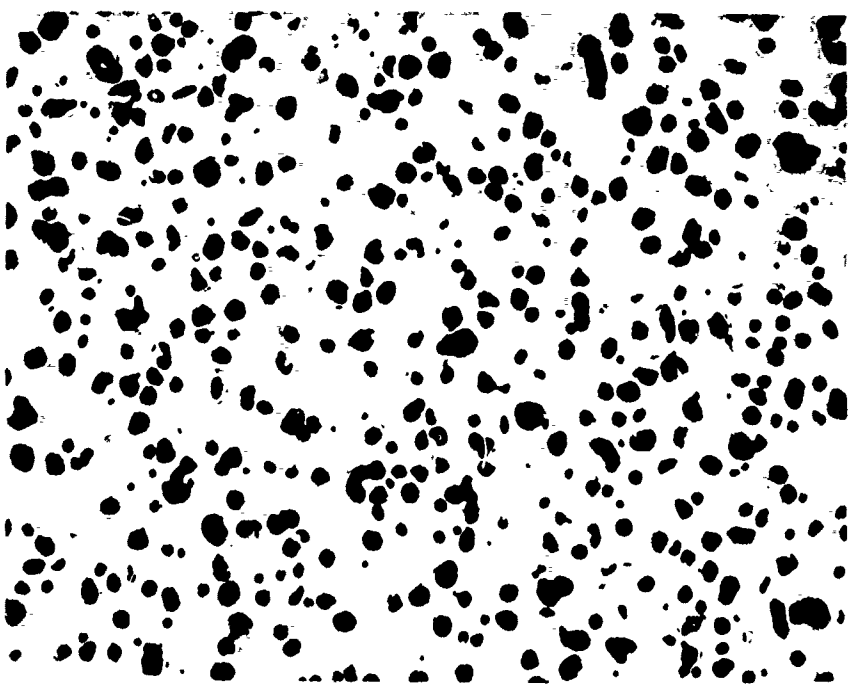

Figure 12. Photomicrographs of Cross Sections of Zirconia Sample (150X)

4. Hafnia

For this series of runs, a 9-inch length of $^1/_4$ inch O. D., $^3/_{16}$ inch I. D., 4 per cent lime stabilized, impervious hafnia tube was used. It had a density of 9.51 gm/cm^3 and a porosity of about 5 per cent. The manufacturer's chemical analysis of the hafnia sample is given in Table 16 and the spectrographic analysis performed at this Laboratory is given in Table 17.

TABLE 16

MANUFACTURER'S ANALYSIS OF HAFNIA, IMPURITIES

Compound	Per Cent
ZrO_2	2.5 to 3
Al_2O_3	0.012 to 0.1
Fe_2O_3	0.012 to 0.1
Cb_2O_5	0.05 to 0.1
TiO_2	0.01 to 0.2
CaO	4
Total other oxides	0.1

TABLE 17

SPECTROGRAPHIC ANALYSIS OF HAFNIA SPECIMEN

Element	Per Cent
Ca	greater than 0.1
Zr	greater than 0.1
Si	0.01 to 0.1
Al	"
Mg	"
Ti	"
Y	"
Fe	"
Cu	"
Mn	"
Cr	"

The photomicrographs of the hot zone and cold zone hafnia cross sections are shown in Figure 13 with a magnification of 150 X. The hafnia microstructure is little affected by heating to temperatures of 2000°C. A secondary phase appears in both the hot and cold zones of the specimen.

Cold Zone

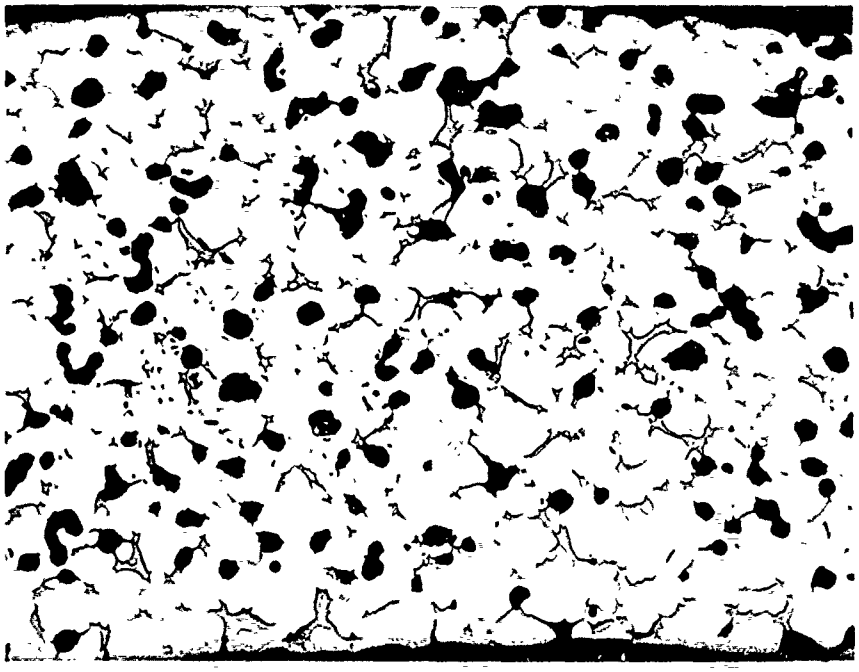

Hot Zone

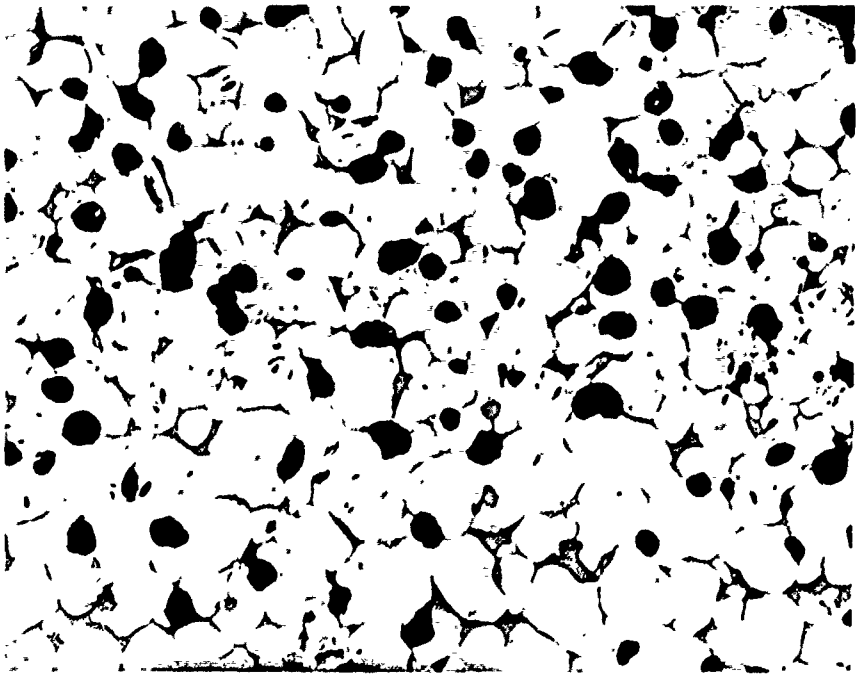

Figure 13. Photomicrograph of Cross Sections of Hafnia Sample (150X)

5. Thoria

A 9-inch length of $^3/_8$ inch O.D. x $^9/_{32}$ inch I.D., slip cast, impervious thoria tube was used. It had a porosity of 5 per cent and a density of 9.12 gm/cm^3. Table 18 gives the manufacturer's chemical analysis of the thoria sample, and Table 19 gives the spectrographic analysis performed at this Laboratory. Even though the manufacturer quotes 5000 ppm ZrO_2, zirconium was not detected by spectrographic analysis. Two identical samples were used since one developed a leak after it had been used for one series of runs.

TABLE 18

MANUFACTURER'S ANALYSIS OF THORIA—IMPURITIES

Compound	Parts per Million
CaO	81
MgO	332
SiO_2	193
Al_2O_3	81
ZrO_2	5000

TABLE 19

SPECTROGRAPHIC ANALYSIS OF THORIA SPECIMEN

Element	Per Cent
Mg	0.01 to 0.1
Si	"
Al	"
Fe	"
Mn	less than 0.01

As can be seen in Figure 14, the photomicrographs of the hot zone and cold zone thoria cross sections with a magnification of 150 show no visible difference between the hot and cold zones. There is a slight evidence of grain structure and the pore structure is finer than in the other two oxides mentioned previously.

In all of the oxides studied, the pores are nearly spherical and are not interconnected to the extent that diffusion through the pores occurs. This was verified by the imperviousness of the samples to nitrogen and argon in the temperature range in which these studies were made. The photomicrographs appear to give a higher porosity than the 5 per cent quoted by the manufacturer. Helium and mercury density measurements will be carried out to resolve this discrepancy.

Cold Zone

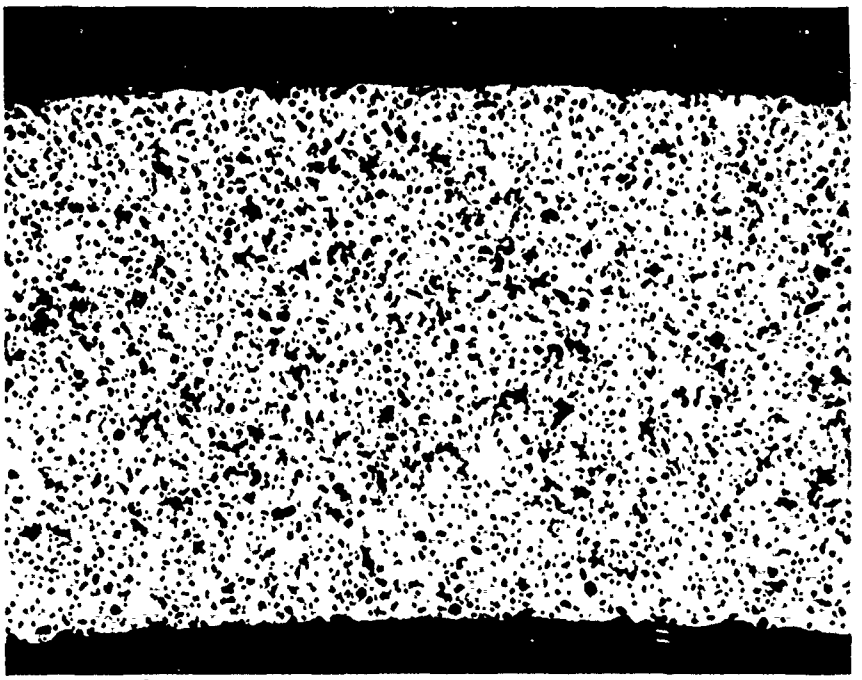

Hot Zone

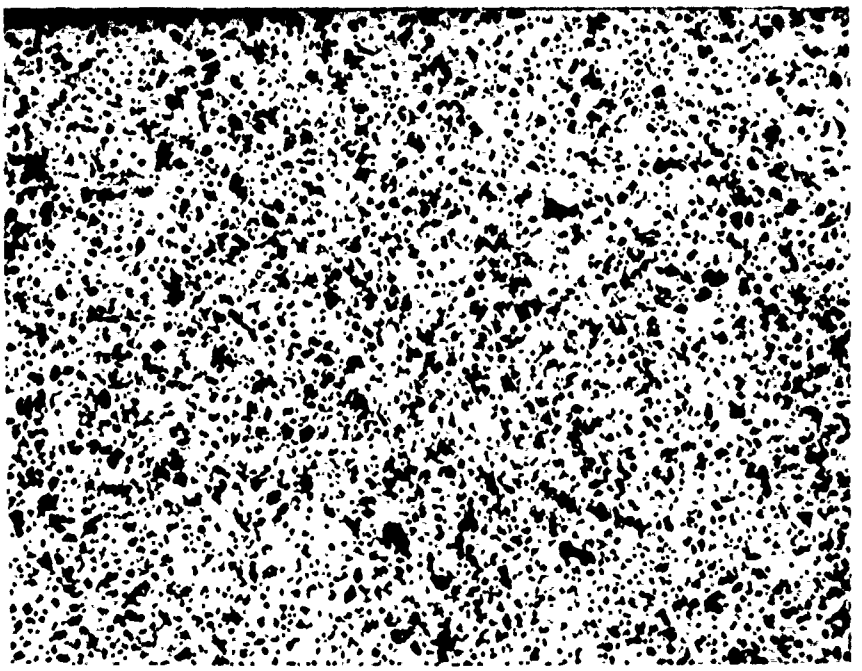

Figure 14. Photomicrographs of Cross Sections of Thoria Sample (150 X)

Results

1. Permeability of Rhodium to Oxygen

The permeability of rhodium to oxygen has been studied between 1290° to 1510°C. At higher temperatures, the evaporation of rhodium is quite rapid and rhodium mirrors formed on the glass walls of the vacuum system. The background pressure decreased as the temperature was raised. This is attributed to a gettering effect caused either by reaction of rhodium vapor with oxygen or by adsorption of oxygen on freshly deposited rhodium surfaces.

The pressure dependence of the permeability is given in Figure 15. The hysteresis on increasing and decreasing pressure is believed to be due to the gettering effect. The data on decreasing pressure should be more accurate since the saturation of the getter is more likely. The oxygen was almost all converted to carbon dioxide before it left the diffusion cell, presumably due to interactions with the carbon in the stainless steel extension tube. The pressure dependence of the permeability was not the same for all the runs made. A half order dependence in pressure, as would be expected from theory, is about the average dependence.

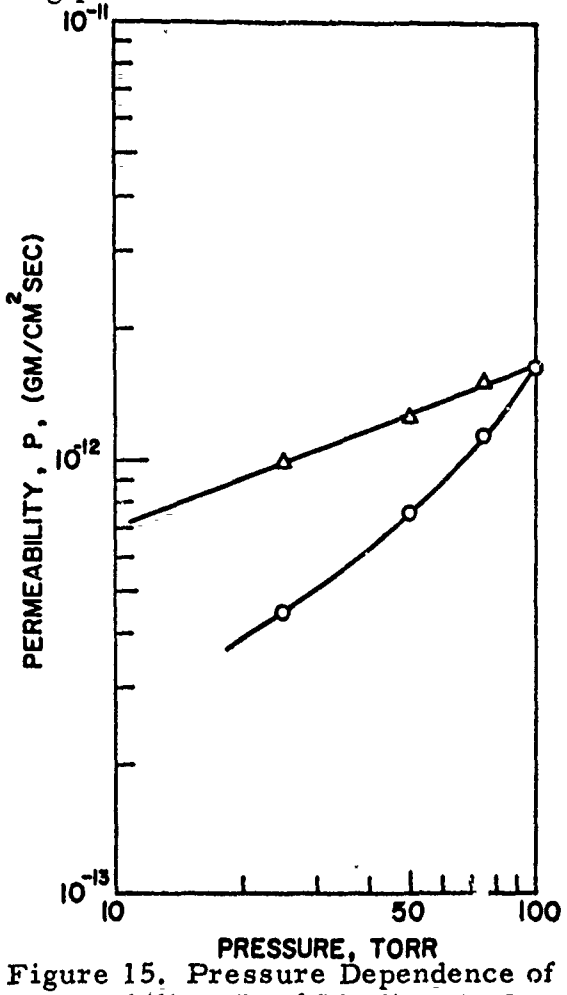

Figure 15. Pressure Dependence of Permeability, P, of Rhodium to Oxygen at 1400°C

O increasing pressure
Δ decreasing pressure

The temperature dependence of the permeability constant, $P\ell$, at 50 and 75 torr oxygen pressure is shown in Figure 16. Only three points are given in this figure; this is due to another characteristic of rhodium. The 0.015 inch rhodium sample was initially nonporous but after exposure to oxygen at elevated temperatures, porosity, as indicated by argon permeation, would develop. At first the porosity developed in the welded portions; it later developed all over the sample. The data shown in Figure 16 were from the only series where as many as three runs were made before the sample became porous. At the time these data were taken, the grain structure of the sample was visible and grain size of the order of 1 mm was observed. These data give a permeability constant of

$$P\ell = 3.63 \times 10^{2} e^{-116,600/RT} \text{ gm/cm sec}$$

where P is the permeability and ℓ is the sample thickness.

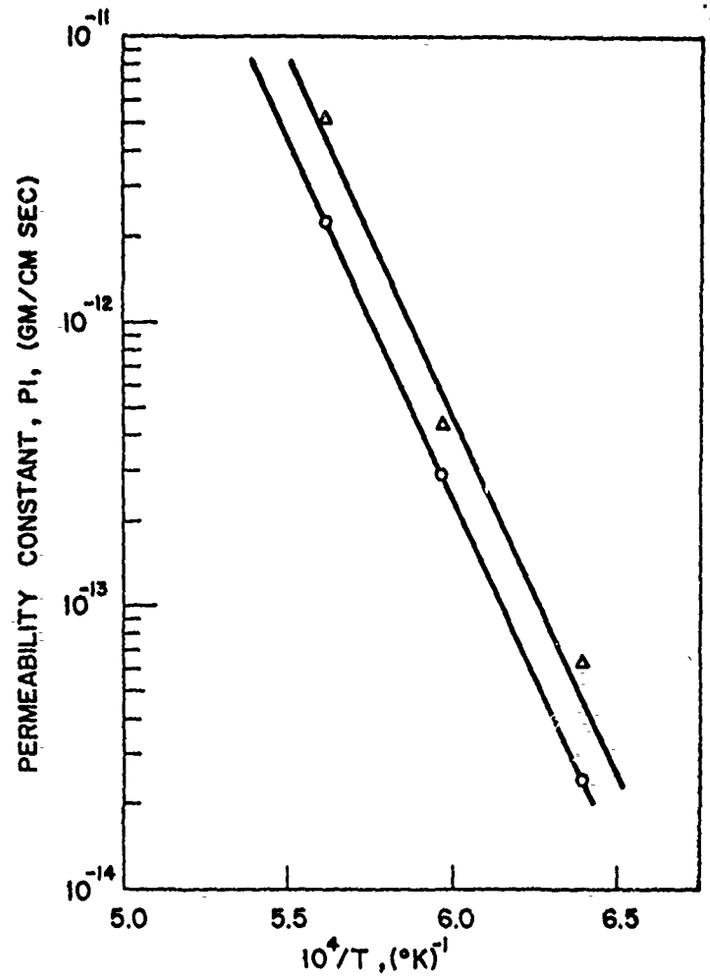

Figure 16. Temperature Dependence of the Permeability Constant, Pl, for Rhodium to Oxygen
O 50 torr pressure
Δ 75 torr pressure

2. Permeability of Iridium to Oxygen

The first iridium sample was heated in air to 2200°C for 150 minutes with the outer jacket of the cell removed. Only if the diffusivity was less than 10^{-8} cm^2 sec^{-1} would the oxygen appear later than 150 minutes. No oxygen was observed inside the cup during this whole run. A permeability of $< 10^{-14}$gm cm^{-2} sec^{-1} was calculated. At the end of the experiment, the wall thickness was measured directly and found to be 0.014 inch thick, one thousandth less than originally. This decrease in wall thickness was due to the iridium reacting with the oxygen in the air to form volatile iridium oxide. The total diameter had decreased at the hot end by 5 per cent and the end of the cup bowed in.

The permeability of a second sample of iridium to oxygen was studied by exposing the inside of the iridium thimble to 50 torr of oxygen for 90 minutes at 1075°, 1175°, 1400°, 1635°, and 1820°C. The iridium thimble was the same as noted previously except that the end was 0.010 inch thick. During

all of these runs, no trace of oxygen permeation was observed. The rhodium data as shown in Figure 16 gave a lowest measured value of the permeability of about 10^{-12} gm cm^{-2} sec^{-1}, a value which could be determined within 10 per cent. This sensitivity is used to determine that the permeability of 0.010 inch iridium to 50 torr of oxygen was $<10^{-13}$ gm cm^{-2} sec^{-1}. This experimentally determined sensitivity limit is more realistic than the theoretical value of 10^{-14} gm cm^{-2} sec^{-1}, since it is based on actual permeation of oxygen through rhodium. Therefore, it will be used to define the limit of oxygen permeation in iridium rather than the value of 10^{-14} gm cm^{-2} sec^{-1} given previously.

3. Permeability of Iridium to Carbon

Carbon permeability was determined by measuring the amount of carbon dioxide formed by oxygen streaming on the inside of a heated iridium thimble which was coated with carbon on the outside. A certain amount of background carbon dioxide was always present due to the interactions of carbon in the stainless steel and oxygen; this was always subtracted out. Since iridium was found to be impervious to oxygen, it is valid to assume where the background is subtracted out that the quantity of carbon dioxide formed is a function of the amount of carbon diffused through the iridium.

Meaningful results are obtained only when there is a sufficient excess of oxygen to convert all of the carbon to carbon dioxide. In this case, the rate-determining step is diffusion through the solid, not reaction on the surface or diffusion through the gas. Even with the end of the tube at the highest temperatures where appreciable carbon monoxide is in equilibrium with carbon dioxide and oxygen, only carbon dioxide is seen because the gas passes down the iridium tube where the temperature is cooler and where the equilibrium is shifted toward carbon dioxide. Iridium is a good catalyst for this conversion.

Figure 17 is an Arrhenius plot of the permeability constant for iridium to carbon. The data in Figure 17 were taken for two iridium tubes, one 0.015 inch thick on the end and the other 0.010 inch thick. Above 1900°C, the carbon diffusion was too fast for the carbon to react quantitatively with practical oxygen flows. Below about 1450°C, the data were uncertain. With the 0.010 inch sample the correction for the blank (taken without carbon on the end of the tube) was too large to get meaningful data below 1400°C. Between 1400° and 1900°C the activation energy obtained for the two samples agreed within experimental error. The pre-exponential factor in the Arrhenius equation differs for the two samples. This difference can be due to the uncertainty in estimating the area of carbon in contact with the iridium since some of the carbon painted on the end of the tube flaked off for both samples. The permeability constant for an average of the two samples is given by

$$P = 2.75 \times 10^{-4} e^{-56,400/RT} \text{ gm/cm sec} \quad .$$

There is no noticeable induction period before the diffused carbon appears as carbon dioxide at the omegatron; experimental conditions were such that an induction period greater than five minutes would have been detected.

The calculated diffusivity is greater than 10^{-7} cm^2 sec^{-1} and the calculated average solubility of carbon in iridium is less than 10^{-2} gm cm^{-3}.

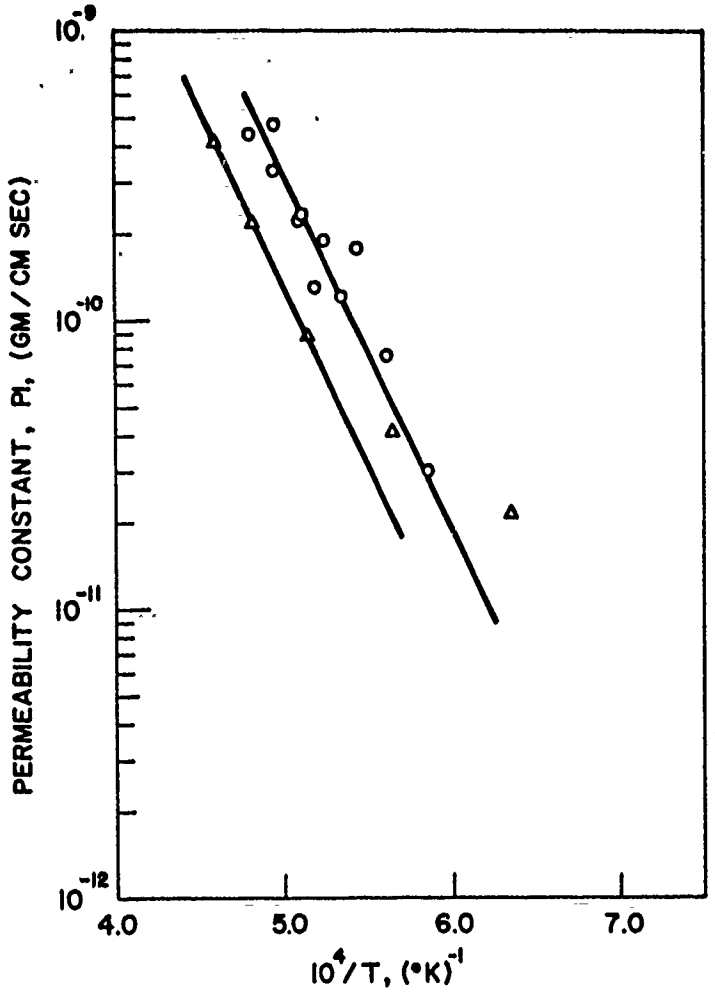

Figure 17. Temperature Dependence of Permeability Constant, Pl, of Iridium to Carbon
O 0.010 inch thick sample
Δ 0.015 inch thick sample

4. Permeability of Zirconia to Oxygen

Oxygen permeates the zirconia tube as a function of time after oxygen is admitted to the inside of the tube in a way nearly like that described by Equation 4. Figure 18 shows this time dependence at 1120°C. Figure 19 shows the steady state permeability as a function of oxygen pressure at 1275°C, the effect is very slight. The slope of the line demonstrates a one-fourth power dependence on the oxygen pressure.

Permeability versus temperature data at 25 and 50 torr oxygen pressure gave the same Arrhenius slope indicating that the pressure dependence of the permeability did not change with temperature.

When the carbon monoxide pressure on the vacuum side of the tube was varied from 2×10^{-3} torr to 5×10^{-1} torr, no change in permeation occurred, indicating zero order dependence.

The temperature dependence of the permeability constant of zirconia at 25 torr oxygen pressure is shown in Figure 20. The permeability constant is given by the expression

$$P\ell = 7.85 \times 10^{-2}\, e^{-55,700/RT} \text{ gm/cm sec}$$

from 1110° to 2060°C.

Diffusivities have been obtained by fitting the gas flow versus time curve at one-half steady state value with the theoretical curve as shown in Figure 18. The temperature dependence of the diffusivity is given in Figure 21. It can be represented by

$$D = 1.85 \times 10^{2}\, e^{-57,600/RT} \text{ cm}^2/\text{sec}$$

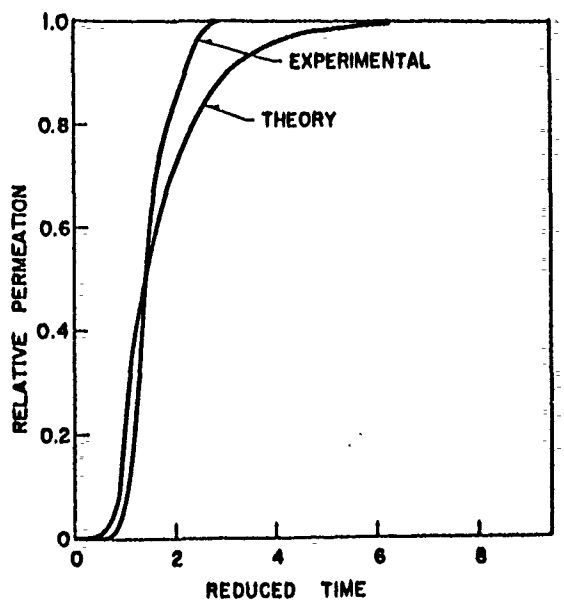

Figure 18. Time Dependence of Permeation of $Zr_{0.92}\, Ca_{0.08} O_{1.92}$ to Oxygen at 1120°C

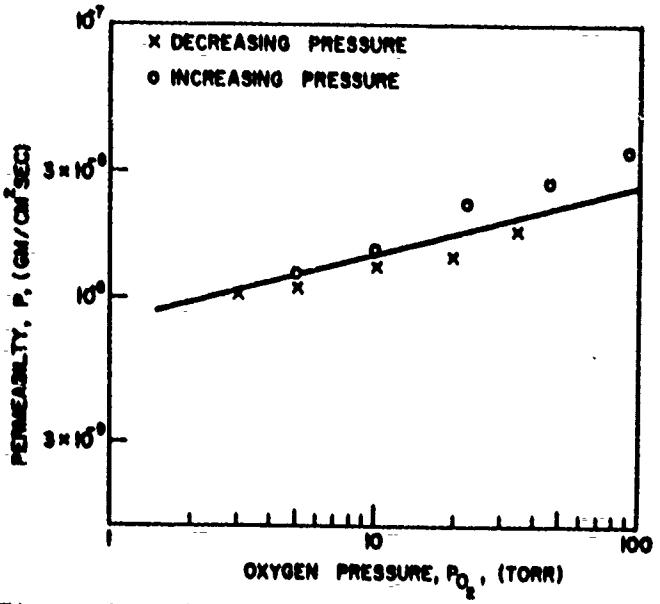

Figure 19. Pressure Dependence of Permeability, P, of $Zr_{0.92}Ca_{0.08}O_{1.92}$ to Oxygen

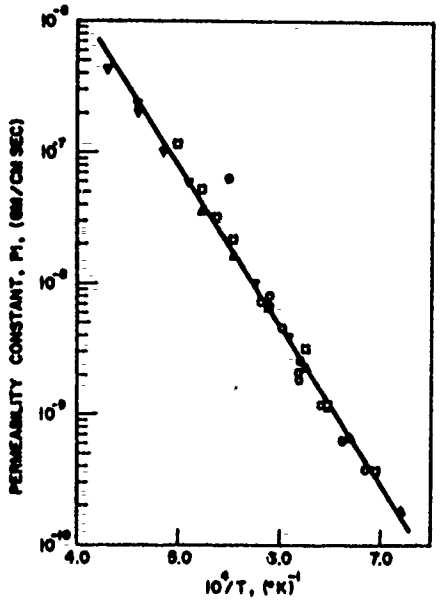

Figure 20. Temperature Dependence of Permeability Constant, $P \cdot l$, of $Zr_{0.92}Ca_{0.08}O_{1.92}$ to Oxygen

	Length of Hot Zone	Wall Thickness
O	2.5 cm	0.12 cm
□	1.3 "	0.12 "
Δ	1.3 "	0.074 "
∇	1.6 "	0.074 "

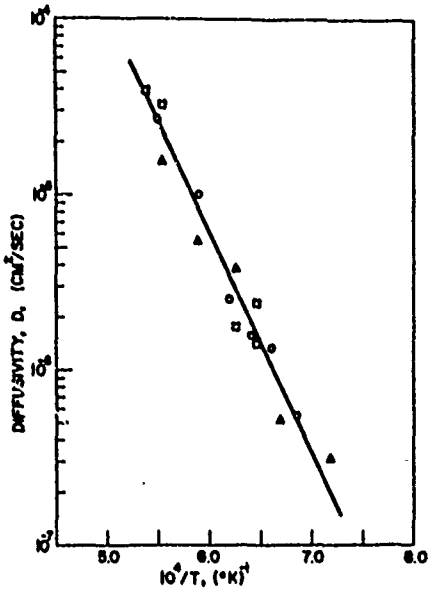

Figure 21. Temperature Dependence of Diffusivity, D, of $Zr_{0.92}Ca_{0.08}O_{1.92}$ to Oxygen

Length of Hot Zone	Wall Thickness
○ 2.5 cm	0.12 cm
□ 1.3 "	0.12 "
△ 1.3 "	0.074 "

No diffusivities could be obtained at the higher temperatures because the oxygen permeated through the sample at a rate that was too fast to be measured with the presently used experimental setup.

The data in Figures 20 and 21 include points taken with different areas of the tube in the hot zone and two different thicknesses. The thickness was changed by grinding the tube to half the wall thickness in the region of the hot zone. (from 0.12 to 0.074 cm). Both the permeability constant, $P \cdot l$, and the diffusivity, D, obtained from these data are independent of the area and thickness indicating that diffusion through the sample and not surface processes is governing the permeation.

5. Permeability of Hafnia to Oxygen

The results for hafnia are quite similar to those obtained for zirconia. Figure 22 gives the dependence of the permeability on oxygen pressure at 1430°C. A one-fourth power dependence of the permeability on pressure was observed. Figure 23 gives the temperature dependence of the permeability constant at 25 torr oxygen pressure and Figure 24 gives the temperature dependence of the diffusivity obtained from the time dependence of permeation.

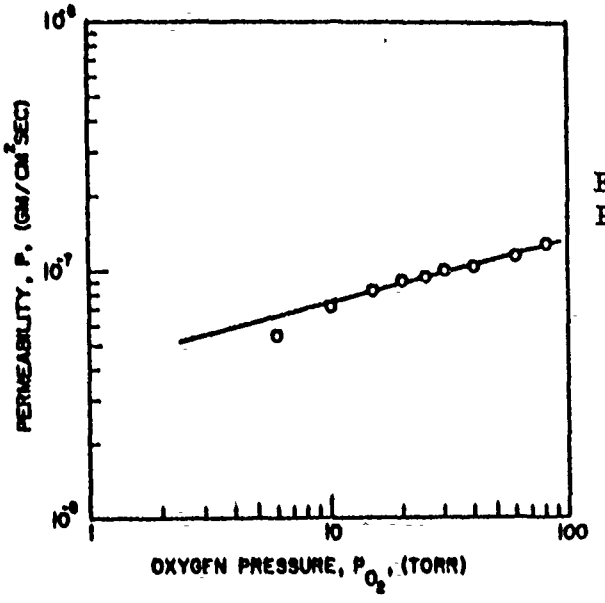

Figure 22. Pressure Dependence of Permeability, P, of $Hf_{0.86}Ca_{0.14}O_{1.86}$ to Oxygen at 1430°C

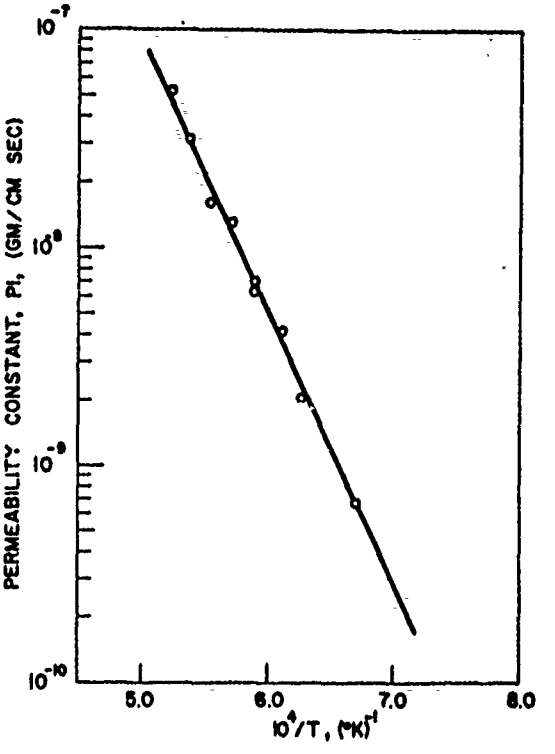

Figure 23. Temperature Dependence of Permeability Constant, $P \cdot l$, of $Hf_{0.86}Ca_{0.14}O_{1.86}$ to Oxygen

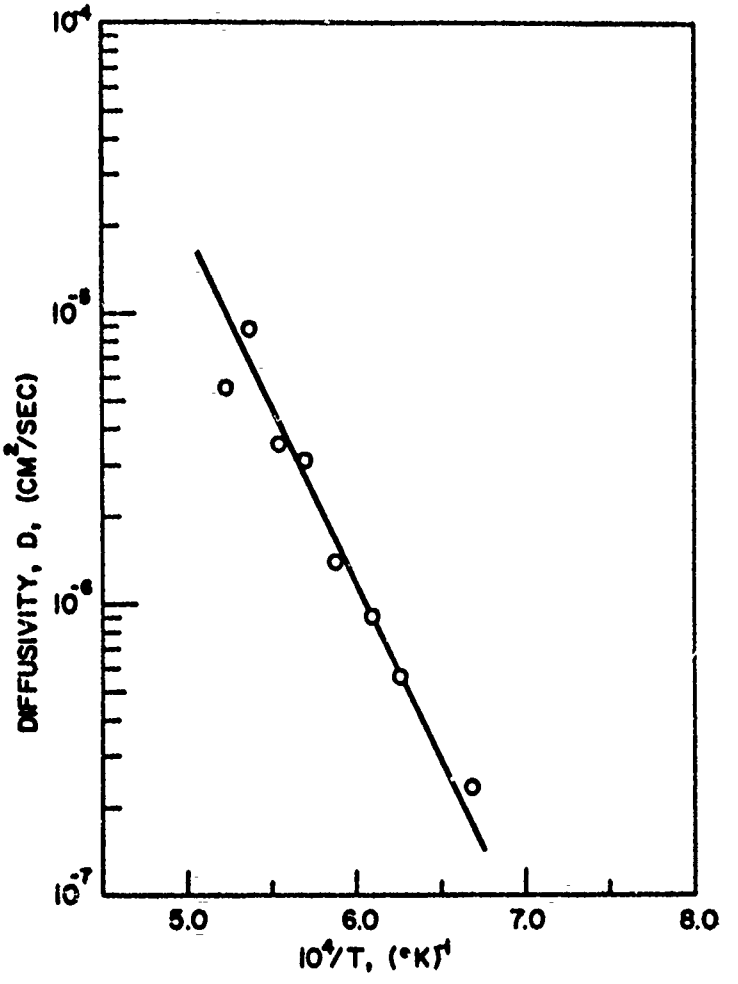

Figure 24. Temperature Dependence of Diffusivity, D, of $Hf_{0.86}Ca_{0.14}O_{1.86}$ to Oxygen

From 1220° to 1640°C, the permeability constant of a 0.074 cm thick hafnia sample to oxygen is given by

$$P\ell = 2.02 \times 10^{-1} e^{-58,500/RT} \text{ gm/cm sec} .$$

The diffusivity, over the same temperature range, is given by

$$D = 2.18 \times 10^{1} e^{-55,700/RT} \text{ cm}^2/\text{sec} .$$

6. Permeability of Thoria to Oxygen

The results on the permeability of thoria to oxygen differed from those of zirconia and hafnia. The time dependence of the permeation indicates a higher value of the diffusivity with a time constant too short for evaluation.

The oxygen pressure dependence was found to be a function of temperature. Values of the slopes of permeability versus pressure on a log plot were 0.33 at 1220°C, 0.23 at 1440°C, and 0.13 at 1640°C.

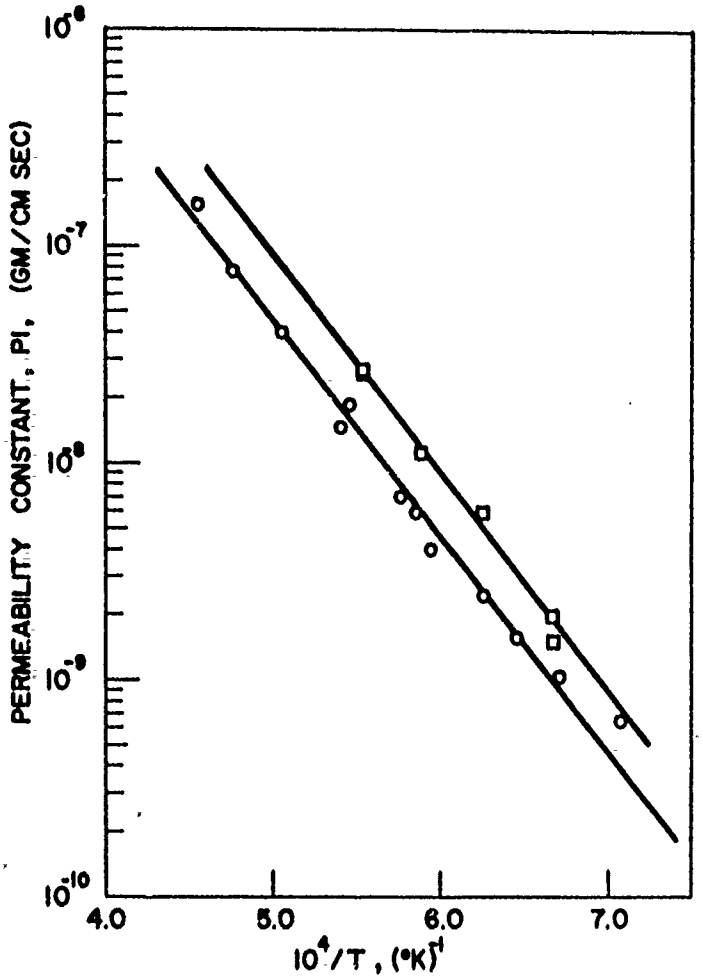

Figure 25. Temperature Dependence of the Permeability Constant, $P\ell$, of ThO_2 to Oxygen
□ Sample 1 O Sample 2

Figure 25 shows the temperature dependence of the permeability constant of thoria at 25 torr oxygen pressure on two independent samples. (High temperature data were taken at 50 torr pressure and corrected to 25 torr.) Sample 1 developed a leak after one series of runs and could not be used for any further studies. During three series of runs on Sample 2 using the alumina washers, the permeability decreased with each successive series. (A series of runs consisted of measuring the permeability of the sample at different temperatures in the range of 1100° to 1600°C with each temperature being higher than the previous one.) It was initially hypothesized that the decrease in permeability was due to grain growth in the thoria when it reached 1600°C; however, later examinations revealed the presence of alumina on the surface of the thoria as well as a decrease in the thickness of the spaces. When the sample was reheated later to 1800°C with tantalum washers, the permeability returned to the initial value shown in Figure 25, indicating that the alumina was causing the decrease in the permeability.

The permeability constant of Sample 2 is given by

$$P\ell = 4.68 \times 10^{-3}\, e^{-46,100/RT} \text{ gm/cm sec}$$

from 1140° to 1930°C. The thickness of the sample was 0.089 cm.

Discussion of Permeation through Oxides

The permeability of a membrane is given by

$$P = D \frac{\Delta C}{\ell} \quad .$$

It is useful to make the initial assumption that the concentration at one boundary is low with respect to the concentration at the other boundary so that $\Delta C = C$. This in fact is the assumption made in the calculation of the diffusivity from the time dependence of the permeation. In this case,

$$P\ell = DC \quad . \tag{7}$$

Equation 7 can be checked from the independent determination of the permeability and the diffusivity and from other measurements related to diffusion of oxygen reported in the literature. For this purpose, the concentration of diffusing species was converted to a fraction of sites occupied in order to get all the determinations in units of cm^2/sec. This is done by dividing the permeability times thickness by the density of oxygen in the normal lattice. The normal lattice sites are, of course, occupied by vacancies during vacancy diffusion. If interstitial diffusion is occurring, the additional premise is made that the number of interstitial sites equals the number of normal oxygen sites.

The effect of porosity is worth considering. If the pores do not pass oxygen freely, the true permeability is slightly larger than the measured permeability. Since some of the material on the ends of the pores will not contribute to the permeation, porosity will lead to a measured permeability that is smaller than the true permeability. If the holes do allow oxygen to pass through easily, then the true permeability will be smaller than that measured. Unless there are long channels, this effect will be small. As will be shown later the permeabilities obtained here give a smaller diffusion constant than other measurements indicating that there is no large error in this direction.

Figure 26 shows the diffusion constant (diffusivity multiplied by the concentration) versus temperature on an Arrhenius plot for zirconia. Line 1 was obtained from the permeability times the thickness as given in Figure 20. Lines 2, 6, and 7 were obtained from oxidation of zirconium. Lines 4 and 5 were obtained from oxidation of partially reduced zirconia. Line 3 was obtained from self-diffusion coefficients and electrical conductivity, both of which include a concentration term. Line 8 was obtained by multiplying the diffusivity as given in Figure 21 by the nominal 8 per cent oxygen vacancy concentration.

The reasons for the variation in the results shown in Figure 26 can be explored by examining the nature of the diffusing species in zirconia. Calcia doped zirconia has been shown to be an anion deficient oxide[34] which exhibits ionic rather than electronic conductivity at high temperatures.[29,35] For pure zirconia, the type of conductivity varies with oxygen pressure indicating the possibility of both n and p type conductance.[36] Both electronic and ionic conductance have been suggested for the "pure" material.[30,31,37] Undoubtedly,

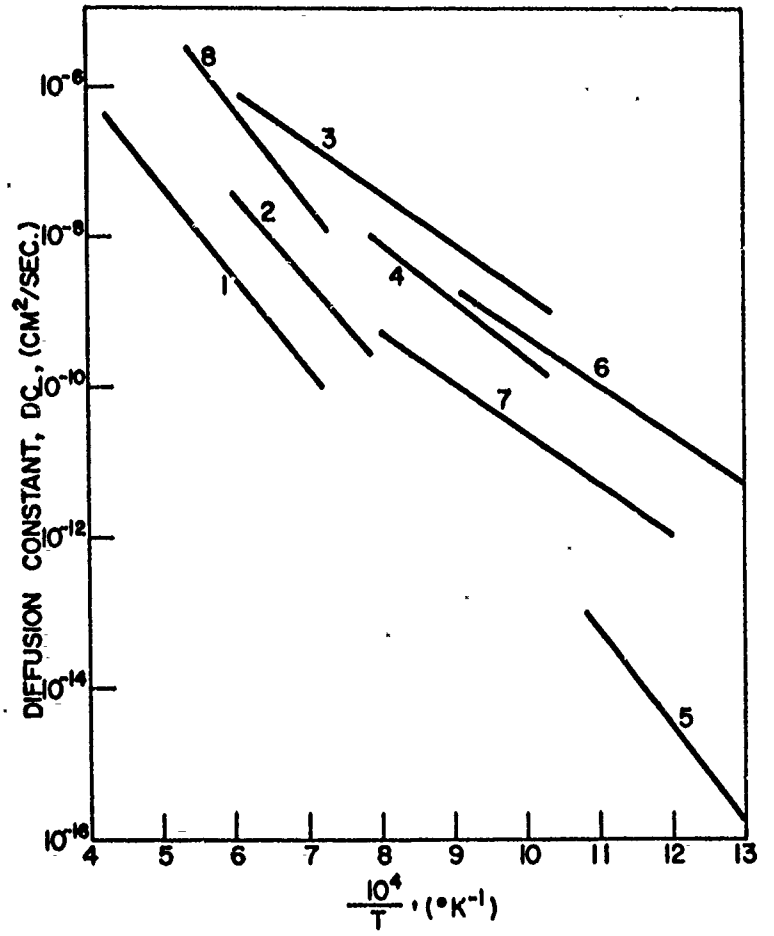

Figure 26. Diffusion Constants for Zirconia

1. Permeability of $Zr_{0.92}Ca_{0.08}O_{1.92}$ (this work).
2. Oxidation of a liquid zirconium tin alloy.[28]
3. Self-diffusion measurements with O^{18} plus electrical conductivity on $Zr_{0.85}Ca_{0.15}O_{1.85}$.[29]
4. Oxidation of $ZrO_{1.994}$ (following color change).[30]
5. Oxidation of $ZrO_{1.975}$ (weight uptake).[31]
6. Oxidation of zirconium.[32]
7. Oxidation of zirconium.[33]
8. From time dependence of permeation of $Zr_{0.92}Ca_{0.08}O_{1.92}$ and nominal vacancy concentration (this work).

impurities play an important role in these studies. Cation diffusion is many orders of magnitude slower than anion diffusion.[38] A grain boundary effect on the ionic conductivity was present below 1000 °C but absent above this temperature.[39]

The mechanism of oxygen diffusion through zirconia is tentatively discussed as follows:

The addition of calcia must depress the concentration of electrons, e^-, while increasing the oxygen vacancy concentration according to the following equilibria:

$$\text{Nil} \rightarrow \square_O^{++} + 2e^- + \tfrac{1}{2}O_2 \qquad (8)$$

$$CaO \rightarrow (Ca\square_{Zr})^{=} + \square_O^{++} + ZrO_2 \qquad (9)$$

where $\square_O^{++}$ is an oxygen ion vacancy and $(Ca\square_{Zr})^{=}$ is a calcium ion in a zirconium ion lattice site.

Apparently, the formation of electron holes, h^+, by the equilibrium

$$\tfrac{1}{2}O_2 + \square_O^{++} \rightarrow 2h^+ \qquad (10)$$

does not occur to a sufficient extent to contribute to the electrical conductivity.[29] However, the rate of oxidation of the metal (as well as for oxidation of partially reduced oxides or for transport of oxygen across a membrane) is governed by the slowest of the charge carriers.[40] Thus, the diffusion coefficient of calcia doped zirconia obtained by self-diffusion measurements and electrical conductivity measurements had the highest value of any other shown in Figure 26 both because of the high vacancy concentration and because the diffusion of the faster charge species is measured. The diffusion coefficient obtained by the permeability measurement is the lowest of the group because it is the only other calcia doped sample and, hence, the one in which the electron concentration is suppressed. The spread in the diffusion coefficients obtained by oxidation experiments could be explained by variations in impurity content.

The permeability of the calcia doped zirconia seems to be limited by the transport of electron holes. Equation 10 gives an equilibrium

$$[h^+] = K(P_{O_2})^{1/4}[\square_O^{++}]^{1/2} \quad . \qquad (11)$$

For the calcia doped material the concentration of oxygen vacancies is approximately equal to the calcium concentration and nearly independent of oxygen pressure. The permeability is given by

$$P = D_{(h^+)}\frac{[h^+]_1 - [h^+]_2}{\ell} \quad . \qquad (12)$$

It can be assumed that the electron hole concentration on the vacuum (or carbon monoxide) side of the membrane is extremely low so that by combining Equations 11 and 12 and equating oxygen vacancy and calcium concentrations, the following equation is obtained:

$$P\cdot\ell = D_{h^+} \cdot K(P_{O_2})^{1/4}[(Ca\square_{Zr})^{=}]^{1/2} \quad . \qquad (13)$$

This equation predicts a quarter power dependence of oxygen pressure and a zero order dependence on the carbon monoxide pressure; this agrees with the experimental data.

Equation 13 also shows why the diffusivity obtained by the time dependence of permeation did not give the same diffusion coefficient as that obtained from the permeability (lines 1 and 8 in Figure 26) when the oxygen ion vacancy was used.

From a comparison of the permeabilities and diffusivities, a concentration of imperfections (in this case, electron holes) of about 5×10^{-4} per lattice site was obtained nearly independent of temperature. If the foregoing analysis is correct, the heat of formation of these holes according to Equation 10 is close to zero.

The transport number of electrons in stabilized zirconia has been of some interest because of its use as a high temperature electrolyte. A value of $< 5 \times 10^{-3}$ for the transport number of electrons at 1100°C has been reported.[41] Comparing the diffusion constant obtained from the permeability measurements with the oxygen vacancy self-diffusion measurement[29] gives a transport number for electron holes of about 10^{-3} in stabilized zirconia.

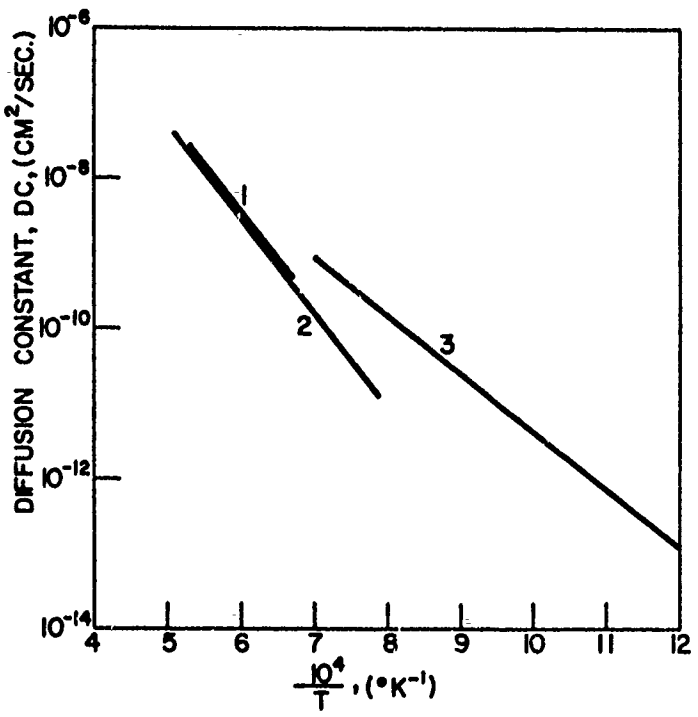

Figure 27. Diffusion Constants for Hafnia

1. This work.
2. Oxidation of hafnium tin alloy.[28]
3. Oxidation of hafnium.[42]

There are much less data available in the literature relating to oxygen diffusion in hafnia. Figure 27 is a plot of the diffusion constant for hafnia obtained from this work and from two studies on oxidation of the metal. It appears that the mechanism proposed for zirconia is also valid for hafnia.

No mechanism for diffusion can be given for thoria. The change in pressure dependence of the permeability with temperature suggests a change in mechanism over this temperature range. Although data for oxidation of the metal, self-diffusion coefficients for oxygen, and electrical conductance measurements are available in the literature, there appears to be too much variation between the different results to make meaningful comparisons. This can be seen in Figure 28.

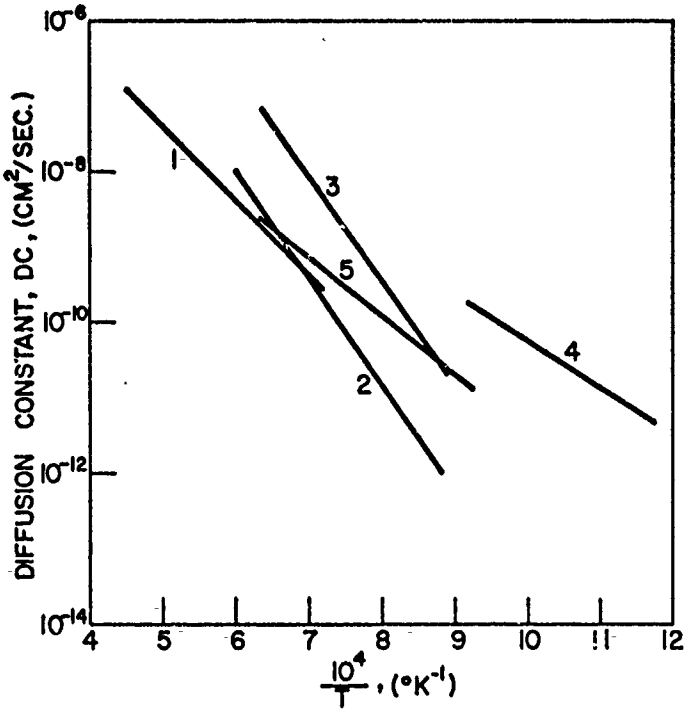

Figure 28. Diffusion Constants for Thoria

1. This work.
2. Self-diffusion coefficient.[43]
3. Oxidation of thorium.[44]
4. Oxidation thorium-tin alloy.[28]
5. Electrical conductivity.[45]

Summary

The permeability to oxygen of a number of prospective coating materials has been measured. The permeability of iridium to carbon has also been measured. These measurements have been made in the temperature region of 1100° to 2200°C. The dependence on oxygen pressure between 10 and 100 torr has also been studied. In all cases, a fractional order in pressure dependence has been observed.

The permeability constant for zirconia and hafnia has been interpreted as due to oxygen vacancies and electron holes moving through the crystal lattice. For thoria, both oxygen vacancies and interstitials may occur. Diffusion of oxygen in rhodium and carbon in iridium occurs due to interstitial solution in the metal lattice.

Except for the zirconia and hafnia which were lime stabilized, these results have been obtained on polycrystalline materials of the highest available purity. The data taken here as well as other information available in the literature appear to indicate that grain boundary diffusion is not contributing markedly to the permeability.

The effect of impurities on the permeability can be appreciable. Zirconia and hafnia must be stabilized to prevent fracturing on temperature cycling. Further impurities would have only a slight effect although the major stabilizing agent may be changed. Doping of thoria may be useful and further work in this area will be considered.

Figure 29 presents the temperature dependence of the permeability constant for the materials studied in this work. The diffusion constants of the three oxides have been obtained from these data and compared with data in the literature. A reasonable agreement is obtained. The permeability constant, $P \cdot \ell$, for these materials is given by the equation

$$P \cdot \ell = A\, e^{-E/RT} \quad . \quad . \qquad (14)$$

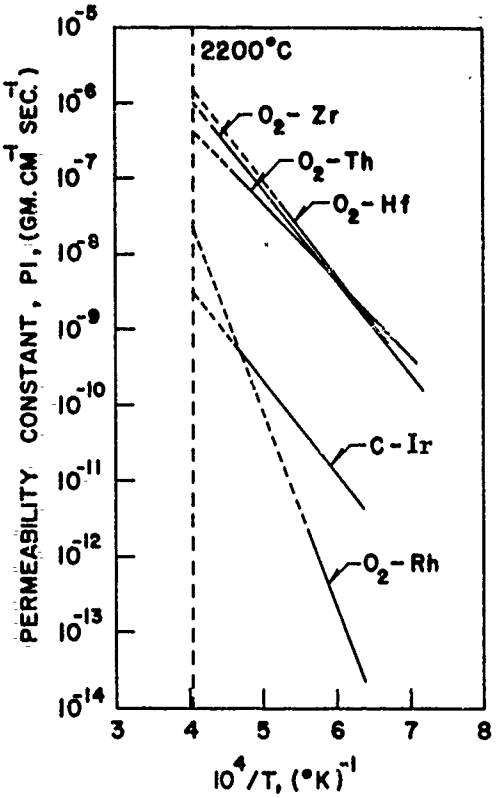

Figure 29. Permeability Constant, $P\ell$, versus Temperature of Materials Studied Here

Table 20 lists the values of A and E obtained here and the permeability constant extrapolated to 2200°C.

TABLE 20

PERMEABILITY CONSTANT, $P\ell$

Material	Diffusing Species	Oxygen Pressure (torr)	A (gm/cm sec)	E (kcal/mole)	$P\ell$ at 2200°C (gm/cm sec)
$Zr_{0.92}Ca_{0.08}O_{1.92}$	O	25	7.85×10^{-2}	55.7	1.0×10^{-6}
$Hf_{0.86}Ca_{0.14}O_{1.86}$	O	25	2.02×10^{-1}	58.5	1.5×10^{-6}
ThO_2	O	25	4.68×10^{-3}	46.1	4.2×10^{-7}
Rh	O	50	3.63×10^{2}	116.6	2.2×10^{-10}*
Ir	O	150	--	--	$< 3 \times 10^{-15}$
Ir	C	--	2.75×10^{-4}	56.4	3.1×10^{-9}

* Calculated at 1800°C since rhodium is molten at 2200°C.

Recommendations

On the basis of this work, the following recommendations can be made for the continuation of the diffusion studies:

1. Samples of thoria doped with trivalent and pentavalent impurities, such as alumina, yttria, or vanadia, would be useful in exploring the effect of impurities. This doping, by changing the vacancy or interstitial concentration, may decrease the permeability.

2. Zirconia and hafnia must be stabilized. If the electron holes are trapped by this stabilizing cation, the permeability will be effected. Calcia stabilized zirconia and hafnia have been studied and a yttria stabilized zirconia sample has been ordered to test this idea.

3. The permeability of beryllia to oxygen should also be determined. Although there is quite a bit of information available on diffusion in beryllia, it seems desirable to have actual permeabilities measured. This work is actually under way at present.

4. The permeabilities of at least some of the mixed oxides, such as $ThO_2 \cdot ZrO_2$, $SrO \cdot ZrO_2$, $BaO \cdot ZrO_2$, $3BeO \cdot 2ZrO_2$, $ZrO_2 \cdot SiO_2$, $CaO \cdot ZrO_2$, and $HfO_2 \cdot SiO_2$, should be investigated in the same way as has been done for the single oxides. Procurement of impervious tubes of some of these materials is being explored.

5. Carbon diffusion should be studied in the compounds HfC, ZrC, ThC, ThC_2, HfB_2, and ZrB_2, which have been selected as promising materials for intermediate layers of coatings. It has been shown in the discussion of oxygen diffusion in the oxides that the permeability is more closely related to the parabolic oxidation constant than to self-diffusion measurements. Since carbon is not a gaseous species whose permeation can be measured directly, it might be best to study carburization of metals to determine the diffusion properties of carbon in carbides. However, since carbon dissolves in these metals as well as reacting with them, the interpretation may be difficult.

6. Studies of diffusion of radioactive carbon by sectioning and counting techniques or by surface activity techniques are straightforward and the methods can be applied both to self-diffusion of carbon in the carbides and diffusion of carbon in the borides. The interpretation of the self-diffusion results must be considered with care. However, since the electrons are quite free in these materials, electronic conduction will not limit the rate. Also, the carbon atom is a small interstitial atom in a metal lattice and, hence, would be expected to be the diffusing species.

VIII. MECHANICAL COMPATABILITY OF IRIDIUM WITH GRAPHITE

TASK B1-2

Introduction

The mechanical (structural) compatability of a coating with a graphite substrate depends on numerous parameters. The thermal expansion properties of a coating and the substrate should be closely matched. Since thermal gradients may produce stresses even in systems with perfectly matched thermal expansion, the coating to graphite bond should be as strong as possible. The mechanical compatability will further depend upon the thickness and brittleness of the coating, its tensile and compressive strength, microstructure, porosity, and purity (including carbon content) of the coating. Furthermore, the lowest eutectic temperature in the carbon-coating materials system constitutes the upper temperature limit where the coating can provide oxidation protection for graphite.

From existing vapor pressure and thermodynamic data, iridium appeared particularly promising as a single layer coating. Measurements on bulk iridium can be used only for predicting a few of the parameters that determine the structural compatability (e.g., eutectic temperature, thermal expansion, thermal conductivity). In general, the properties of an iridium coating will be strongly dependent on the method by which the coating is applied. The selection of a coating method will depend on the desired coating thickness, since some methods (e.g., sputtering) are practical for very thin films only, whereas others (e.g., flame spraying) produce relatively thick coatings. From the standpoint of mechanical compatability, the thinnest coating capable of maintaining the required oxidation protection is desirable. If protection for an extended time period is needed, changes in the film properties occurring at the service temperature due to grain growth, annealing and/or carbon diffusion also need to be investigated. An exhaustive literature survey on the physical and chemical properties of iridium and the possible methods of iridium plating was reported in a Special Summary Report[1].

Thermal Expansion Measurements

To obtain maximum thermal shock resistance and to prevent cracking, the thermal expansion of the graphite substrate should closely match that of the coating. Furthermore, the substrate should exhibit a minimum degree of anisotropy. The thermal expansion of iridium, determined by Holborn[46] and coworkers, is listed in Table 21. These measurements date back to 1904, and since there is doubt concerning the purity of the iridium used, a redetermination was carried out on iridium wire of 99.95 per cent purity, using a high temperature X-ray camera. Excellent agreement with Holborn's results was obtained.

TABLE 21

COEFFICIENT OF THERMAL EXPANSION OF IRIDIUM AND OF GRAPHITE INCH/INCH °C x 10^6

Temperature	Iridium	Graphite A		Graphite B		Graphite C***
		With Grain	Against Grain	Against Grain	With Grain	Against Grain
40-100	6.5	3.4	4.3	5.4	4.2	5.0
100-200	6.9*	3.6	5.2	6.2	5.3	5.0
200-300	7.3*	4.0	5.6	6.4	5.7	5.5
300-400	7.6*	4.4	5.7	7.2	6.0	5.5
1000-1200	9.4	5.5	7.0	8.2	7.6	8.0
1200-1400	9.6	6.0	7.5	8.9	7.9	8.0
1400-1600	10.2	7.0	8.5	9.2	8.4	8.8
1600-1800	10.6	7.5	9.0	9.5	8.6	9.0
1800-2000	11.0**	8.0	9.5	10.1	9.0	9.2
2000-2200	---	8.5	10.5	10.2	9.3	9.5
2200-2400	---	9.0	10.5	10.6	9.6	10.0

* Interpolated
** Extrapolated
*** This material was very isotropic. The temperature dependence of the expansion coefficient was therefore measured only in one direction.

A search for a suitable graphite substrate showed that most commercial grades are either too anisotropic or have expansion coefficients too low for compatability with iridium as a coating material. Experimental graphite grades produced by Union Carbide Corporation, Carbon Products Division, were therefore used for the compatability studies. The thermal expansion coefficients of these experimental grades were determined with a high temperature dilatometer and are also listed in Table 21. The fine-grained and easily machinable graphite "A" was used only for exploratory experiments where isotropy and a close match of thermal expansion was not particularly important. Photomicrographs of graphites "B" and "C" which served as substrates for the coating and coating evaluation work are shown in Figures 30 and 31.

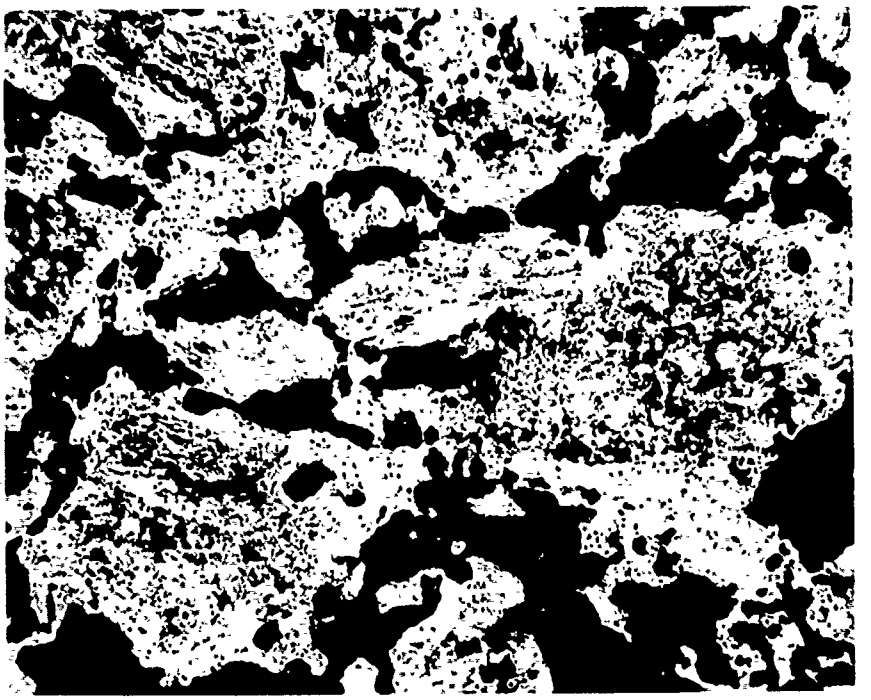

Figure 30. Photomicrograph of Graphite "B"
150 X Magnification

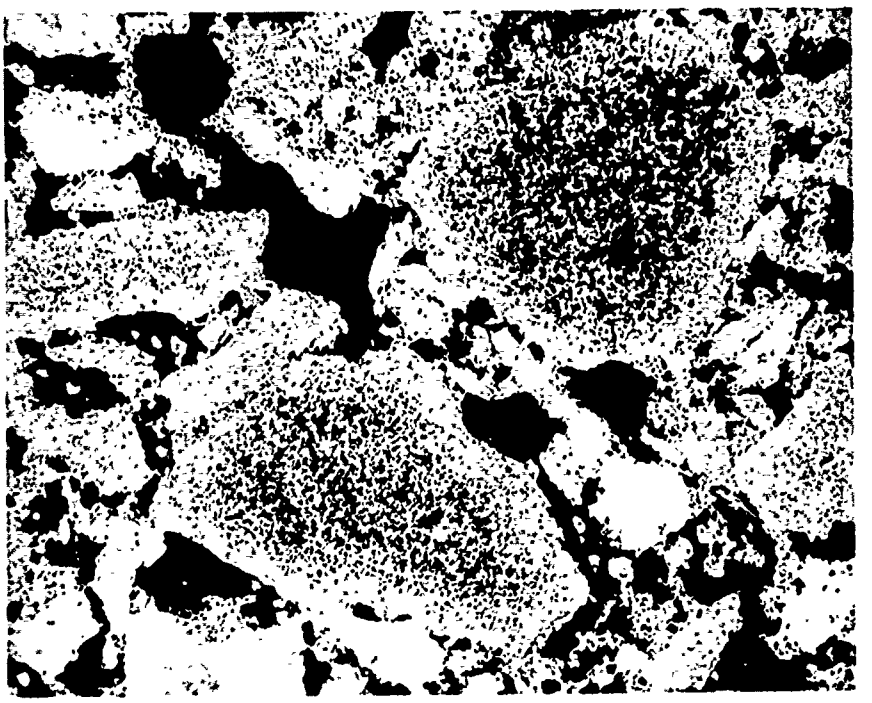

Figure 31. Photomicrograph of Graphite "C"
150 X Magnification

Investigation of the Carbon Iridium Bond and the Carbon-Iridium Eutectic Temperature

The objective of this phase of the program was to investigate possible high temperature reactions between carbon and iridium and to find means of obtaining a strong carbon-iridium bond. All iridium used in this work was obtained from Engelhard Industries, Baker Platinum Division. Each lot (sheet, foil, wire, and powder) was analyzed spectroscopically and found to be at least 99.7 per cent pure. The main impurities were rhodium and platinum, but traces of copper, lead, iron, magnesium, aluminum, nickel, and silicon were also detected. In preliminary experiments, flat sheets of iridium (1 cm^2 x 0.25 mm thick) were placed between two pieces of graphite (2.5 cm diameter x 1.3 cm high) and heated in argon for half-an-hour at 2600°, 2750°, and 3000°C respectively. These temperatures are higher than the melting point of pure iridium (2450°C). Only the pressure of the weight of the upper graphite section which was approximately 13 grams was present. The graphite pieces were strongly bonded together by this treatment. Iridium did not flow out but was retained by surface tension to an area roughly the size and shape of the iridium sheets used. The bonded specimens were cut in half along a plane normal to the joint and one-half was broken to obtain an estimate of the bond strength. Failure of all three specimens occurred in the bulk graphite (Carbon Products' type AGW) rather than at the carbon-iridium interface. The results of the break-test for the sample heated to 2750°C are shown in Figure 32.

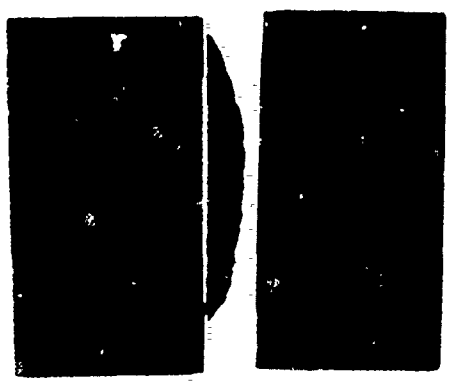

Figure 32. Break-Test on Graphite Bonded with Iridium at 2750°C

Half of each specimen was polished and examined with a microscope. The photomicrographs are shown in Figures 33, 34, and 35. Carbon is dissolved by molten iridium in proportionally larger amounts with increasing temperature and recrystallizes from the melt on cooling. The strength of the carbon-iridium bond is presumedly a direct result of this process of dissolution and reprecipitation of carbon.

Figure 33. Carbon-Iridium Bond Obtained by Heating to 2600°C, 185 X Magnification

Figure 34. Carbon-Iridium Bond Obtained by Heating to 2750°C, 185 X Magnification

Figure 35. Carbon-Iridium Bond Obtained by Heating to 3000°C, 185 X Magnification

The literature indicates that graphite is wet by molten metals only when a carbide is formed [47,48]. A search for a possible iridium carbide was therefore conducted, but none was found. For this investigation, a 0.25 mm diameter iridium wire was coated with colloidal graphite of spectroscopic purity, mounted in a high temperature X-ray camera. and heated to 1950 ± 10°C for sixty-six hours. Debye patterns obtained at 1300°, 1500°, 1900°, and 2100°C showed only the presence of iridium and graphite. The presence of even one per cent of iridium carbide on the surface of the iridium wire would have been detected. When an attempt was made to obtain a Debye pattern at 2200°C, the iridium wire melted, although the iridium-carbide eutectic temperature has been reported to be 2296 ± 16°C[49]. The eutectic temperature was therefore redetermined and found to be 2110 ± 25°C.

The determination of the eutectic temperature was carried out by embedding short pieces of iridium wire (0.25 mm diameter) and narrow strips of 0.04 mm thick iridium foil in carbon black contained in a graphite capsule. The carbon black had previously been purified by heating in a chlorine atmosphere to 2900°C. The capsules were heated in a graphite tube furna e to the desired temperature and held there for three hours. Temperatures were read through a sight tube with a L & N optical pyrometer which had been calibrated against an NBS calibrated standard. Visual inspection under a microscope showed no signs of melting on either foil or wire after heating to 2100°C. When

the temperature was increased 10 degrees (2110°C), the foil had melted whereas the wire showed only traces of melting at the ends. Finally, when heated to 2120°C, both the wire and the foil melted. The stated uncertainty of ±25°C takes into account possible errors in temperature readings (about ± 10°C) and also the inevitable temperature variations in a resistance furnace during a three hour bake (about ± 15°C).

Metallographic examination of the eutectic composition showed very little free carbon. Since there is reason to believe that the solubility of carbon in solid platinum group metals is very low[50], it is estimated that the eutectic concentration of carbon in iridium is less than 5 weight per cent. A quantitative determination of the carbon-iridium phase diagram has been deferred until the need for this information is sufficiently urgent to justify the effort. The experiments also provided a clue to the influence of the slow rate of carbon diffusion in iridium on the observed eutectic temperature. When hold times of only half-an-hour were used, the temperature had to be raised to 2150° for iridium to melt. The large discrepancy in the eutectic temperature as determined here and by Nadler and Kempter can be explained in part by the fact that these authors employed heating times of only five minutes.

Coating Experiments

The results of the above investigations indicate that a strongly adherent iridium coating should be obtainable by fusing iridium to a graphite substrate. In preliminary experiments, small ($^1/_2$ inch diameter by 1 inch long) graphite rods were tightly wrapped in thin (0.037 mm = 1.5 mil) iridium foil and heated by induction to 2200°C. Iridium fused to the substrate, but the melt had a tendency to run off and the coating was therefore not uniform. However, the adherence of iridium to graphite was again found to be excellent, since the bulk graphite rather than the carbon-iridium interface separated under mechanical stress.

When iridium was applied by a slurry dipping technique, very uniform and adherent coatings could be produced. Polished graphite specimens were dipped into a slurry made from xylene (8 weight per cent) and milled iridium powder having an average particle size of 2.3 microns, as measured with a Fisher subsieve sizer (0.5 to 15 microns). Xylene was then driven off by slow heating in argon to 400°C. After this treatment, the film of iridium powder was sufficiently adherent so that with reasonable care the specimens could be weighed and inspected without damage. The iridium uptake depended on the time the specimen was left in the slurry (about five to ten seconds). A single dipping operation produced a coating between 0.0005 and 0.0007 inch thick. The specimens were then placed in a graphite capsule and supported in such a manner that the coated portion had no contact with the capsule wall. The capsules were heated in a graphite tube furnace in an argon atmosphere to 1950°C and held there for one hour to outgas the graphite substrate. After one hour at 1950°C, the temperature was raised to either 2120° or to 2140°C for a hold time of one half hour.

Heating to 2120°C produced a very smooth, strongly adherent "sintered" coating. The strong adherence may well result from the formation of an eutectic melt at the iridium-graphite interface although the hold time at 2120°C was not long enough to cause the coating to fuse all the way through. One advantage of "sintered" coatings is that they may be built up to any desired thickness by repeating the dipping and heat treatment procedure.

Heating to 2140°C for half-an-hour or 2150°C for quarter-of-an-hour produced fused coatings with surfaces not quite so smooth as the "sintered" coatings. The maximum thickness of fused coatings is limited due to a tendency for the melt to run off. Metallographic inspection showed that the fused coatings contained recrystallized graphite that came out of solution when the iridium solidified. Since the graphite crystallites have a tendency to grow normal to the substrate surface, the coating can be very thin in some places. To evaluate these sintered coatings, oxidation and thermal shock tests were conducted. The first oxidation test was carried out on a specimen made from AGW graphite (5 inches long by $^3/_8$ inch diameter), coated three times with iridium over a length of 4 inches. The first coating was fused on by heating to 2140°C and the second and third were "sintered". The total thickness of the iridium coat was approximately 2 mils. The upper one inch of the specimen was mounted inside an induction coil and heated to 2050° ± 50°C for fifteen minutes in air; the lower end was cooled by a water spray. The specimen lost 0.048 grams during this test. Visual inspection showed that the coating had developed a few cracks on cooling, due to the large mismatch in thermal expansion of type AGW graphite and iridium. Therefore, another oxidation test was carried out on another specimen made from an experimental graphite grade with a higher coefficient of thermal expansion (Graphite B in Table 21). This specimen, 4 inches long by $^3/_8$ inch diameter, was coated with iridium over a length of approximately 3 inches to an average total coating thickness of 2.4 mils. Total weight of iridium on the sample was 3.41 grams. The upper section of the specimen (approximately 1.2 inches) was again heated in air to 2050° ± 50°C for a period of one hour while the uncoated lower end was cooled by a spray of water. Total weight loss during the oxidation test was 0.41 gram. The same specimen was subsequently tested for thermal shock resistance by repeated cycling ten times in air between 550°C (below red heat) and 2000°C. Each cycle consisted of a one minute heating period, a one minute hold at 2000°C, and a cooling period of forty-five seconds. The specimen survived without cracks or other damage to the coating and the weight loss during the thermal shock test was 0.04 gram. Figures 36 and 37 show the specimen before and after the tests. The total weight loss due to the oxidation and thermal shock tests was 0.45 grams. If all the weight loss is due to evaporation of iridium, this should have resulted in observable dimensional changes due to a decrease in thickness of the iridium coating, but no such change could be measured. The specimen was therefore cut in half along the longitudinal axis and it was found that some graphite underneath the coating had been eroded by oxidation. An approximate calculation of the volume of eroded graphite indicated that about 80 per cent of the weight change was due to oxidation of the graphite substrate.

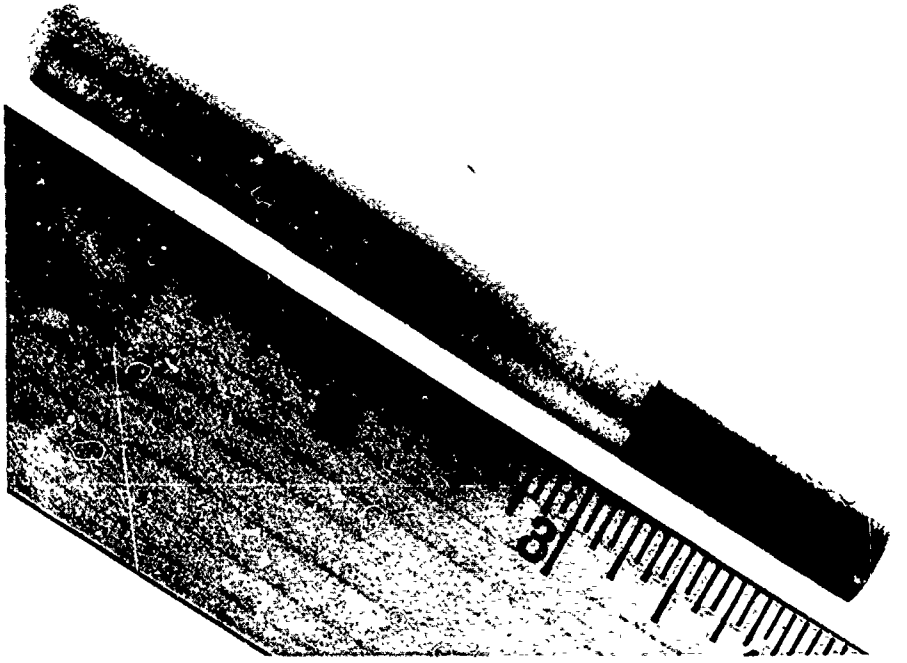

Figure 36. Iridium Coated Test Specimen

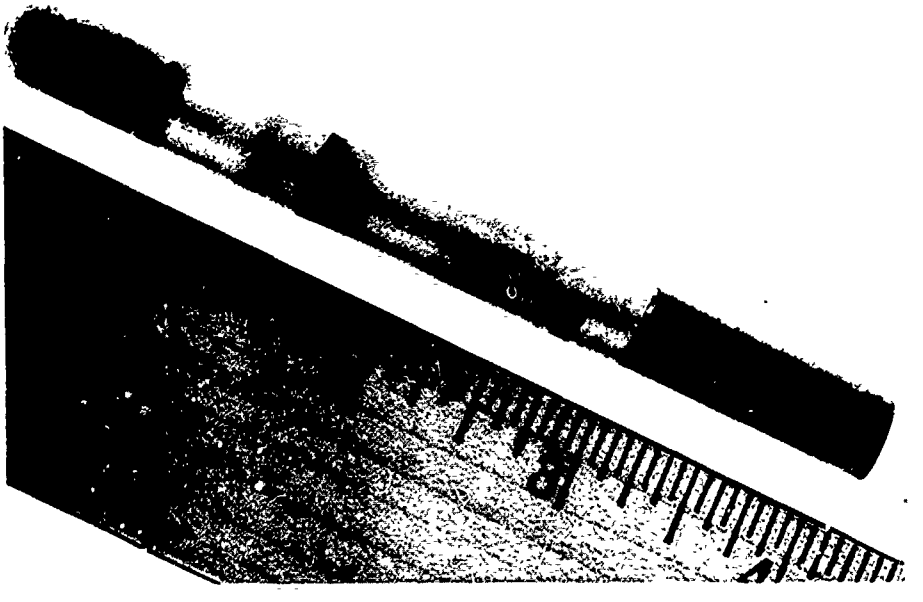

Figure 37. Iridium Coated Test Specimen After Oxidation and Thermal Shock Tests

Subsequent metallographic examinations of the sintered iridium coatings revealed that the coatings contained both pores and pinholes. Typical defects are shown in Figures 38 and 39.

Figure 38. Pores in a Sintered Iridium Coating, Coating Thickness 0.002 inch.

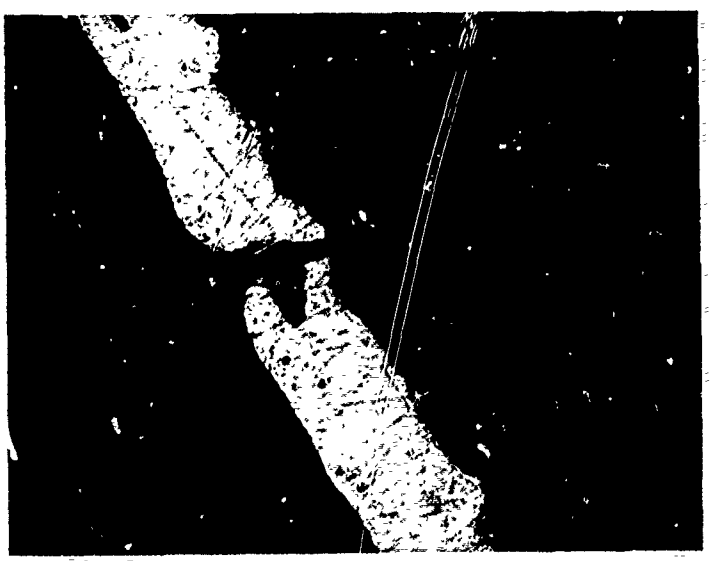

Figure 39. Pinhole in a Sintered Iridium Coating, Coating Thickness 0.002 inch.

Variations in the coating [illegible] t particle size distribution was tried, but did not [illegible] osity. Vacuum sintering had an adverse effect, [illegible] ack and peel.

Foil-Clad Iridium Coatings

The sintered iridium coatings did not present any mechanical compatibility problems. The graphite-to-iridium bond was strong and the coatings survived repeated thermal cycling to 2000° C without damage. However, because of the porous nature of these coatings, it was felt that an investigation of the mechanical compatibility of dense iridium coatings with graphite should be carried out. Since at the time no satisfactory method of applying a dense iridium coating to graphite had been determined, a cladding procedure was employed.

The thinnest (0.0015 inch) commercially available (Engelhard Industries, Baker Platinum Division) iridium foil was used. As received, the foil was very brittle. It was therefore annealed by heating to 1500° C and quenching in water. Two turns of foil were then tightly wrapped around the central 3 inches of a rod ($\frac{1}{2}$ inch diameter by 6 inches long) made from graphite "C". The foil was secured with molybdenum wire since iridium wire was found to be too brittle for this purpose. The assembly was then heated in an argon atmosphere to 1700° C for half-an-hour---high enough to cause sufficient sintering of the iridium foil to keep it in place, but low enough to prevent reaction between iridium and molybdenum, which occurs extensively at 1750° to 1800° C. The molybdenum wire was then removed and the two turns of iridium foil further self-bonded by sintering at 2100° C in argon for half-an-hour to one hour.

Repeated efforts to obtain good bonding between the foil and the graphite substrate were unsuccessful. There was no bonding unless a liquid interface was formed; yet when the temperature was raised high enough to form the eutectic melt, the melting process could not be controlled. The problem was finally solved by removing the iridium cylinder from the substrate and force-fitting it onto another graphite rod which had previously been coated with a one mil coat of sintered iridium. The diameter of the second substrate was 0.0006 inch larger than that of the first and the sintered iridium surface had been mirror finished with 4/0 polishing paper. The entire assembly was then coated three additional times by slurry dipping and sintering at 2120° C, thus increasing the coating thickness (including the two layers of foil) between 0.005 and 0.006 inch. Since there was a mismatch of approximately 20 per cent in the thermal expansions of graphite "C" and of iridium (see Table 1), circular cracks formed in the sintered coating at both ends of the foil cover. Although these cracks could be readily filled by redipping or by painting with iridium slurry, they always reappeared on sintering. The previous coatings (consisting solely of sintered iridium powder) had never shown any tendency to crack, possibly because the CTE of sintered iridium may be lower than that of the solid metal. A new graphite grade with a thermal expansion coefficient of approximately 7×10^{-6} inch/inch/° C (at room temperature) will be required

to minimize the thermal stress problem.

The foil-cladding method is a complex procedure and is limited to small substrate sizes because iridium foil is available in a maximum size of 3 inches x 6 inches only. Alternate methods of applying a dense iridium coating were therefore investigated.

Electrodeposition of Iridium

A cursory investigation of electroplating processes as a means of applying a dense adherent coating of iridium to graphite was carried out. Based on previous work by Withers and Ritt[51] a molten sodium cyanide-potassium cyanide electrolyte was used. Withers and Ritt electrodeposited iridium on metals which had previously been plated with nickel and/or gold. The present work shows that dense iridium deposits can be plated directly on graphite.

The apparatus used in this investigation consisted of an electric furnace (made from Hevi-Duty type 3708 SP heating units and Johns-Manville JM-2000 firebrick) 3 inches ID x 8 inches deep, a quartz envelope 4.0 cm ID x 30 cm deep, and a Morganite fused alumina salt container 3.8 cm ID x 16.5 cm deep. The anode was a semi-cylindrical sheet of 0.025 cm iridium 14.0 cm long and 1.2 cm wide; the cathodes were 0.25 inch rods of copper, molybdenum, or tantalum or 0.5 inch rods of polished ATJ graphite. The system was closed with a water cooled Teflon stopper (which served both as a cap and a cathode lead bearing) and flushed with 5 CFH of argon. While running, the cathode was rotated at ~60 RPM (see Figure 40).

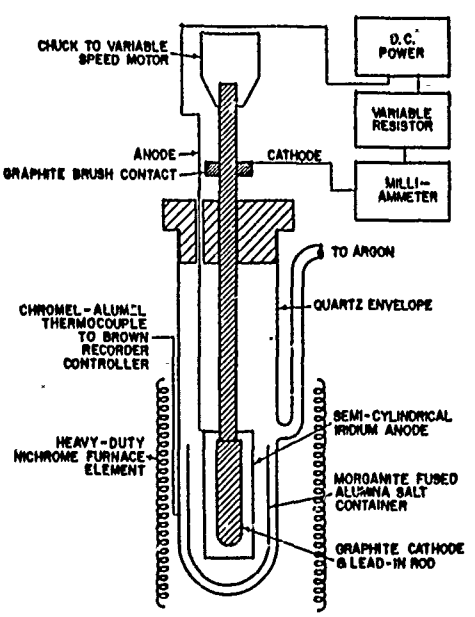

Figure 40. Cell Arrangement for Electroplating Iridium

The bath temperature was controlled and monitored with a Brown recorder-controller using a chromel-alumel thermocouple. The power supply for plating was a 1.5 volt battery. The current could be adjusted with a 0 to 10 ohm potentiometer and was measured with a triplet milliammeter.

The electrolyte consisted of 70 ^{w}/o sodium cyanide and 30 ^{w}/o potassium cyanide in which an iridium complex was formed by the passage of alternating current (10 ma/cm^2) between two iridium electrodes for a time sufficient to bring the iridium concentration to ~6 gms/liter.

The cell was run at ~600°C at an average current density of 10 ma/cm^2. The cathode efficiency was less than 50 per cent based on the trivalent iridium cation, probably due to the relatively large ratio of the anode-to-cathode area in these exploratory experiments.

Several graphite cylinders 0.5 inch diameter x 4 inches long were plated with 1 to 4 mils of iridium. The coatings were uniform and continuous. Metallographic examinations revealed the columnar nature of the deposit as shown in Figure 41 which depicts a 4 mil iridium plate, a. c. electroetched in 0.2 N HCl for three hours at ~0.3 amps/cm^2.

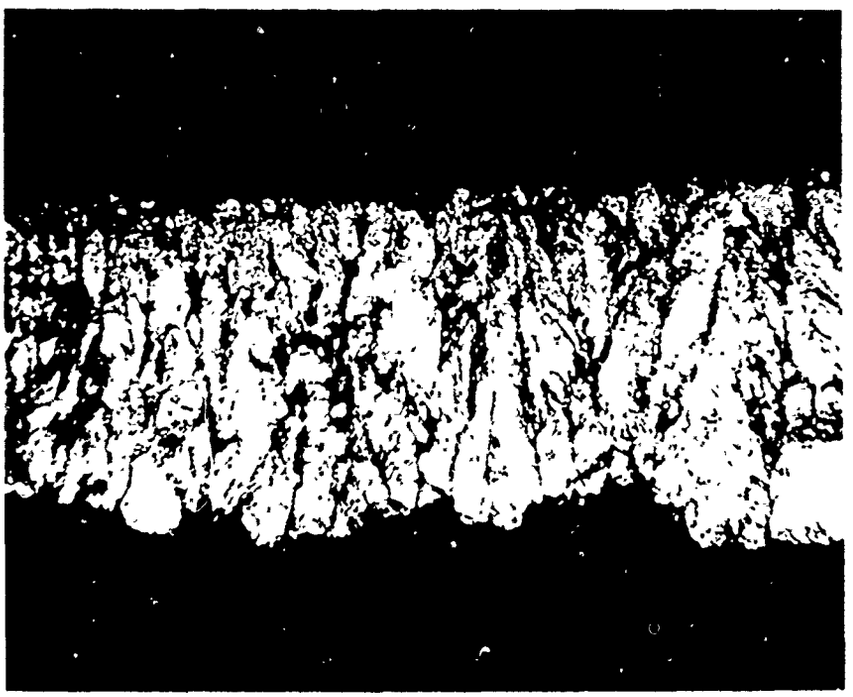

Figure 41. 4 Mil Iridium Plate, 500X Magnification

The major problem in electroplating a graphite substrate is salt penetration. The graphite absorbs ~10 per cent salt by volume which on heating will vaporize and rupture the coatings.

One sample having a 1.5 mil coating was drilled ($^1/_4$ inch diameter) axially from the uncoated end and heated in vacuum in an attempt to remove the salts without disrupting the coating. A portion of the side wall of the sample was then heated with a gas-oxygen torch to 2100 ±50°C for one hour, resulting in a weight loss of 0.185 gms. This test shows that the 1.5 mil electroplate offered considerable protection.

Electrodeposits of iridium were also obtained on specimens which had previously been coated with iridium by the slurry-dip and sintering method previously described. Salt penetration was less severe than when unprotected graphite was used as substrate; however, some salt did penetrate the pores of the sintered coating, causing disruptive effects when the specimens were subsequently heated to 2000°C.

Vapor Deposition of Iridium

The vapor deposition of iridium has previously received little attention. Reviews of vapor plating methods mention the deposition of iridium via decomposition of the iridium carbonylhalides, $IrCl_2(CO)_2$ or $IrCl(CO)_3$ [52, 53]. The original paper by Reerink [54] is concerned with the plating of platinum and states that iridium cannot be deposited by this method. However, a later patent granted to the same author [55] does include iridium in its claims. Hieber and coworkers [56] prepared the iridium carbonylhalides, but their method is very complex and the yields are extremely low.

A cursory investigation of the vapor deposition of iridium by the decomposition of $IrCl_3$ was therefore conducted. The published investigations of the iridium-chlorine system are old and of questionable reliability, and there are no kinetic data on either the formation or decomposition of $IrCl_3$. According to the literature, [57, 58] $IrCl_3$ is formed at 650°C from the elements. At a chlorine pressure of one atmosphere, $IrCl_3$ is reported to decompose to $IrCl_2$ at 772°C and to IrCl at 780°C. Finally, at 800°C, IrCl decomposes into the elements. However, according to recent work at General Atomic, General Dynamics[59], $IrCl_2$ and IrCl have been reported to be nonexistent.

In the coating experiments, a stream of Cl_2 saturated with $IrCl_2$ was passed over a graphite specimen which was heated by induction and previously coated with iridium by the slurry dip method. With the specimen at 850°C, a small amount of iridium was deposited; but the deposition was slow, nonuniform, and the iridium deposits did not adhere well. Most of the $IrCl_3$ rather than decomposing, condensed in the cooler portions of the apparatus beyond the decomposition zone. In an effort to increase the rate of decomposition, the substrate temperature was raised in separate experiments to 900°, 1000° 1200°, 1400°, and 1800°C respectively. There was no iridium deposition in the

900° and 1000°C runs; whereas, at the higher temperatures part of the original iridium coating on the specimen was removed. However, during the 1800°C run, a very dense and uniform iridium coating was deposited on the walls of the quartz tube. Thus, an iridium coating should indeed be obtainable by this method; but further work has been discontinued since it was felt that the development of a coating method utilizing the $IrCl_3$ would require an investigation of the vapor pressure and the kinetics of formation and decomposition of this compound, a study which is beyond the scope of this program.

The vapor deposition of iridium via the various iridium carbonyl compounds is at present under investigation and appears very promising. No vapor pressure or thermodynamic data are available for tetrairidium dodecacarbonyl, $Ir_4(CO)_{12}$. Hieber[60] who first reported the preparation treated anhydrous $IrCl_3$ with CO at 350 atmosphere. According to Hieber $Ir_4(CO)_{12}$ can be purified by sublimation in carbon monoxide at 210°C in a copper lined autoclave at 140°C. The copper serves as the halogen acceptor, forming CuCOCl during the reaction. Anhydrous $IrCl_3$ is prepared either by drying commercially available $IrCl_3 \cdot H_2O$ in chlorine at 300°C or by treating iridium metal with Cl_2 at 650° to 700°C. The latter method was employed for this investigation, using ball milled iridium scrap left over from previous work. The extent of conversion to the chloride was followed by measuring the weight gain. The starting material used for the following reactions contained at least 98 per cent $IrCl_3$.

In the first synthesis attempt, 10 gms of $IrCl_3$ were mixed with shredded quartz wool (to prevent caking) and heated in a copper-lined autoclave (volume 100 cc) to 140°C. The CO pressure at 140°C was 5000 psi. After several days, the pressure was unchanged, indicating that little or no reaction had occurred. The autoclave temperature was raised in 15° increment to 185°C at which time the initial pressure of 6000 psi began to drop slowly. After three weeks at 185°C, the pressure remained steady at approximately 5000 psi. Since the volume of CO contained outside the autoclave in connectors and leads was unknown, the theoretical pressure drop assuming complete reaction could not be calculated. The reaction was terminated at this point and the weight gain was found to be 4.62 gms. This value is to be compared with a theoretical weight gain of 5.65 grams including the weight gain due to formation of CuCOCl. Sublimation of the reaction products in a stream of CO at 210°C yieldedtwo different iridium compounds: cubic yellow crystals of $Ir_4(CO)_{12}$ and a small quantitiy of a far more volatile dark purple crystalline iridium carbonyl or chlorocarbonyl. A chemical analysis of this purple substance has not yet been obtained, but it is likely an intermediate product in the formation of $Ir_4(CO)_{12}$. None of the purple material was obtained when the formation of $Ir_4(CO)_{12}$ was carried to completion in four days at 225°C and 6500 psi CO pressure. In a third experiment, $IrCl_3$ was treated for three days at 210°C and 7000 psi CO pressure. The weight gain again indicated incomplete reaction, and the reaction product contained some of the purple iridium carbonyl compound.

Yellow iridium carbonyl $Ir_4(CO)_{12}$ was found to decompose thermally at 220°C at a carbon monoxide pressure of one atmosphere, and at about 170°C in vacuo. Even at 220°C, the vapor pressure of $Ir_4(CO)_{12}$ is so low that the substance is not particularly suitable for vapor plating. However, vapor deposition of iridium was successfully achieved using the more volatile purple iridium carbonyl compound. The apparatus used is shown in Figure 42. The carbonyl was placed on a sintered quartz disk in a vertical quartz tube and heated to sublimation temperature (175° to 210°C, depending on CO pressure) in a tube furnace, while the graphite substrate immediately above the tube furnace was heated by induction to approximately 500°C. For deposition at atmospheric pressure, previously dried CO was fed through the bottom end of the tube. For deposition of iridium at reduced pressures, the CO stream was restricted by a very fine capillary, and the pressure in the reaction tube was maintained below one mm Hg with a two-stage mechanical pump. In the exploratory experiments carried out so far, deposition at reduced pressure appeared to give denser and better adherent coatings; whereas deposition at atmospheric pressure produced a more uniform coating thickness. Further variables, such as the geometry and the temperature of the graphite substrate, CO flow rate, and optimum pressure are presently under investigation.

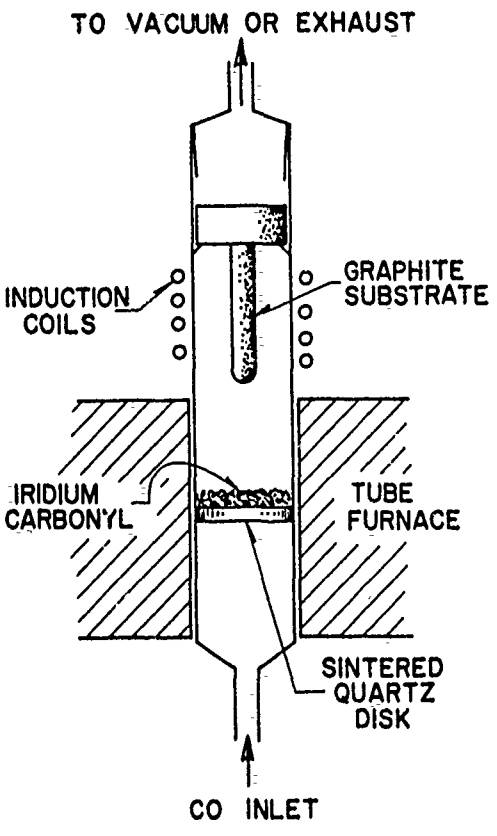

Figure 42. Apparatus for Iridium Vapor Plating

Since the purple carbonyl compound used in the above experiments may well be an intermediate in the reaction which terminates in the formation of $Ir_4(CO)_{12}$, synthesis to obtain large quantities is difficult. Experiments were therefore conducted to convert the more easily obtainable $Ir_4(CO)_{12}$ to a more volatile class of compounds, the iridiumchlorocarbonyls, $Ir(CO)_2Cl_2$ and $Ir(CO)_3Cl$. These compounds have been previously prepared by Hieber[56] by passing CO over $IrCl_3 \cdot H_2O$ at 150°C, but the yields were very low (under 16 per cent) in part due to spontaneous decomposition in the presence of water vapor.

In our own experiments, a previously dried mixture of 80 per cent CO and 20 per cent Cl_2 was passed over $Ir_4(CO)_{12}$. At 250°C, iridiumcarbonyl was quantitatively converted in a slow reaction to a canary yellow, needle-crystalline substance which condensed in the cooler section of the of the reaction tube. No chemical analysis has yet been obtained but the material exhibits all the properties of Hieber's $Ir(CO)_2Cl_2$, including the instability to water vapor. It can be sublimed in a CO atmosphere with only minor thermal decomposition at temperatures between 250° and 270°C, and it has been used successfully for iridium vapor deposition in the same apparatus as described above. CO at one atmosphere pressure was used as a carrier gas and the sublimation temperature was 260°C.

IX. REACTIONS OF IRIDIUM AND RHODIUM WITH BARRIER MATERIALS

One multilayer approach to the formulation of protective coatings for graphite involves iridium and rhodium as the external coating separated from the substrate graphite by an intermediate layer of some refractory material which is chemically stable both with respect to carbon and the external layer. An initial consideration for the intermediate layer materials has been directed to the carbides of hafnium, zirconium, and thorium, and the diborides of hafnium and zirconium due to their favorable high temperature physical and chemical properties. A lack of pertinent data on the reactions of the platinum metals with the carbides and diborides has prompted this investigation.

The specific reactions studied were:

Ir + HfC	→	Products	(1)
Ir + ZrC	→	"	(2)
Ir + ThC_2	→	"	(3)
Rh + HfC	→	"	(4)
Rh + ZrC	→	"	(5)
Rh+ ThC_2	→	"	(6)
Ir + ZrB_2	→	"	(7)
Ir + HfB_2	→	'	(8)
Rh + ZrB_2	→	"	(9)
Rh + HfB+	→	"	(10)

Experimental

The rhodium and iridium powders were supplied by the Baker Platinum Division of Engelhard Industries. Elemental spectrographic analyses of the iridium revealed minor impurities of rhodium and platinum along with traces of copper, lead, iron, magnesium, aluminum, nickel, and silicon. The purity of the iridium powder was stated to be 99.8 per cent and our analyses supported this specification.

The carbides and borides of hafnium, zirconium, and thorium were supplied by Atomergic Chemetals Company in powder form. The results of chemical analyses are given in Table 22. The X-ray diffraction patterns of these materials obtained from the Analytical Service Group revealed a minor unidentifiable impurity in the zirconium diboride and minor amounts of hafnium carbide in the hafnium diborides.

The induction heating apparatus used for conducting this investigation is shown in Figure 43. At the left of the photograph is a vacuum furnace consisting of a high frequency induction heated crucible assembly, a quartz envelope, and an optical window. The latter was used for monitoring the temperature with an optical pyrometer. The susceptor assembly consisted of a 1.25 inch O.D. x 1-inch I.D. x 2 inches high ATJ graphite crucible

TABLE 22

CHEMICAL ANALYSES OF BORIDES AND CARBIDES

	ZrB_2		ZrC		HfB_2		HfC	
Element	Theoretical	Found	Theoretical	Found	Theoretical	Found	Theoretical	Found
Zr	80.9	79.21	88.4	86.57				
Hf					89.2	88.86	93.7	93.66
C		1.04	11.6	11.30		0.36	6.3	6.04
B	19.1	18.22		0.45	10.8	10.24		
N		0.21		0.58				
O		1.16		0.18		0.66		0.53
H		0.10		0.17		0.07		0.09
Total		99.94%		99.25%		100.19%		100.32%

completely enclosed by 0.25-inch graphite felt, grade WDF, the top of which contains a 0.2-inch diameter sight hole for making the temperature readings.

The differential thermal analysis apparatus is shown in Figure 44. The ZT graphite sample and reference crucibles (1) are supported by the platinum-platinum 10 per cent rhodium differential thermocouple. The couple assembly (2) is then placed in a quartz envelope (3) which is in turn placed in a Sentry Model "VH" tube furnace, and (4) evacuated. The system is then filled with argon and purged at the rate of 30 cc/min. The temperature is increased uniformly (~ 300°C per hour) by means of a motor driven stepless transformer. The output from the differential thermocouple is fed to a Leeds and Northrup microvolt amplifier (8) and recorded on a Leeds and Northrup adjustable range, adjustable zero, recorder (9). A potentiometer (10) is used to monitor the sample temperature.

The reactions of iridium and rhodium with the intermediate layer materials were conducted in ZT graphite capsules 0.25-inch I.D. x 0.37-in O.D. x 0.37-inch high, either in vacuum or at reduced pressures of He. The capsules containing the reactants were heated by electrical induction and held at a constant temperature.

In a typical experiment, 0.435-gram of powdered iridium (2.25 mmoles) was thoroughly mixed with 0.145-gram of powdered hafnium carbide (0.76 mmoles), placed in the graphite reaction capsule and weighed. The loaded capsule was inserted into the furnace and the entire system evacuated to less than 1 mm Hg pressure. The furnace was heated to 2050°C and held for thirty minutes, after which the power supply was turned off and an atmosphere of helium admitted for rapid cooling. The graphite reaction capsule was removed and its weight recorded, after which the sample was crushed and submitted for X-ray analysis. In some cases,

ILLUSTRATIONS (Cont'd)

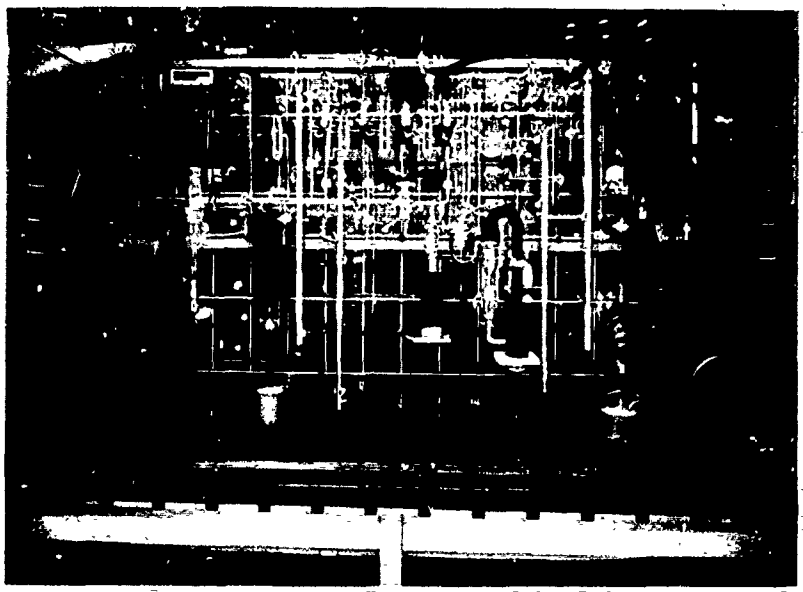

Figure 43. Induction Heated Vacuum Furnace, Gas Collection, and Toepler Systems

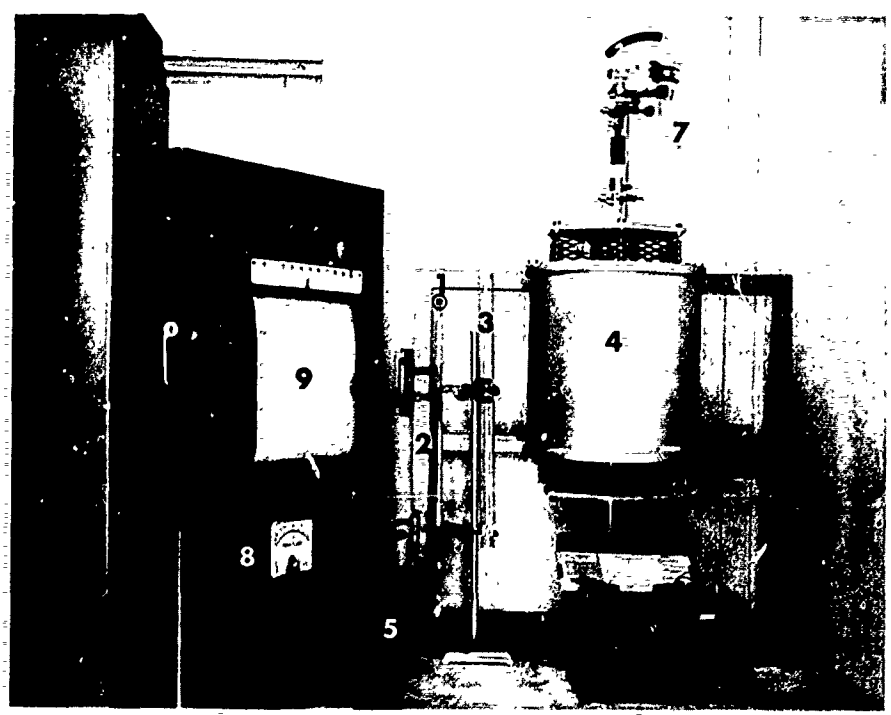

Figure 44. Differential Thermal Analysis Apparatus

pressures of helium gas up to 760 mm Hg were substituted as a heat sink for low temperature runs. Metallographic analysis was performed on the heated samples wherever possible.

The differential thermal analysis data were taken using high purity alumina in the reference crucible. In a typical experiment, a sample similar to the one mentioned above was prepared and then placed in a ZT graphite crucible shown in Figure 45. The apparatus was assembled,

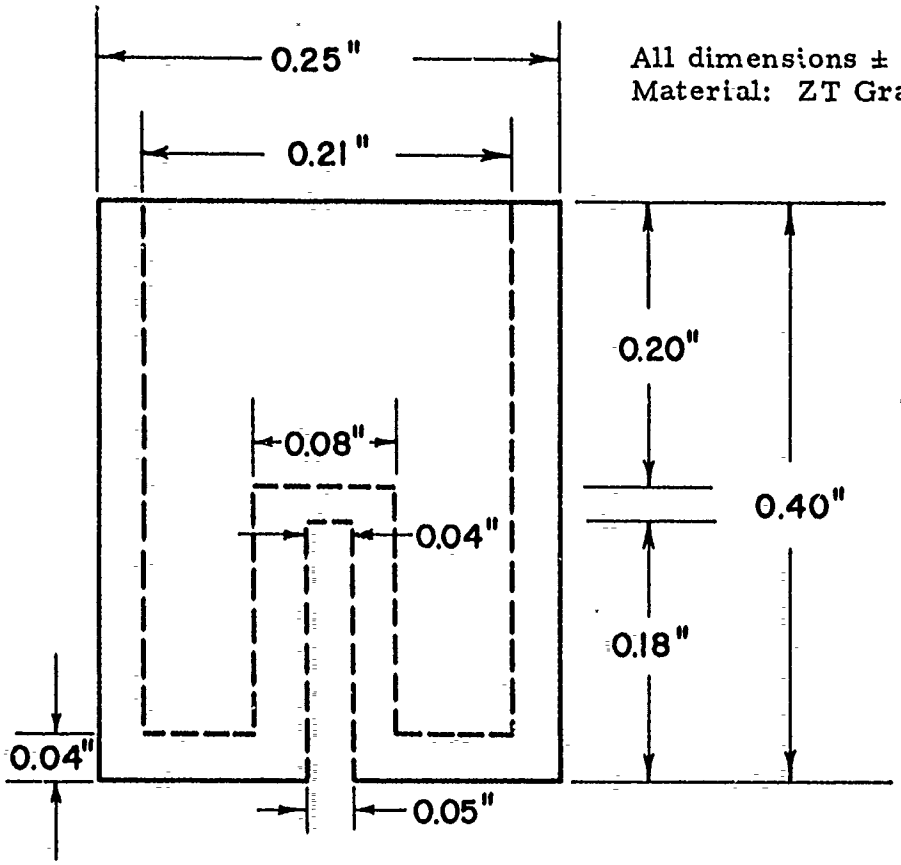

Taper Thermowell:

0.04" top dia.
0.05" bottom dia.

Figure 45. DTA Capsule

evacuated, and flushed continuously with argon. The temperature was raised to 1450°C at a linear rate of 300°C per hour, and the resulting curves were recorded with the Leeds and Northrup strip chart recorder.

The experimental results obtained from the treatment of HfC, ZrC, and ThC with the metals iridium and rhodium are subject to a variety of

interpretations and conclusions. It must be remembered that in dealing with intermetallic species or phases, slight variations of dissolution of one or more components into an intermetallic phase may not cause gross physical or chemical property differences while the converse is true in the case of studies conducted on covalently or ionic bonded inorganic compounds. Therefore, a systematic presentation of possible interpretations will be discussed and compared with the experimental results.

Treatment of hafnium carbide with iridium between 1200° to 2200°C resulted in the formation of an intermetallic phase of AB_3 type reported by Dwight.[61] An equation representing the possible reaction can be written as follows:

$$3Ir + HfC \rightarrow HfIr_3 + C.$$

In Table 23 can be found the d values of the starting materials, Dwight's d values for $HfIr_3$, and our experimentally determined d values. Calculations

TABLE 23

X-RAY DATA FOR HfC + 3Ir REACTION

HfC[62] d, Å	Ir[63] d, Å	$HfIr_3$[64] d, Å	Product d, Å
2.68	2.2170	3.94	
2.321	2.9197	2.78	
1.641	1.3575	2.27	2.260
1.399	1.1574	1.96	1.957
1.340	1.1082	1.39	1.388
1.160	0.9598	1.187	1.185
1.065	0.8808	1.135	1.135
1.038	0.8586	0.980	0.9845
0.9473	0.7838	0.901	0.9039
0.8932		0.879	0.8813
0.8204			0.8047
0.7845			
0.7735			

from our data yield a lattice constant of 3.94 Å, while Dwight reports a^o = 3.935 Å. It is interesting to note that irrespective of the stoichiometry of the starting mixture, $HfIr_3$ was the only product even though species such as HfIr, $HfIr_2$, and Hf_3Ir_2 are known, strongly suggesting that these other

species are unstable with respect to disproportionation in our reaction system and experimental conditions.

The difference in lattice parameters can be partially rationalized if some carbon has been included in the lattice network. The superlattice lines were not detected which indicates a disordered system lending support to some carbon inclusion, although the difference in atomic scattering may be small. An effort is being made to anneal the phase properly and find the superlattice lines. It should also be noted that in the phase diagram of Hf and Ir, a solid solution of Hf or Ir can exist on either side of the $HfIr_3$ eutectic which may or may not result in a measurable shift of the lattice constant. In any event, if the disorder-order transformation is effected and the superlattice lines found, definite proof of the exact composition of the product of this reaction will have been made.

A similar phenomenon occurs when zirconium carbide and iridium are heated together at 1200°C or above. An equation representing the probable reaction is:

$$3\ Ir + ZrC \rightarrow ZrIr_3 + C.$$

An intermetallic phase is formed and X-ray data of this phase are given in Table 24. It was also found that heating to 2100°C resulted in melting

TABLE 24

X-RAY DATA FOR ZrC + 3Ir REACTION

$ZrIr_3$ d, Å*	Product d, Å
2.276	2.27
1.971	1.97
1.394	1.39
1.189	1.19
1.138	1.14
.985	.986
.904	
.882	

*Calculated from the lattice constant given by Dwight.

of the reaction mixture. Although there has been reported only one phase of zirconium-iridium, $ZrIr_3$, there may well be others as is the case in the hafnium-iridium system; but our data reveal only phases similar to $ZrIr_3$ are found even when ZrC is in a sixfold excess.

A reaction between iridium and thorium dicarbide was effected by heating a suitable mixture to 1950°C and a representative equation may be:

$$2Ir + ThC_2 \rightarrow ThIr_2 + C.$$

A minimum reaction temperature has not been established for this reaction. It was found that liquefaction of the mixture occurred on heating to 2150°C. The X-ray diffractometer data on the products given in Table 25 agree well with published work.

TABLE 25

X-RAY DATA FOR ThC_2 + 2Ir REACTION

$ThIr_2$* d, Å	Product d, Å
2.70	2.70
2.31	2.31
2.21	2.21
1.91	
1.56	1.56
1.47	1.47
1.35	1.35
1.21	1.23
1.16	1.17
1.15	1.15
1.02	
.997	
.958	
.905	

*ASTM Powder Diffraction file 12-533.

When the carbides of hafnium and zirconium were treated with rhodium at temperatures in excess of 1000° and 1200°C, respectively, a solid solution was found. Table 26 gives the d-spacings from X-ray studies and

TABLE 26

X-RAY DATA FOR HfC + 3Rh AND ZrC+3Rh REACTIONS

$HfRh_3$* d, Å	HfC + 3Rh Product d, Å	$ZrRh_3$* d, Å	ZrC + 3Rh Product d, Å
2.258	2.291	2.267	2.296
1.955	1.984	1.963	1.989
1.383	1.397	1.388	1.409
1.179	1.198	1.184	1.202
1.129	1.147	1.133	1.150
.977		.982	
.897		.901	
.874		.878	

* Calculated from lattice constants given by Dwight.

comparison with reported values of AB_3 type structures is not good agreement. Reasons for this disagreement are not apparent and more effort will be necessary to determine the correct interpretation. Equations illustrating possible reactions are:

$$3Rh + HfC \rightarrow HfRh_3 + C,$$

$$3Rh + ZrC \rightarrow ZrH_3 + C.$$

Treatment of rhodium with thorium dicarbide at 1900°C in vacuo resulted in a homogeneous melt which when cooled to room temperature yielded a solid material whose X-ray diffraction pattern exhibited lines different from those of the starting materials. Identification of these lines with known compounds was unsuccessful, i.e., no lines of thorium carbide or rhodium were present, strongly suggesting a chemical reaction or a solid solution had occurred. Due to the low melting point (1900°C) of this reaction mixture, no further investigation seemed warranted at this time.

When the borides of zirconium, hafnium, and thorium are treated with iridium and rhodium, a vigorous reaction ensues as evidenced by large heats of reaction from the differential thermal analysis data. In Table 27

TABLE 27

MINIMUM REACTION TEMPERATURES DETECTED BY DIFFERENTIAL THERMAL ANALYSIS

Reactants	Temperature, °C
4.75 Ir + ZrB_2	1220 ± 5
4.75 Ir + HfB_2	1235 ± 5
4.75 Rh + ZrB_2	1195 ± 5
4.75 Rh + HfB_2	1165 ± 5

are given the minimum temperatures where sharp peaks are found. These four systems were heated finally in vacuo to 1430°C and held for thirty minutes. The photomicrographs in Figures 46 through 49 indicate very little void areas; i.e., the black spots and the resultant mixtures are very dense. Metallographic examination yielded the following:

(1) In Figures 46 through 49, the irregular shaped particles are isotropic (cubic) as determined by polarized light.

(2) In Figures 46 through 49, the matrix phase is anisotropic.

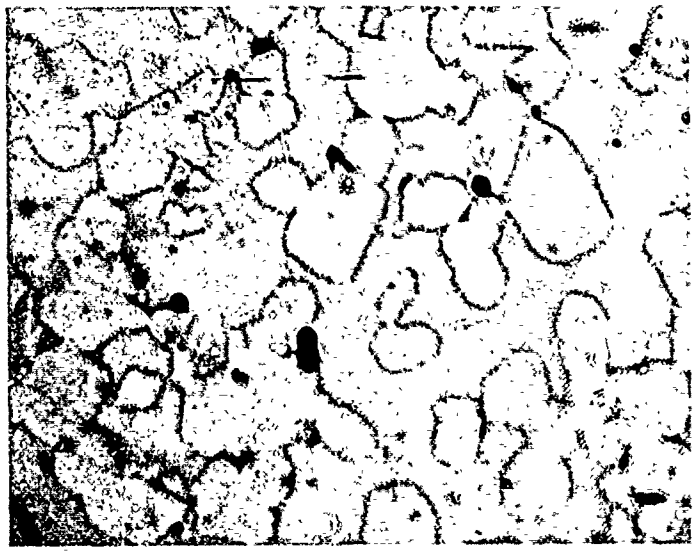

Figure 46. Reaction Product of Ir + ZrB_2 Held in Vacuo at 1430°C for 30 Minutes 533 X Magnification

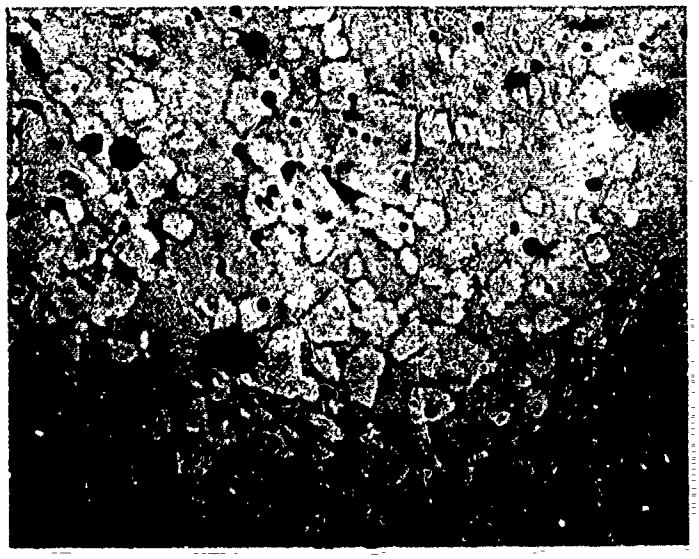

Figure 47. Reaction Product of Ir + HfB_2 Held in Vacuo at 1430°C for 30 Minutes 533 X Magnification

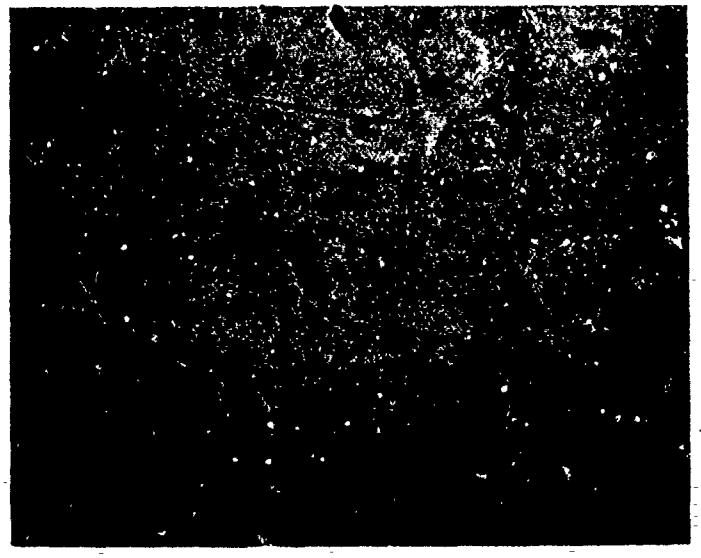

Figure 48. Reaction Product of Rh and ZrB_2 Held in Vacuo at 1430°C for 30 Minutes 533 X Magnification

Figure 49. Reaction Produ..t of Rh and HfB_2 Held in Vacuo at 1430°C for 30 Minutes 533 X Magnification

(3) In Figure 49, a minor phase was observed at the grain boundaries of the matrix phase and this was found to be anisotropic.

X-ray diffraction patterns of these specimens exhibited no lines associated with the starting materials, nor was it possible to accurately identify any of the reaction products. However, cubic components, identified by metallographic examination, were found in each of the four unidentifiable X-ray patterns.

The four major lines from the diffraction patterns of each sample are given in Table 28. It can be seen that the d values are not in exact accordance with those reported by Dwight for the pertinent cubic structures of

TABLE 28

X-RAY DATA FOR THE REACTIONS OF THE BORIDES WITH IRIDIUM AND RHODIUM (FOUR MOST INTENSE PEAKS)

$ZrIr_3$* d, Å	Product 4.75Ir+ZrB_2 d, Å	$HfIr_3$* d, Å	Product 4.75Ir+HfB_2 d, Å	$ZrRh_3$* d, Å	Product 4.75Rh+ZrB_2 d, Å	$HfRh_3$* d, Å	Product 4.75Rh+HfB_2 d, Å
2.276	2.316	2.27	2.319	2.267	2.322	2.258	2.319
1.971	2.005	1.96	2.004	1.963	2.013	1.955	2.010
1.394	1.420	1.39	1.417	1.388	1.425	1.383	1.420
1.189	1.210	1.187	1.209	1.184	1.216	1.179	1.213

* Calculated from lattice constants given by Dwight.

type AB_3. This may be due in part to boron inclusion in the lattice of the solid solution since, to a first approximation from the values of the atomic radii, boron could easily fit in and expand the lattice. An interesting comparison can be made from Table 29 in which Dwight's values, our values, and values using Goldschmidt radii are included. Our values fall in between those of Dwight and Goldschmidt indicating most likely an expanded cubic lattice of a solid solution of the AB_3 type with some inclusion of boron. The matrix phase is most likely a solid solution high in boride content.

Additional experimental evidence of chemical reactions in these systems can be found in the results of diamond pyramid microhardness tests. These values are given in Table 30.

TABLE 29

REACTIONS OF PLATINUM METALS WITH REFRACTORY DIBORIDES—INVESTIGATION OF PRODUCTS

System	a_o	Composition	a'_o	a''_o
4.75 Ir + ZrB_2	4.013 ± 0.003	$ZrIr_3$	3.943	4.171
4.75 Ir + HfB_2	4.008 ± 0.001	$HfIr_3$	3.935	4.143
4.75 Rh + ZrB	4.020 ± 0.004	$ZrRh_3$	3.927	4.157
4.75 Rh + HfB_2	4.027 ± 0.005	$HfRh_3$	3.911	4.129

a_o = Measured lattice constants.

a'_o = Dwight's reported values for ordered AB_3 phases[61]

a''_o = Lattice constants calculated from CN 12 radii of the components.

TABLE 30

DIAMOND PYRAMID MICROHARDNESS OF REACTION PRODUCTS (DPH_{100} g LOAD)

Reactants	DPH_{100} g = (kgs/mm^2)	
	Particles	Matrix
4.75 Ir + ZrB_2	1250	1150
4.75 Ir + HfB_2	1225	850
4.75 Rh + ZrB_2	1250	900
4.75 Rh + HfB_2	820	790
Ir	~300	
Rh	~300	
HfB_2	~2000	
ZrB_2	~2000	

X. CHEMICAL REACTIONS OF OXIDES

TASK B2-1

Introduction

On the basis of existing thermochemical and physical data[1], the oxides ThO_2, HfO_2, ZrO_2, and BeO have been selected as promising materials for further study as high temperature oxidation barriers. Considering these compounds as coatings directly on a graphite substrate requires information concerning the chemical reaction kinetics which describe interactions of graphite with the oxygen barriers. Even though the oxides are thermodynamically unstable with respect to carbon at 2200°C, the reaction rates may be low enough to justify an investigation of the factors controlling these rates.

Literature values for minimum reaction temperatures between these oxides and graphite are often misleading in that temperatures cited for a zero free energy change are based on equilibrium data; i.e., a CO partial pressure of one atmosphere being defined as the standard state. A more realistic criterion for minimum reaction is that temperature corresponding to a low pressure of CO; e.g., $P_{CO} = 1.3 \times 10^{-3}$ atmosphere (1 torr). This minimum temperature could then be calculated from free energy functions at various temperatures which contain the enthalpy and entropy terms. In addition to minimum reaction temperature data, kinetic information is very important for these systems, since a solid state diffusion controlled reaction could result in a "practical compatibility" of metal oxide and graphite.

Experimental

Investigation of the chemical kinetics concerning the graphite reduction of the refractory metal oxides was carried out by employing spectroscopic grade natural graphite (Union Carbide Grade SP-1) and the metal oxide. The graphite was previously heated to 2200°C in vacuo and then blanketed with dry argon and transferred to a glove box flushed with dry, deoxygenated nitrogen. The metal oxide and graphite were weighed, thoroughly mixed in the dry nitrogen atmosphere, and transferred to a crucible of AUC graphite. This crucible was shielded with 10 mil molybdenum sheet and was pretreated in the same fashion as the reactant graphite.

In a typical experiment, approximately 2.5 mmoles oxide (-325 mesh) were thoroughly mixed with a 20-fold mmole excess of -325 mesh graphite and loaded into the crucible. An additional 4 or 5 mmoles of graphite were added to the top of the reaction mixture. The crucible was then transferred from the glove box to the vacuum line, evacuated to 10^{-5} torr, and heated by induction. The rate of carbon monoxide evolution was followed by means of a mercury manometer. The temperature of the reaction was measured with a calibrated optical pyrometer by viewing the charge through a sight hole under blackbody conditions. The noncondensable evolved gas was demonstrated to be carbon monoxide by complete conversion to carbon

dioxide at 300°C over copper oxide. The purity of both gases was also established by vapor phase chromatography utilizing a silica gel column operated at 78°C. All solid reaction products were examined by X-ray diffraction.

Materials

Thorium dioxide (-325 mesh), obtained from the Zirconium Corporation of America, was examined for purity by chemical analysis and a spectroscopic method:

Calculated for ThO_2:	Th, 87.9; O, 12.1
Found:	Th, 87.37; O, 12.8
Spectroscopic:	Major: Th
	Minor: Al, Mg, Fe, Si
	Trace: Cu

Zirconium dioxide (-325 mesh), obtained from the Zirconium Corporation of America, was dehydrated at 400°C in vacuo and then examined for purity by chemical analysis:

Calculated for ZrO_2:	Zr, 74.0; O, 26.0
Found:	Zr, 74.5; O, 25.3

Beryllium oxide (-325 mesh), obtained from the Brush Beryllium Company, was dried at 400°C in vacuo, and examined for purity

Calculated for BeO:	Be, 36.1; O, 64.9
Found:	Be, 36.55; O, 40.6
Spectroscopic:	Major: Be
	Minor: Mg
	Trace: Fe, B, Mn, Cr, Pb, Si, Ni, Al, Cu, Zn

Hafnium oxide (-325 mesh), obtained from the Zirconium Corporation of America, was dried in a platinum dish at 1000°C for four hours and examined for purity by chemical and spectroscopic analysis:

Calculated for HfO_2:	Hf, 84.7; O, 15.3
Found:	Hf, 83.53; O, 15.0; Fe, 0.60; Si, 0.03
Spectroscopic:	Major: Hf
	Minor: Zr, Al, Fe, Ti, Si, Cu, Mg
	Trace: Ni, Mn, Cr

Hafnium oxide (-325 mesh) fully stabilized with 5 per cent Y_2O_3 was obtained from the Zirconium Corporation of America. This material, contained in a platinum crucible, was dried in air at 800°C for four hours and analyzed.

Calculated for HfO_2+5 w/o Y_2O_3:		Hf, 80.5; O, 15.5
Found:		Hf, 80.63; O, 19.35
Spectroscopic:	Major:	Na, Fe, Si, Hf, Li, Ti, K, Zr, Y
	Minor:	Mg, Mn, Cu, Cr, Ni, Al

Results and Discussion

Beryllium Oxide-Graphite

Beryllium oxide (BeO) is reported to react with graphite at minimum temperatures of 1315°C[65] and 2300°C[66]. The reported reaction rates[67] in moles CO per 10^4 particles of BeO (100 - 140 mesh) per second in the specified temperature ranges are:

$$k = 7.64 \times 10^{-3} e^{-61,300/RT} \quad (2018° \text{ to } 2186°K) \quad (1)$$

$$\text{and } k = 1.01 \times 10^{-10} e^{-40,000/RT} \quad (1788° \text{ to } 2018°K) \quad (2)$$

One may obtain a reaction rate of 1.6×10^{-4} mmoles CO/mmole BeO min^{-1} from Equation (1) at 2100°K, assuming the oxide to be 100 mesh. Since these rate laws were obtained during the very early stages of the reaction, diffusion controlled processes would not be apparent. The kinetics of this reaction are further complicated by the fact that more than one reaction takes place[68].

$$BeO_{(s)} + {}^3/_2 C_{(s)} \rightarrow {}^1/_2 Be_2C_{(s)} + CO_{(g)} \quad (3)$$

$$Be_2C \rightarrow 2Be_{(g)} + C_{(s)} \quad (4)$$

$$Be_{(g)} + CO \rightarrow BeO_{(s)} + C_{(s)} \quad (5)$$

Our results are consistent with this explanation in that after attaining a maximum CO pressure of 52 torr in the reaction system, the pressure dropped to 18 torr. Complete reoxidation of the beryllia by CO (Equation 5) did not take place because the Be had condensed in the relatively cool portion of the vacuum system. This experiment indicated a minimum reaction temperature of 1295°C. The partial pressure of CO, evolved from the reaction represented by Equation (3), was calculated to be 1 torr at 1592°C and one atmosphere at 2227°C[1]. The difference between the experimental minimum reaction temperature (1295°C) and the calculated (1592°C) suggests that the initial reaction does not proceed as described in Equation (3).

Zirconium Oxide-Graphite

Zirconium dioxide is reported to react with graphite at a minimum temperature of 1300°C[65] and 1600°C[66]. The reaction is summarized by the following equation:

$$ZrO_{2(s)} + 3C_{(s)} \rightarrow ZrC_{(s)} + 2CO_{(g)}. \quad (6)$$

Prescott[69] found from equilibrium data that $\Delta F° = 151,800 - 78.68T$, or P_{CO} is one atmosphere at 1657°C. Kutsev et al.[70] report the reaction to proceed according to

$$ZrO_2 + 2.63C \rightarrow ZrC_{0.71}O_{0.08} + 1.92CO, \quad (7)$$

whereas, Zhelankin et al[71] report compositions varying from $ZrC_{0.64}O_{0.06}$ to $ZrC_{0.77}O_{0.00}$ at temperatures of 1930° and 2450°C, respectively. From thermodynamic calculations, the P_{CO} at 1167°C is one torr and one atmosphere at 1657°C. We found the total amount of carbon monoxide evolved to be 90 to 93 per cent of theoretical, based on Equation (6). Hence, our data are consistent with the formation of zirconium oxycarbides (Equation 7).

Zirconium dioxide was reduced with graphite in the temperature range 1875° to 2150°C; a typical plot of CO evolution versus time is shown in Figure 50. In all cases, zero time corresponded to activation of the induction heating unit. Extrapolation of kinetic data obtained at lower temperatures justified the high temperature extrapolation of two minutes.

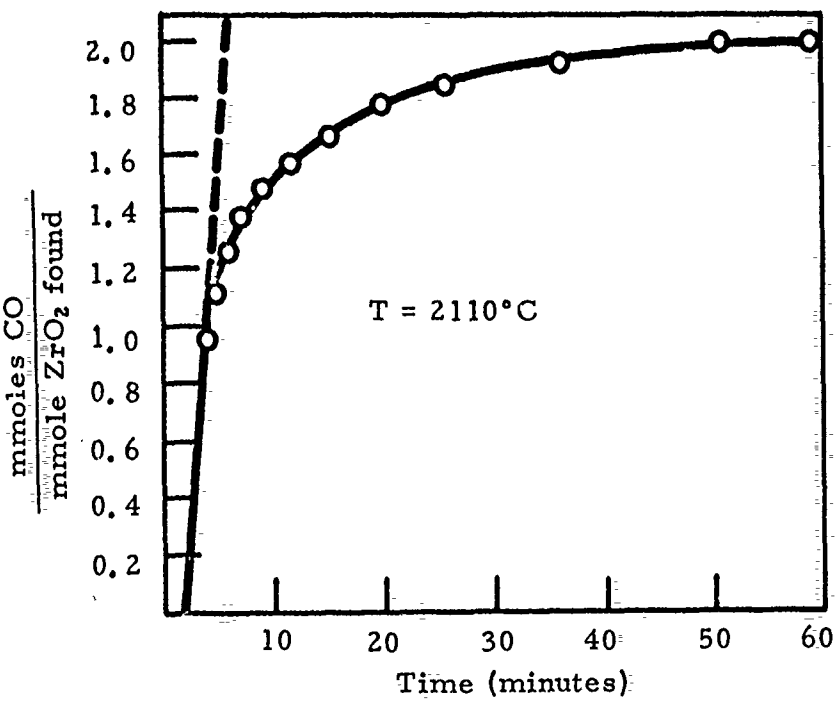

Figure 50. Carbothermic Reduction of Zirconia-Reaction Rate

These rate data have been reduced to mmoles CO/mmole ZrO_2 found (based on the total CO evolved) rather than the amount of ZrO_2 calculated on the basis of sample weight. Table 31 summarizes the observed stoichiometry, reaction temperature, minimum reaction temperature, and product composition. The stoichiometry is consistent with oxycarbide formation (Equation 7).

TABLE 31

CARBOTHERMIC REDUCTION OF ZIRCONIA

ZrO_2 (gms)	Yield, CO (mmoles)		Temperature (°C)		Solid Product	Minimum Reaction Temp. °C *
	Calcd.	Found	Reaction	Final		
0.270	4.37	3.95	2110	2110	ZrC+C	1635
0.210	3.43	3.22	2050	2050	ZrC+C	1595
0.292	4.75	4.66	2025	2140	ZrC+C	-
0.282	4.58	4.55	1960	2110	ZrC+C	1615
0.312	5.08	5.09	1940	2150	ZrC+C	1660
0.304	4.94	4.87	1875	2150	ZrC+C	1565

* Temperature at which sample visibly flashed and CO evolution commenced.

The specific rate constants at various temperatures are summarized in Table 32. From a plot of the log specific rate constant versus $\frac{1}{T°K}$ (Figure 51), an activation energy of 70.8 kcal was calculated by the method of least squares.

TABLE 32

REACTION RATE CONSTANTS - $ZrO_2 + C$

Temperature °C	Rate Constant k ($\frac{\text{mmoles CO}}{\text{mmole } ZrO_2 \text{ min.}}$)	
	Calculated	Observed
2110	0.58	0.48
2050	0.40	0.42
2025	0.34	0.48
1960	0.21	0.21
1940	0.18	0.12
1875	0.14	0.13

The graphite reduction of ZrO_2 obeys the rate equation,

$$\frac{d(CO)}{dt} = 1.8 \times 10^6 \, e^{-70,800/RT}$$

for the first 50 per cent of reaction in the temperature range 1875° to 2110°C. The reaction appears to be solid state diffusion controlled for the latter stages of the reaction, as evidenced by the parabolic shape of kinetic curves. This condition was confirmed in that, after a lower temperature kinetic run, an increase in temperature produced additional carbon monoxide. A minimum reaction temperature range of 1565° to 1660°C was observed with a mean value of 1615°C.

Thorium Oxide-Graphite

The carbothermic reduction of thoria is summarized by the equation

$$ThO_2 + 4C \rightarrow ThC_2 + 2CO.$$

The free energy change, $\Delta F° = 176,970 - 73.89T$, for this reaction was reported by Prescott et al.[72] for the temperature range 1707° to 2068°C. The partial pressure of CO was calculated to be one atmosphere at 2122°C. Nadler et al.[73] reported the ThO_2 reduction to the dicarbide in the temperature range 1650° to 1730°C. Thermodynamic data are not available for ThC_2 at high temperatures; therefore, a minimum reaction temperature could not be calculated. A typical kinetic plot is shown in Figure 52.

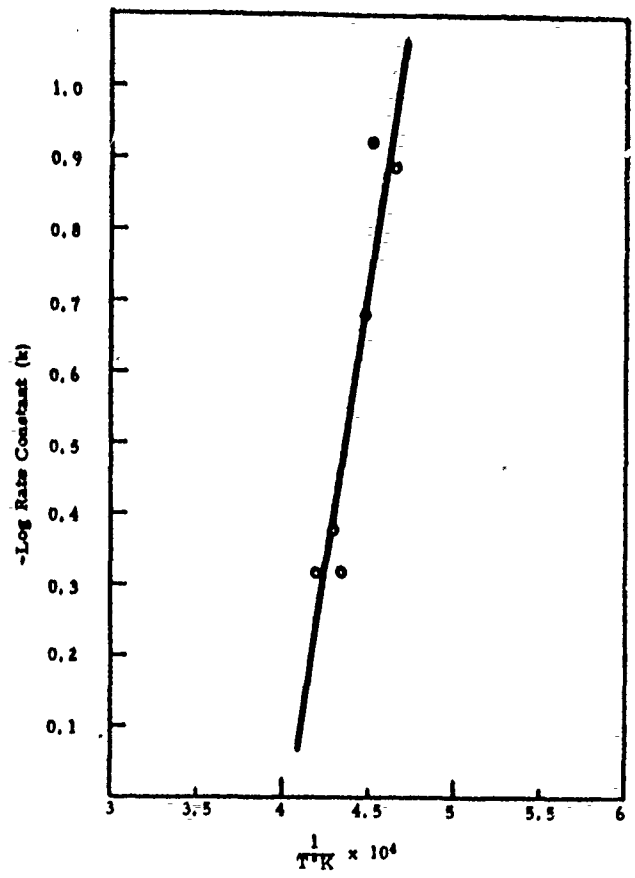

Figure 51. Variation of Carbothermic Reduction Rate Constants with Temperature—Zirconia

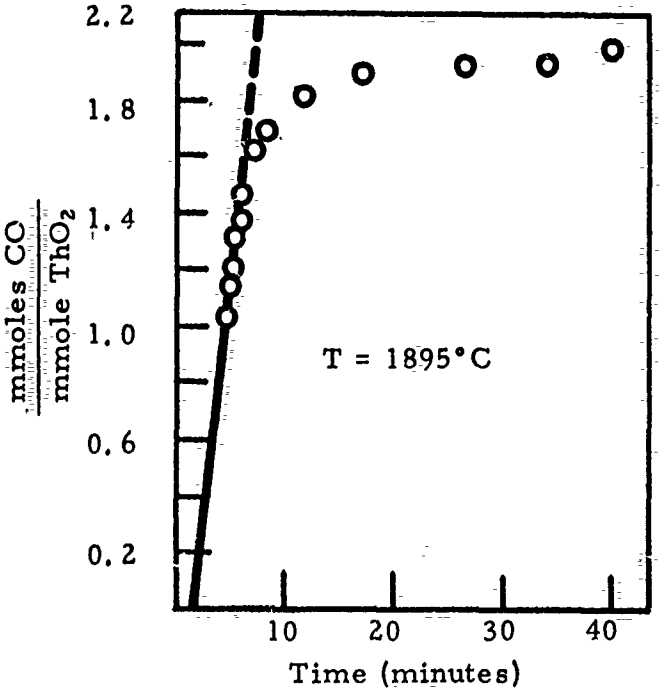

Figure 52. Carbothermic Reduction of Thoria Reaction Rate

The stoichiometry and reaction temperatures are summarized in Table 33. The initial reaction rate, $\frac{dCO}{dt}$, was found to be a constant value at a given temperature in the range 1780° to 2200°C. The rate constants at various temperatures are summarized in Table 34.

TABLE 33

CARBOTHERMIC REDUCTION OF THORIA

ThO_2 (gms)	Yield, CO (mmoles)		Temperature (°C)		Solid Product	Minimum Reaction Temp. °C*
	Calcd.	Found	Reaction	Final		
0.539	4.08	4.01	2100	2100	ThC_2+C	1640
0.512	3.98	3.97	2005	2005	ThC_2+C	1690
0.505	3.82	3.88	1930	2050	ThC_2+C	1615
0.462	3.50	3.58	1895	1895	ThC_2+C	1640
0.545	4.13	4.20	1780	2100	ThC_2+C	1605
0.000	0.00	0.10	2210	2210	C	-

* Temperature at which sample visibly flashed and CO evolution commenced.

TABLE 34

REACTION RATE CONSTANTS—ThO_2 + C

Temperature of Reaction °C	Rate Constant k ($\frac{\text{mmoles CO}}{\text{mmoles } ThO_2 \text{ min}}$)	
	Calculated	Observed
2100	0.63	0.58
2005	0.45	0.63
1930	0.34	0.20
1895	0.30	0.33
1780	0.20	0.20

The scatter found in the rate constants may be attributed to difficulties inherent in reactions involving finely divided materials. From the plot log rate constant versus $\frac{1}{T°K}$ in Figure 53, an activation energy of 36.4 kcals was obtained by the method of least squares. The rate law for the reaction $ThO_2 + 4C \rightarrow ThC_2 + 2CO$ in the temperature range 1780° to 2100°C is:

$$\frac{dCO}{dt} = 1.4 \times 10^3 \, e^{-36,400/RT} \, \frac{\text{mmoles CO}}{\text{mmole } ThO_2 \text{ min.}}$$

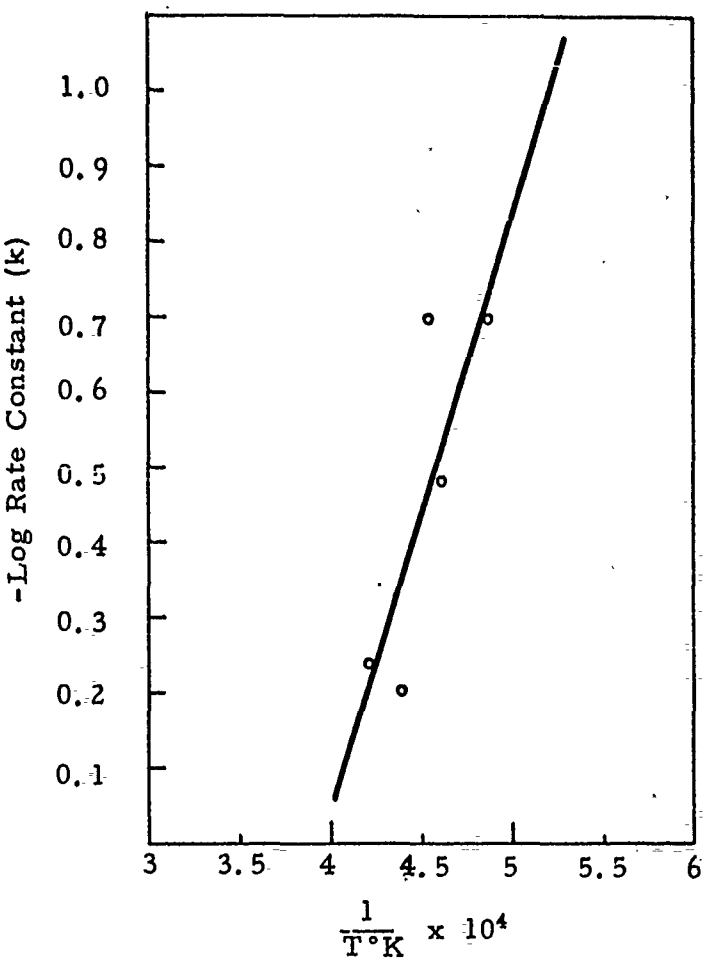

Figure 53. Variation of Carbothermic Reduction Rate Constants with Temperature — Thoria

For the temperature range investigated, ionic diffusion is quite rapid as evidenced by a linear rate law. If solid state diffusion were slow, one would expect a decrease in the reaction rate with increase in time, as the product phase increased in thickness. However, considerable lattice diffusion would be expected above 1500°C which is the Tammann temperature of ThO_2 because atom mobility would be expected to be greater in the product layer, ThC_2, which has a lower melting point than the oxide[74]. The derived rate law predicts that the reaction rate is ten times faster at 2200°C than at 1800°C; at the higher temperature, a carbon monoxide evolution of 0.3 mmoles/mmole ThO_2/min. was calculated. A minimum reaction temperature of 1640°C ± 30°C was observed.

Hafnium Oxide-Graphite

The reaction of hafnium dioxide with graphite[75] is summarized by

$$HfO_2 + 2.9C \rightleftharpoons HfC_{0.95} + 1.95CO.$$

The free energy change for this reaction in the temperature range 1750° to 2000°K was found from equilibrium data to be in accord with $\Delta F° = 132,300 - 66T$ or P_{CO} = one atmosphere at 1732°C.

The stoichiometry and reaction temperatures for this graphite reduction of HfO_2 are summarized in Table 35.

TABLE 35

CARBOTHERMIC REDUCTION OF HAFNIA

HfO_2 (gms)	Yield, CO (mmoles) Calcd.	Found	Temperature °C Reaction	Final	Solid Product	Minimum Reaction Temp. °C*
0.504	4.80	4.99	1740	1980	HfC+C	1750
0.517	4.93	5.10	1920	2150	HfC+C	1700
0.502	4.78	4.96	1930	2100	HfC+C	1750
0.505	4.81	4.90	2050	2050	HfC+C	1800
0.500	4.75	4.94	2160	2160	HfC+C	1755
0.508	4.84	4.93	2200	2200	HfC+C	1660

* Temperature at which sample visibly flashed and CO evolution commenced.

A typical kinetic plot is shown in Figure 54; the rate constants presented in Table 36 were obtained from the slope of the various kinetic plots.

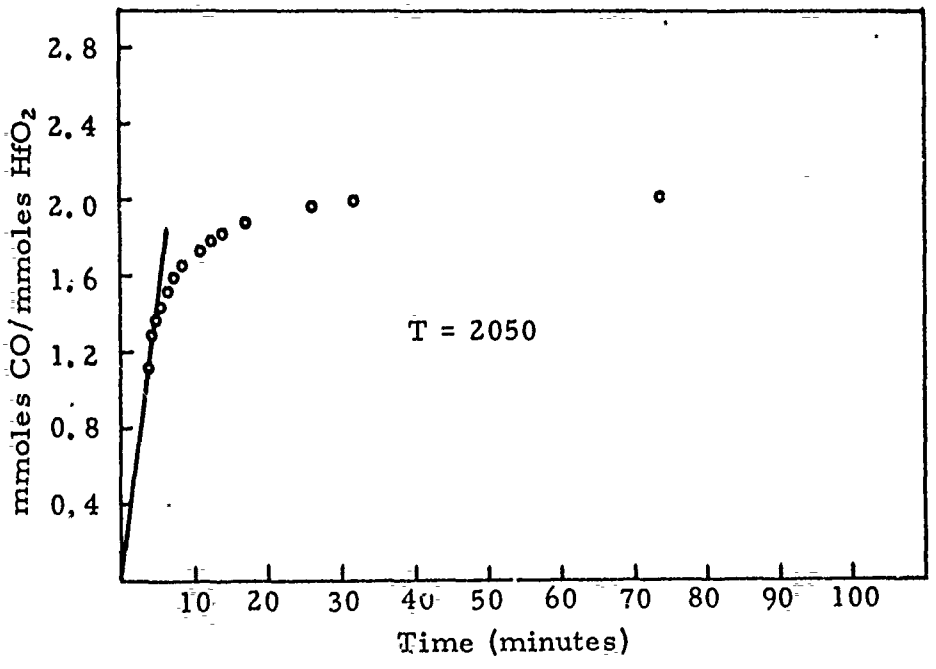

Figure 54. Carbothermic Reduction of Hafnia Reaction Rate

TABLE 36

REACTION RATE CONSTANT - $HfO_2 + C$

Temperature of Reaction °C	Rate Constant k ($\frac{\text{mmoles CO}}{\text{minutes}}$)	
	Calcd.	Observed
1740	0.26	0.25
1920	0.29	0.29
1930	0.30	0.35
2050	0.32	0.30
2160	0.35	0.34
2200	0.35	0.39

The variation of rate constant with temperature is shown in Figure 55. An activation energy of 7.1 kcal/mole was obtained by the method of least squares. This value is considerably lower than that for the reduction of ZrO_2 (70.8 kcal) or ThO_2 (36.4 kcal).

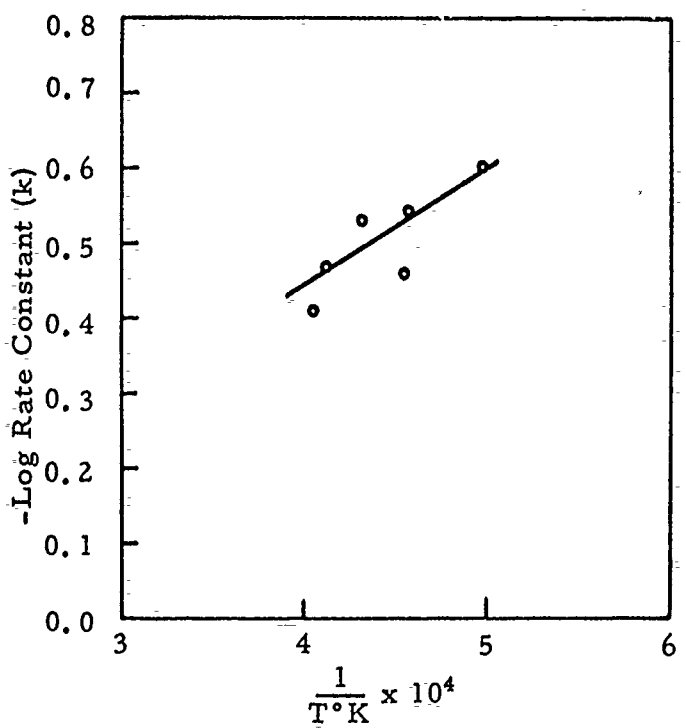

Figure 55. Variation of Carbothermic Reduction Rate Constants with Temperature — Hafnia

An average minimum reaction temperature of 1734°C was observed. The observed flashing of the reaction mixture during the initial reaction was much more severe than for the reduction of ThO_2 and ZrO_2; in fact, 70 per cent of the kinetic experiments with HfO_2 were failures because the reaction mixture was expelled from the containing crucible. It is interesting to note that the observed average minimum reaction temperature, 1734°C, is in the temperature range for the phase transition from monoclinic to the cubic HfO_2; i.e., 1700° to 1800°C[76].

Possibly this phase transition afforded particle sizes less than -325 mesh or a more reactive form of HfO_2. A more reactive form is suggested by the small temperature effect in the reaction rate, i.e., low activation energy (7.1 kcal). The rate law calculated for the carbothermic reduction of HfO_2 to HfC and CO, in the temperature range 1740° to 2200°C, was found to be consistent with

$$\frac{dCO}{dt} = 1.5\, e^{-7100/RT} \frac{\text{mmoles CO}}{\text{mmoles } HfO_2 \text{ min.}}$$

In order to determine if the phase transition, which occurs in HfO_2, was responsible for the low activation energy, the carbothermic reduction data wereinvestigated utilizing HfO_2 fully stabilized with 5 per cent Y_2O_3. The stoichiometry, minimum reaction temperature, and product composition are summarized in Table 37. A typical kinetic plot appears in Figure 56.

TABLE 37

SUMMARY OF CARBOTHERMIC REDUCTION DATA OF HfO_2 STABILIZED WITH Y_2O_3

Total Sample Weight (gms)	Yield, CO, based on HfO_2 present (mmoles)		Temperature, °C		Solid Reaction Product	Minimum Reaction Temp., °C *
	Calcd.	Found	Reaction	Final		
0.528	5.10	5.12	2060	2100	HfC, HfO_2, Y_2O_3, C	1750
0.519	5.02	5.09	1950	2025	-	1835
0.512	4.95	5.07	1850	2080	HfC, HfO_2, C	1725
0.518	5.01	5.12	1935	2110	HfC, HfO_2, C	1760
0.508	4.92	4.90	1960	2070	HfC, HfO_2, C	1800

* Temperature at which sample visibly flashed and CO evolution commenced.

It appears that during the HfO_2 phase transition a relatively low energy barrier towards reduction is present. This is born out by the fact that when the phase transition was eliminated an activation energy of 48.6 kcal was determined compared to previously cited 7.1 kcal. An average minimum reaction temperature of 1776°C was observed compared with 1734°C for pure HfO_2. In Table 37 under solid reaction products, traces of HfO_2 and Y_2O_3 were found in amounts barely detectable by X-ray diffraction.

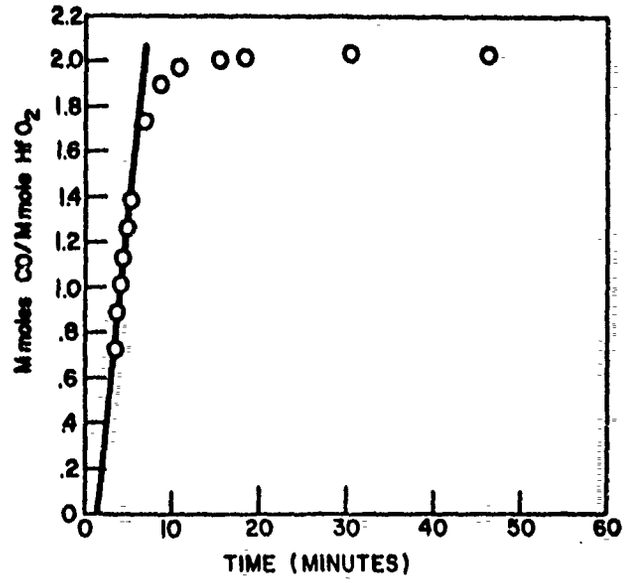

Figure 56. Carbothermic Reduction of Stabilized HfO_2—Reaction Rate

The variation of reaction rate constant with temperature is shown in Figure 57 and summarized in Table 38. A least squares treatment of these data resulted in a calculated activation energy of 48.5 kcal and a rate law consistent with

$$\frac{dCO}{dt} = 2 \times 10^4 e^{-48,600/RT} \frac{\text{mmoles CO}}{\text{mmole } HfO_2 \text{ min.}}$$

in the temperature range 1850° to 2060°C.

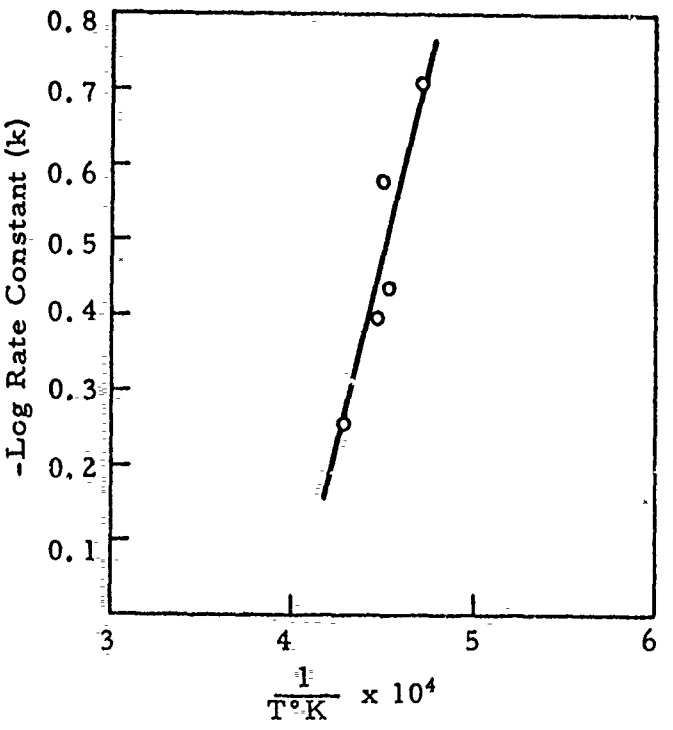

Figure 57. Variation of Reaction Rate Constant with Temperature— Stabilized Hafnia

TABLE 38

REACTION RATE CONSTANT – HfO_2 (Y_2O_3 STABILIZED) + C

Temperature °C	Rate Constant k ($\frac{\text{mmoles CO}}{\text{mmoles } HfO_2 \text{ min}}$)	
	Calculated	Observed
1850	0.200	0.196
1935	0.311	0.370
1950	0.336	0.263
1960	0.352	0.400
2060	0.564	0.560

Future Investigations

Methods and techniques are currently being developed to study the reaction of compacted ATJ graphite with refractory oxide pellets of ThO_2, HfO_2 (stabilized with Y_2O_3) and ZrO_2 (stabilized with Y_2O_3). It is hoped this study will further our understanding of the carbothermic reaction mechanism while also yielding kinetic data under conditions of minimum reaction rate.

XI. CHEMICAL REACTION OF GRAPHITE WITH THE DIBORIDES

Task D-2

There is an abundance of literature on the reactions of the borides of Hf and Zr with graphite; most of the recent work indicates a eutectic at temperatures 500° to 600°C below the melting points of the borides.

Brewer et al.[77] concluded that ZrB_2 is "stable in the presence of graphite" through experimentation with Zr, B, and C.

Glasser[78] hot pressed ZrB_2 in graphite molds at 1.3 tsi and noted chemical reaction only above 2865°C, and Feisel[79] treated ZrB_2 compacts with graphite to form a liquid phase at 2500°C. Popper[80] reports a liquid phase is produced during hot pressing at ZrB_2 in graphite molds at 2300°C, while Wood[81] related that ZrB_2 forms a liquid phase with graphite at 2200° to 2300°C.

Chown et al.[82] coated graphite with slurries of the borides and sintered the coatings in a graphite tube furnace under argon. The most desirable coatings were formed at the eutectic point, usually around 600°C less than the melting point of the borides. "Evidence indicates that the coatings were formed via the melting of boride-carbon and carbide-metal eutectics."

Edwards et al.[43] contained various borides in spectroscopic grade graphite and determined that a liquid phase results at ~500°C below the reported melting points of the borides. See Table 39.

TABLE 39

LIQUEFACTION OF BORIDES IN CONTACT WITH GRAPHITE[43]

Boride	Published Melting Point, °C	Liquefaction Temperature, °C	Sample Type
TiB_2	2790 - 2980	2550 - 2600	Chip
		2500	Powder
ZrB_2	2990 - 3040	2475 - 2525	Chip
		2425	Chip
		2400	Powder
HfB_2	3062 - 3250	2600	Powder
WB	2400 - 2900	2375 - 2425	Powder
TaB	>2000	2725	Powder
NbB_2	3000	2525 - 2550	Powder

Edwards contends that since the liquefaction temperature must depend strongly on the intimacy of contact of the borides with graphite, "it seems probable that bonded coatings would liquefy at lower temperatures than were observed in these experiments where the borides were in loose contact with the graphite."

Nowotny et al.[84] investigated the Hf-B-C and the Zr-B-C systems and demonstrated the stability of the borides with carbon, the carbides, and boron carbide. Although their data are for the 1400°C section of the phase diagram, our work shows that it is highly probable that they hold for temperatures in excess of 2400°C.

Our data reveal that ZrB_2 and HfB_2 are stable in the presence of graphite up to the eutectic melting point, approximately 2500°C. Layers of the borides upon graphite may perform satisfactorily at temperatures greater than 2200°C at reasonable pressures when protected from oxidation. However, at these temperatures in vacuo, the vapor pressure of boron over the diborides is significant and may well result in the eventual conversion of thin boride layers to their respective carbides; this should in no way interfere with the borides used as a barrier layer in the proposed coating systems.

Experimental

The ZrB_2, ZrC, and HfB_2 used in the following experiments are characterized in Section IV on Page 83. The boron carbide assay showed 78.3 per cent B, 20.9 per cent C, 0.3 per cent Fe, 0.2 per cent Si, and 0.1 per cent Al. The graphite was spectrographic grade powder designated as SP-2.

The apparatus used in this task is the same as that described in Figure 43.

Graphite crucibles, ZT grade, containing varying amounts of ZrB_2 powder were heated to 2420°C under 0.8 atmosphere of helium and held for thirty minutes. The samples melted and upon cooling the resolidified specimen was submitted for X-ray diffraction and metallographic analyses. In an effort to determine the liquefaction temperature, equimolar amounts of ZrB_2 and graphite powders were pressed into pellets 0.25 inch diameter x 0.5 inch long and heated to 2450°C in vacuo for fifteen minutes. No melting was detected. Further heating to 2480°C produced a melt. Upon cooling, the sample was submitted for X-ray analysis.

A 0.43 gram sample of equimolar amounts of B_4C and ZrB_2 was placed in an ATJ graphite crucible and heated in vacuo to 2175°C for one hour. Upon cooling, the mixture was slightly sintered, and no color change occurred. This specimen was then subjected to X-ray analysis.

A 0.435 gram sample of equimolar amounts of B_4C and ZrC (2.76 mmoles each) was placed in an ATJ graphite crucible and heated in vacuo to 2340°C for one hour. No melting of the sample occurred, but a high degree of sintering was observed. After cooling to room temperature, an X-ray analysis was performed.

R. V. Sara[85] carried out an experiment in which a powdered mixture of equimolar quantities of C and HfB_2 were pressed into a pellet and then heated slowly to high temperatures to determine the liquidus temperature. Liquefaction was noted in the black body cavity at 2500°C.

Some preliminary experiments were conducted in which thin (generally 2 to 3 mils thick) boride coatings were applied to bullet-shaped (0.5 inch diameter x 1.25 inch long) ATJ graphite cylinders by a slurry-dip technique. The specimens were then heated in vacuo to a predetermined temperature and held at temperature for one hour after which the samples were submitted for X-ray analysis.

In two similar experiments with the boride-coated graphite cylinders, the samples were heated in an argon atmosphere at 2210°C for three hours. Table 40 summarizes the experimental conditions and results of the X-ray analyses.

TABLE 40

PRODUCTS OF DIBORIDE EXPERIMENTS
ON 0.5 INCH GRAPHITE CYLINDERS

HfB_2 on Graphite			ZrB_2 on Graphite		
Temp.	Atm.	Products*	Temp.	Atm.	Products*
1970	Vacuo****	HfB_2, minor HfC**	1875	Vacuo	ZrB_2
2130	Vacuo	HfB_2, HfC	2070	Vacuo	ZrB_2, ZrC
2260	Vacuo	HfC, minor HfB_2	2340	Vacuo	ZrC (no B product was detected)
2210	Argon	HfB_2, minor HfC**	2210	Argon	ZrB_2, minor ZrC***

* Determined by X-ray diffraction.
** Approximately same magnitude as starting material.
*** Impurity materials present in starting material not found in resultant product.
****<1 mm of Hg helium pressure.

Summary of Results

The results of the chemical reactions carried out are summarized by the following equations:

$$ZrB_2 + C \text{ (graphite)} \xrightarrow[He]{2420^\circ C} \text{no reaction}$$

$$B_4C + 2ZrC \xrightarrow[\text{vacuo}]{2340^\circ C} 2ZrB_2 + 3C$$

$$B_4C + ZrB_2 \xrightarrow[\text{vacuo}]{2175^\circ C} \text{no reaction}$$

$$HfB_2 + C \text{ (graphite} \xrightarrow[\text{vacuo}]{2500^\circ C} \text{no reaction}$$

These results clearly agree with Nowotny's Zr-B-C and Hf-B-C phase diagrams which show that ZrB_2 and HfB_2 are stable in the presence of graphite up to 1400°C and further, it has been found that this stability extends to the eutectic temperature of approximately 2500°C for ZrB_2 and C and HfB_2 and C. It may also be noted in the case of ZrB_2 that the temperature at which ZrB_2 and C form a liquid vary depending upon the composition of the mixture as evidenced by the powdered ZrB_2 in graphite melting at 2420°C while a pressed pellet of equimolar composition did not melt until 2480°C.

The zirconium and hafnium boride-coated graphite cylinders undergo a chemical reaction in vacuo (< 1 mm of Hg) to yield the respective carbides; while in the presence of an argon environment, no chemical reaction was observed. The explanation for this anomalous behavior can be easily rationalized if one recalls the vapor pressure of boron over ZrB_2 at 2100°C is approximately 0.01 mm Hg[86,87], thus the overall reaction sequence is the dissociation of ZrB_2 to elemental Zr which undergoes a fast reaction with carbon at 2100°C to produce ZrC. The same argument applies in the case of the HfB_2-coated graphite cylinders.

Discussion

Zirconium diboride does not undergo a chemical reaction with graphite up to the eutectic point of approximately 2500°C where liquefaction occurs to give a ZrB_2-C melt. Metallographic analyses of the melt after solidification illustrate the distinct presence of a carbon phase crystallizing within the zirconium diboride matrix phase as shown in Figures 58 and 59. The X-ray data give only lines associated with graphite and ZrB_2. In order to verify further that ZrB_2 is the stable phase in the system Zr-B-C, two additional experimental observations were made. Treatment of ZrB_2 with B_4C at 2175°C in a graphite crucible resulted in no chemical reaction. If ZrC was the stable phase, it would have been produced in large amounts. To give evidence of the unstability of ZrC, B_4C was mixed with ZrC and the mixture heated to 2340°C in a graphite container. The products were ZrB_2 and carbon; thus the conclusion can be reached that ZrB_2 is the only stable phase when compounds of zirconium and boron plus carbon are placed in contact with each other and heated to high temperatures.

Figure 58. Zirconium D[illegible]ride and Carbon (graphite) heated at 24[illegible]C 533 X Magnification

Figure 59. Zirconium Diboride and Carbon (graphite) heated at 2420°C, 133 X Magnification

Sara[85] carried out an experiment in which a powdered mixture of equimolar quantities of C and HfB_2 were pressed into a pellet and then heated slowly to high temperatures to determine the liquidus temperature. A liquefaction was noted in the black body cavity at 2500°C. X-ray diffraction detected some HfC in the specimen; however, the starting material contained small amounts of both the carbide and oxide; and therefore, it may be assumed that the carbide came from these impurities and that the boride is stable at these temperatures.

The results obtained from the heating of boride-coated graphite cylinders in argon and in vacuum are shown in Table 40. They reveal an apparent anomaly with respect to the stability of ZrB_2 and HfB_2 in the presence of carbon. In the cases where the diboride and carbon were heated in vacuo the carbide was formed, while heating the diboride-carbon samples in argon atmsopheres gave essentially no chemical reaction. It has been shown that ZrB_2 and HfB_2 undergo thermal decomposition in vacuo above 2100°C according to the following equation:

$$ZrB_2(s) \rightarrow Zr(g) + 2B(g). \qquad (1)$$

It has further been demonstrated that if the ZrB_2 is contained in a graphite cell in vacuo at 2100°C, the following reaction occurs:

$$Zr(g) + C(s) \rightarrow ZrC(s). \qquad (2)$$

Thus, the overall reaction sequence may be obtained by addition of Equation (1) and Equation (2) to give:

$$ZrB_2(s) + C(s) \rightarrow ZrC(s) + 2B(g)$$

Even though the carbides of Zr and Hf are formed from the borides in the presence of carbon, they do so only in vacuo and since heating of space hardware occurs after entering regions of measurable pressure, the decomposition of ZrB_2 will be suppressed, and coupled with this is the fact that the ZrB_2 will be present as a "sandwiched" barrier layer, thus decreasing the mean free path for vaporization to a minimum.

XII. ARC PLASMA OXIDATION TESTS

Cincinnati Tests

Three iridium-clad graphite rods and two JTA* refractory based graphite composites were tested for oxidation resistance in the arc plasma torch facilities of the Cincinnati Testing Laboratory (CTL) Division, Studebaker Corporation, Cincinnati, Ohio. The tests were conducted during the period March 18, 1964, to April 1, 1964.

All of the graphite specimens had a 5-mil coating of iridium; two specimens were tested in simulated air at atmospheric pressure to temperatures in excess of 2000°C and one specimen was tested at a reduced stagnation pressure of 48 torr.

The JTA specimens were also tested at atmospheric and subatmospheric pressures for comparison with the iridium-clad materials.

Torch Test Facilities

The primary elements of CTL's plasma torch testing facilities include a 1.5 megawatt arc plasma generator, vacuum test chamber, steam ejector system, and control console with instrumentation and recording equipment. A power transformer and d.c. converter, water supply tank, pump and cooler, and gas flow and metering manifold operates in support of the test equipment.

The 1.5 megawatt arc plasma generator was operated using simulated air (22 per cent oxygen, 78 per cent nitrogen mixture) at flow rates of approximately 0.02 lb/sec and a net enthalpy ranging from 4200 to 5400 BTU/lbs. The surface temperature was measured near the center of the arc impact area and was continuously recorded using a Latronics Coloratio Pyrometer, Model BG 222. This pyrometer measures temperatures using the ratio of intensities of two color bands (red and blue); and, therefore, no emissivity corrections are necessary.

All test runs were recorded on 16 mm color film, but due to the length of the runs the camera was generally operated only for thirty seconds in each two-minute period. The test specimens consisted of rods 5 inches long x 0.5-inch in diameter. In the case of the iridium-coated specimens, the protective cladding extended only over the central 3 inches of the rods, although one end was somewhat protected by an additional coating consisting of sintered iridium powder. The preparation of the iridium-coated specimens is described in Section VIII under the heading "Foil-Clad Iridium Coatings." The arc was fired horizontally, impinging on the center of the specimens, which were supported on both ends by water-cooled copper clamps.

*Approximately 40 ^{w}/o ZrB_2, 12 ^{w}/o SiC, 48 ^{w}/o graphite.

Tests at Atmospheric Pressure

Tests were run both at atmospheric and at reduced pressure. For the tests at atmospheric pressure, a one-inch nozzle producing subsonic plasma flow rates was used. Calibration runs at atmospheric pressure indicated that to obtain surface temperatures between 2000° and 2100°C, the distance from the nozzle had to be 1 5/8 inches for the iridium-clad specimens and 2 5/8 inches for the JTA specimens. The stagnation pressure on the surface measured with a transducer was found to be 4 mm Hg above atmospheric pressure. In addition to the calibration runs, two iridium-clad specimens (A-13 and A-15) and one JTA specimen (JTA-1) were tested at atmospheric pressure. A-13 was tested for twenty minutes at an average surface temperature of 2050°C. The exact time-temperature relationships and other pertinent data are given in Table 41.

TABLE 41

TEST SPECIMEN A-13

Pressure: atmospheric Nozzle: 1 inch Distance from nozzle: 1 5/8 inches
Gas flow: 0.0197 lbs/sec Net enthalpy: 5380 BTU/lbs
*Heat flux: 80 BTU/ft^2/sec

Time (seconds)	Temperature, °C	Time (seconds)	Temperature, °C
30	-	630	2065
60	2010	660	2080
90	1940	690	2080
120	1968	720	2162
150	1996	750	2080
180	1955	780	2162
210	2025	810	2245
240	2065	840	2085
270	2025	870	2093
300	2050	900	1995
330	2050	930	2176
360	2025	960	2080
390	1955	990	2100
420	2050	1020	2010
450	1995	1050	2093
480	2050	1080	2050
510	2065	1110	2050
540	1993	1140	2108
570	2055	1170	2108
600	2128	1180	2080

* The only heat flux data available was that measured on a flat plate test specimen 1 inch x 3 inches.

Figure 60 shows the appearance of A-13 after the test. The extreme right of the photograph shows a portion of the uncoated specimen and the slurry dip coat appears at the left (rounded) end. The center portion of the specimen contains the 3-inch length of the cladding, the borders of which

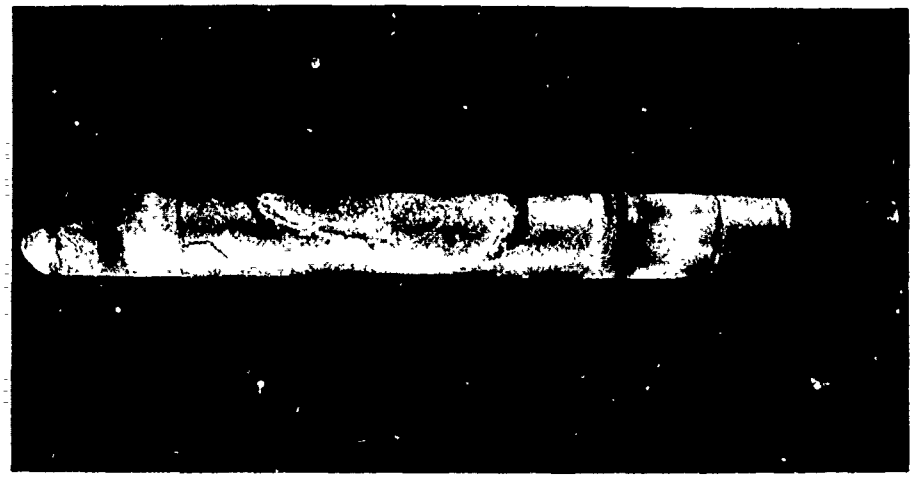

Figure 60. Test Specimen A-13 Iridium-Coated Graphite Oxidized in Air for 20 Minutes at 2050°C at Atmospheric Pressure in an Arc Plasma Jet. Arc Impact Area Appears as Oval-Shaped Light Portion in Center of Photograph.

arc clearly described by the ridges along the specimen. The irregular oval-shaped area in the center of the sample corresponds to the arc plasma impact area. Microscopic examination revealed that in the center of the arc impact area 0.0018-inch iridium had been consumed. On sectioning and metallographic examination, it was found that the coating had remained pore-free and there was no evidence of any erosion of the graphite underneath the coating. The cracks near the outer edges of the coating (Figure 60) developed on cooling and are due to differences in the thermal expansion of iridium and the type of graphite which was used as the substrate.

A cross sectional view of the coating is shown in Figure 61 which is a 133X magnification of the iridium cladding showing a portion of the coating on the side opposite the area upon which the arc plasma impinged. The arrow indicates the exterior of the coating. Surface irregularities represent the very thin slurry coating which covered the iridium sheet. In this particular coating the two turns of iridium that were used for the cladding did not sinter well. The dark area in the center of the metal shows the separation between the two layers of iridium sheet. There appears to be very little erosion on this side of the sample, the surface temperature being much lower than the side contacted by the arc plasma. A section of the coating which was exposed to direct impingement by the arc plasma is shown in Figure 62 (133X magnification). The center of flame contact and the thinnest portion of the remaining coating (see arrow) shows an erosion rate of 1.8 mils for the 20 minutes at 2000°C in the atmospheric tests and is equivalent to 5.4 mils per hour. Again the dark line in the center portion of the light field shows the double layer of the iridium cladding. The erosion had not broken through the 1.5-mil thickness of the exterior sheet.

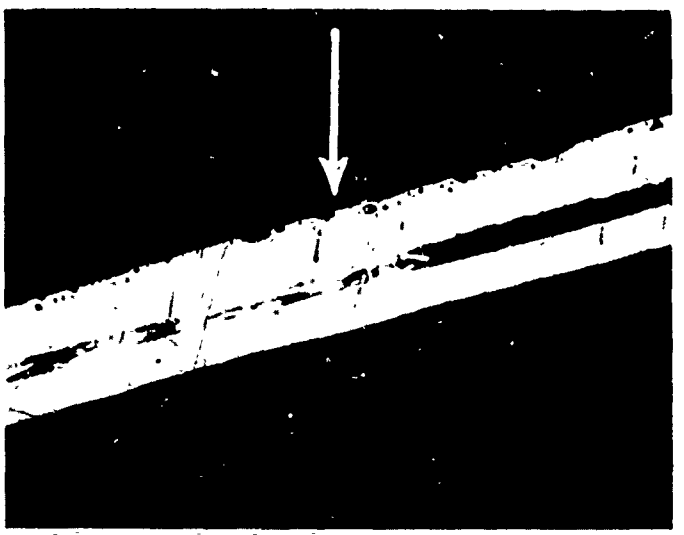

Figure 61. Iridium-Cladding after 20 minutes Oxidation Test at 2000°C at Atmospheric Pressure. The arrow shows a segment of the coating directly opposite the area of arc plasma contact. 133 X Magnification

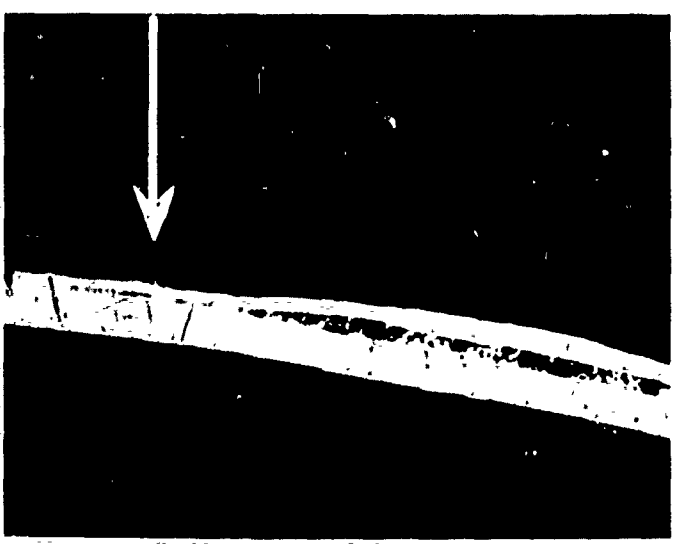

Figure 62. Iridium Cladding after 20 minutes Oxidation Test at 2000°C at Atmospheric Pressure. The arrow shows point of contact with the arc plasma. 133 X Magnification

Specimen A-15 was identical to A-13 and was tested in an identical manner to insure reproducibility of results. This test was also scheduled to last twenty minutes; however, due to arc instability the unprotected end of the sample became so badly eroded after eight minutes that the test had to be terminated to avoid having the sample blown from the support clamps.

The appearance of A-15 after the test is shown in Figure 63. At the left-hand side of the photograph is the portion of the graphite that was uncoated and had eroded to a point so that the test was terminated after eight minutes. The center portion of the test specimen shows the area of contact of the arc plasma. A crack in the center of the coating developed as the sample cooled to room temperature and was probably caused by the differences in the thermal expansion of the iridium and graphite. In general, the test results were the same as for A-13; i. e., the iridium coating had afforded complete protection for the graphite substrate. Due to the shorter testing time, much less iridium (less than 0.001-inch) had been consumed. Time-temperature history and other pertinent data for the test on A-15 are given in Table 42.

Figure 63. Test Specimen A-15 Iridium-Coated Graphite Oxidized in Simulated Air for eight minutes at 2050°C. The left of the photograph shows the deterioration of an uncoated part of the specimen. Center shows the area of arc plasma impact. Shiny area is iridium metal.

TABLE 42

TEST SPECIMEN A-15

Pressure: atmospheric Nozzle: 1 inch Distance from nozzle: $1\frac{5}{8}$ inches
Gas flow: 0.0196 lbs/sec Net enthalpy: 4850 BTU/lbs
* Heat flux: 80 BTU/ft^2/sec

Time (seconds)	Temperature, °C	Time (seconds)	Temperature, °C
30	1955	270	2065
60	2020	300	2080
90	2050	330	2080
120	2065	360	2040
150	2050	390	1995
180	2065	420	1995
210	2080	450	2040
240	2093	460	2040

* The only heat flux data available was that measured on a flat plate test specimen 1 inch x 3 inches.

Specimen JTA-2 was likewise tested for 20 minutes at an average temperature of 2050°C, and its appearance was unchanged except for a white layer in the area of the arc plasma impact. This JTA specimen and that which had been tested at reduced pressure have been turned over to our staff metallographer for investigation of the protective coating and a determination of the phase relationships at the coating-substrate interface. A cross section of the JTA material in the area of the plasma arc impact shows a somewhat uniformly distributed reaction layer around the entire circumference of the specimen with a thickness ranging from 45 to 55 mils for the atmospheric pressure runs and 25 mils thickness for the subatmospheric pressure tests. The detailed test data on JTA-2 are given in Table 43.

Tests at Reduced Pressure

The reduced pressure tests were carried out by firing the plasma arc into a vacuum chamber, where the pressure was maintained at 5 mm Hg by means of a three-stage steam ejector system. A 3-inch supersonic nozzle was used, which for gas flow rates of approximately 0.02 lb/sec gave a calculated plasma velocity of approximately Mach 3.5.

Calibration runs showed that the distance of the specimen from the nozzle had little or no influence on the surface temperature. Temperatures could be adjusted only by varying the input power to the arc plasma generator, which could be done over only a narrow range to prevent arc instability. Fortunately, the conditions were just right for heating an iridium-clad specimen to temperatures between 2050° and 2100°C. The JTA samples, however, could be heated only to 1680°C and a nozzle of different

TABLE 43

TEST SPECIMEN JTA-2

Pressure: atmospheric Nozzle: 1 inch Distance from nozzle: $2\frac{5}{8}$ inches
Gas flow: 0.01999 lbs/sec Net enthalpy: 4170 BTU/lbs
Heat flux: 80 BTU/ft^2/sec

Time (seconds)	Temperature, °C	Time (seconds)	Temperature, °C
30	-	630	1928
60	-	660	1830
90	-	690	1928
120	-	720	1800
150	2080	750	1982
180	2065	780	2012
210	2010	810	1980
240	2100	840	2020
270	2055	870	2068
300	2043	900	2008
330	2093	930	2038
360	1980	960	1985
390	2038	990	2000
420	2024	1020	2010
450	2040	1050	1982
480	2120	1080	2035
510	1928	1110	1982
540	1955	1140	2035
570	1928	1170	2062
600	1982	1180	2065

design would be required to obtain higher temperatures. During the reduced pressure calibration runs, it was also noted that the samples did not heat up uniformly. The hottest zones appeared to be in two areas approximately $\frac{3}{4}$-inch on either side of the center of the plasma arc impact, and it was tentatively assumed that this may be due to a nonuniform flow cross section of the plasma. Surface stagnation pressures were accordingly measured at three spots, at the center, at $\frac{3}{4}$-inch, and at $1\frac{1}{2}$ inches away from the center of the arc impact; and they were found to be 48.3, 46.0, and 35.5 mm Hg, respectively. This variation in pressure does not explain the nonuniform heating and the real reason for it remains unknown. Since temperatures were read from an area close to the center, the measured temperatures may be 50° to 100°C lower than the maximum surface temperatures of the specimen.

An iridium-clad specimen, A-14, was tested under these conditions at temperatures close to 2100°C. After seven minutes, the cathode failed; and the test had to be interrupted. Figure 64 shows a photograph of A-14 after

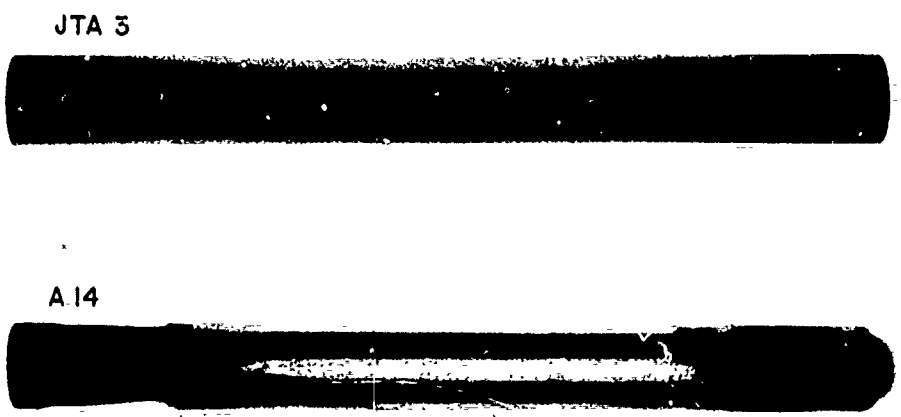

Figure 64. Samples after Oxidation Test at an Air Stagnation Pressure of 48 torr at Supersonic Gas Velocity. A-14 is iridium-clad graphite which was tested at 2000°C for seven minutes. JTA-3 was tested at 1600° to 1700°C for twenty minutes.

the test. There was no discernible erosion of the arc impact area, and the coating appears to be completely unaffected. At the left of the photograph is shown the badly eroded, unprotected end of the graphite rod; since the specimen could no longer be securely clamped, testing was not resumed. The detailed data for this run are given in Table 44.

TABLE 44

TEST SPECIMEN A-14

Pressure: reduced Nozzle: 3 inches Distance from nozzle: 17 1/4 inches
Gas flow: 0.0195 lbs/sec Net enthalpy: 4565 BTU/lbs
*Heat flux: 78 BTU/ft^2/sec

Time (seconds)	Temperature, °C
30	2100
60	2130
90	2093
120	2030
150	2082
180	2078
210	2090
240	2062
270	2060
300	2058
330	2010
360	2043
390	1490
420	Note: Cathode failed

* The only heat flux data available was that measured on a flat plate test specimen 1 inch x 3 inches.

A photograph of the cross section of A-14 magnified 6.7 times appears in Figure 65. The arrow shows the point of the plasma impingement. The top center of the photograph represents the center of arc plasma contact. The cracks in the center of the graphite are not due to the oxidation test. Figure 66 shows a 133 X magnification of the iridium and the iridium-graphite interface at the point of arc plasma contact. The thick, uniform, light portion of the photograph is the iridium cladding, and the irregular portion is the fused iridium coat which was applied by the slurry dip process. This particular specimen shows excellent fusion of the two layers of iridium sheet used for the cladding. The irregularity of the exterior surface of the coat represents a thin layer (1/2-mil thick) of the external slurry dip coating.

As already mentioned, JTA samples could only be heated between 1600° and 1700°C in the reduced pressure runs. One specimen, JTA-3, was tested under these conditions for 20 minutes and a photograph of this specimen is shown in Figure 64. Microscopic examination of the JTA shows a reaction layer 25 mils thick. This specimen will also be investigated further

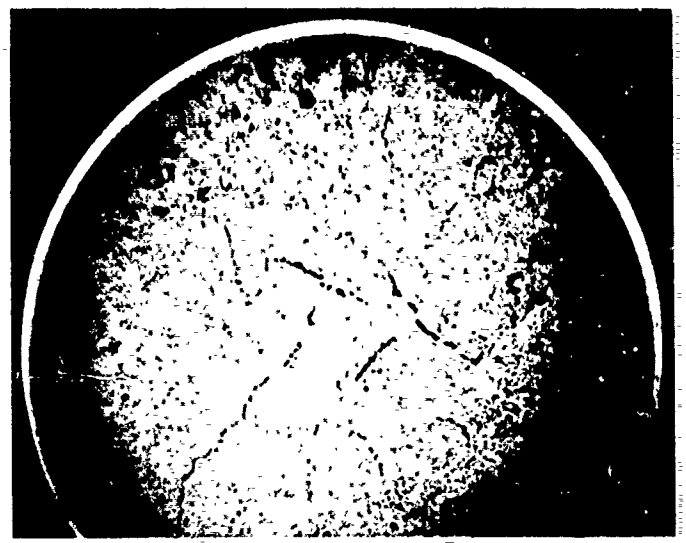

Figure 65. Cross Section of Iridium Coated Graphite after Oxidation test at 2000°C, 48 torr air pressure Supersonic gas Velocity, seven minutes. (6.7 X Magnification)

Figure 66. The Iridium-Coated Graphite after Oxidation at 2000°C, 48 torr air pressure, Showing Area of Arc Plasma Impact (133 X Magnification)

along with the JTA specimen that was tested at atmospheric pressure. The detailed test conditions are given in Table 45.

TABLE 45

TEST SPECIMEN JTA

Pressure: reduced Nozzle: 3 inches Distance from nozzle: 17 1/4 inches
Gas flow: 0.01973 lbs/sec Net enthalpy: 4510 BTU/lbs
Heat flux: 80 BTU/ft^2/sec

Time (seconds)	Temperature, °C	Time (seconds)	Temperature, °C
30	1830	650	1633
60	1727	680	1644
90	1705	710	1650
120	1690	740	1655
150	1732	770	1657
180	1545	800	1667
230	1537	830	1655
260	1558	860	1662
290	1568	890	1662
320	1560	920	1669
350	1580	950	1671
380	1593	980	1677
410	1593	1010	1685
440	1613	1040	1682
470	1621	1070	1687
500	1621	1100	1677
530	1621	1130	1685
560	1627	1160	1690
590	1618	1190	1704
620	1621	1200	1685

Conclusions of Torch Tests

Iridium provided excellent high temperature (2000° to 2100°C) protection for graphite in air at pressures ranging from atmospheric to subatmospheric. An ablation rate of 5.4 mils per hour was observed in the runs at atmospheric pressure; whereas, the ablation rate during the subatmospheric test run was so small that we were unable to measure this quantity. Photomicrographs of the graphite-iridium interface show no erosion of the substrate.

The iridium coating cracked in several places upon cooling after the the tests at atmospheric pressure. This behavior suggests a mechanical incompatibility due to 20 per cent difference in the thermal expansion of iridium and graphite used. The present incompatibility can be eliminated by

using the new especially high CTE (6-7 x 10^{-6} in/in/°C) graphites now under development.

The JTA composite exhibited good oxidation protection in that the external appearance of the specimen did not show any erosion. However, a reaction layer of appreciable thickness did form during the atmospheric test as well as the subatmospheric test. The reaction layer extended to a depth of 55 mils for the 20 minutes, 2000°C atmospheric pressure test and to 25 mils for the 20 minutes, 1600° to 1700°C subatmospheric pressure test.

Thompson Ramo Wooldridge Tests

Plasma torch oxidation tests were also conducted at Thompson Ramo Wooldridge, Inc., Euclid, Ohio, on two iridium-coated graphite samples. The test specimens consisted of rods $^1/_2$-inch diameter x 5 inches long coated with iridium over a length of four inches by the slurry-dip and sintering technique described in Section VIII. The coating thickness varied between 0.002- and 0.003-inch. One test was conducted at atmospheric pressure, the other at reduced pressure. In both cases, the surface temperature in the center of the plasma arc impact area exceeded the carbon-iridium eutectic temperature of 2110°C, so that failure occurred due to melting of the iridium coating. The conditions are listed in Table 46 for the test at atmospheric pressure and in Table 47 for the tests at reduced pressure.

TABLE 46

TEST A, CONDITIONS* AT ATMOSPHERIC PRESSURE

Velocity	2800 to 3000 ft/sec
Plasma Composition	80% N_2, 20% O_2
Plasma Temperature	6500°F (~ 3575°C)
Heat Flux	460 to 500 BTU/ft^2 sec
Distance of Specimen from Nozzle	$^3/_4$-inch
Coating Melted after 70 sec.	

*Data supplied by Thompson Ramo Wooldridge, Inc. personnel.

TABLE 47

TEST B, CONDITIONS* AT REDUCED PRESSURE

Velocity	Unknown
Plasma Composition	80% N_2, 20% O_2
Plasma Temperature	6500°F (~ 3575°C)
Heat Flux	325 BTU/ft^2 sec
Plasma Pressure	18 mm Hg
Tank Pressure	8 mm Hg
Coating Melted after 14 minutes	

*Data supplied by Thompson Ramo Wooldridge, Inc. personnel.

A metallographic examination of the specimen from Test A demonstrated that the failure was due to melting of the iridium coating; i. e., the surface temperature had exceeded the carbon-iridium eutectic temperature of 2115°C. The photomicrographs also show that the coating, which had been deposited by slurry dipping and sintering techniques, was somewhat porous. This porosity may have been a factor contributing to the failure since corrosion of the substrate beneath the coating would tend to facilitate localized overheating.

Figure 67 is a cross sectional view of the test specimen. The numbers drawn in Figure 67 correspond to the areas shown at 60 X magnification in the photomicrographs, Figures 68 through 71. Figure 68, area No. 2 of Figure 67 depicts the essentially undamaged coating. The white area represents the iridium coating; underneath is the graphite substrate. In Figure 69, area No. 3 of Figure 67, the coating is still intact; but the graphite underneath has been burned away as shown by the black portion of the picture. Figure 70, area No. 4 of Figure 67, shows the area of initial breakthrough; the drop of molten iridium is clearly visible (upper left corner of the photograph). The substrate has been completely corroded at the coating-substrate interface. Flaws in the slurry dip coating are demonstrated in Figure 71, area No. 5 of Figure 67, which clearly shows pores in the coating and voids in the substrate material. The latter may be due to corrosion during the oxidation test.

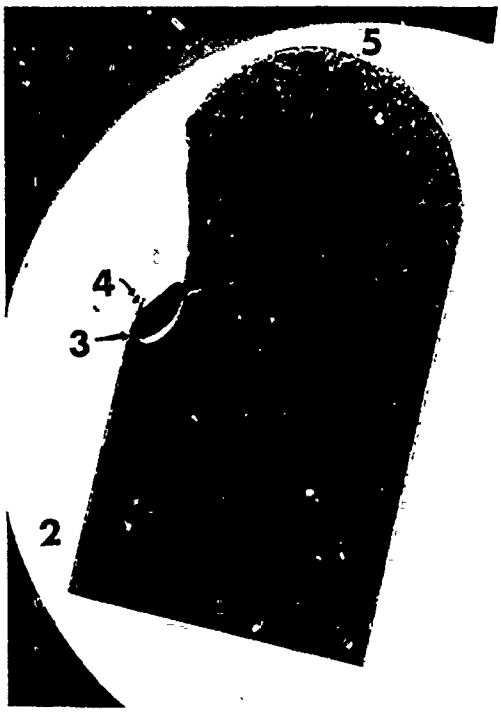

Figure 67. Cross Section of Iridium Coated Graphite

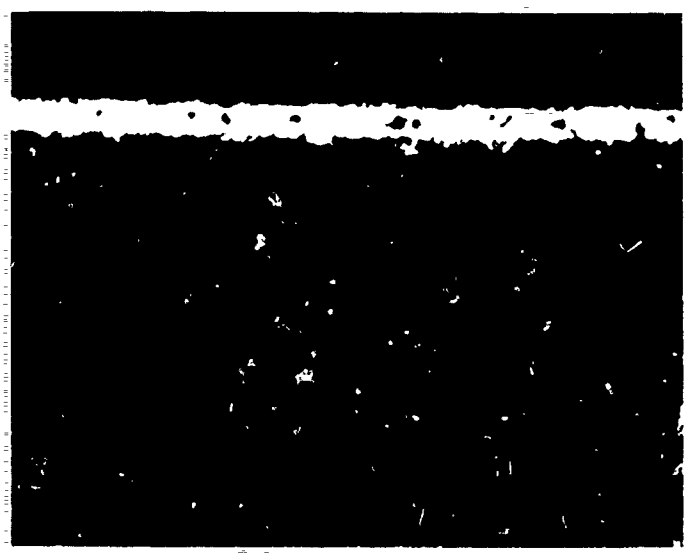

Figure 68. Iridium Coated Graphite — Showing Surface away from Arc Plasma, 50 X Magnification

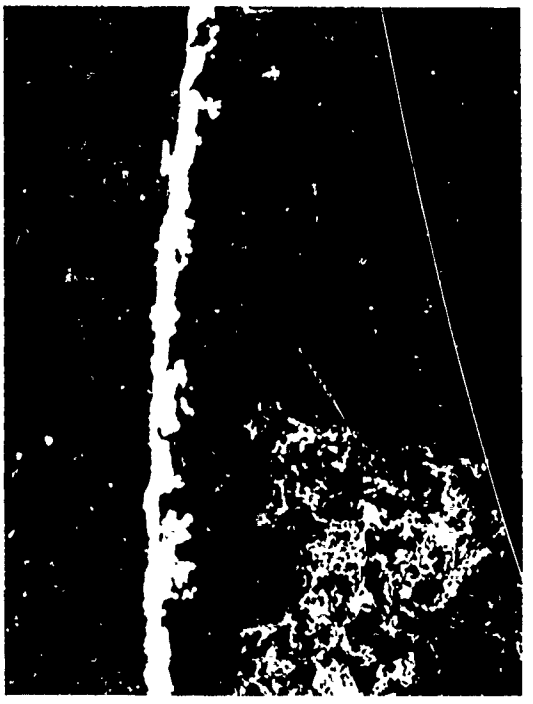

Figure 69. Iridium Coated Graphite — Black Area Shows Corroded Substrate, 60X Magnification

Figure 70. Iridium Coat Showing Globule of Metal which had been Melted at the Area of Arc Impact, 60X Magnification

Figure 71. Iridium Coated Graphite Showing pores in the Coating and Corroded Substrate (black area), 60X Magnification

REFERENCES

1. Criscione, J. M., et al., High Temperature Protective Coatings for Graphite, ML-TDR-64-173, Part I, AF Materials Laboratory, Wright-Patterson Air Force Base, Ohio (June 1964).

2. Passmore, E. M., Boyd, J. E., Neal, L. P., Anderson, C. A., and Lement, B. S., Investigation of Diffusion Barriers or Refractory Metals, WADD TR-60-343, Wright Air Development Division, Wright-Patterson Air Force Base, Ohio (August 1960).

3. Fryburg, G. C., and Petrus, H. M., J. Electrochem. Soc. 108, 496 (1961).

4. Burgess, G. K., and Waltenberg, R. G., Bull. Bur. Standards 13, No. 280, 365 (1916-17).

5. Kubaschewski, O., Z. Electrochem. 49, 446 (1943).

6. Fryburg, G. C., and Murphy, H. M., Trans. AIME 660 (1958).

7. Krier, C. A, and Jaffee, R. I., J. Less Common Metals 5, 441 (1963).

8. Zysk, E. D., Toenshoff, D. A., and Penton, J., Englehard Ind. Tech. Bull. 4, 52 (1963).

9. Crookes, W., Chem. News 105, 229 (1912); C. A. 2, 2895 (1912).

10. Alcock, C. B., and Hooper, G. W., Proc. Roy. Soc. A254, 557 (1960).

11. Cordfunke, E. H. P., and Meyer, G., Rec. Tran. Chim. 81, 495 (1962).

12. Schäfer, H., and Heitland, H. J., Z. Anorg. Allg. Chem. 304, 249 (1960).

13. Gulbransen, E. A., Andrew, K. F., and Brassart, F. A., J. Electrochem. Soc. 110, 476 (1963).

14. Wagner, C., J. Appl. Phys. 29(a), 1295 (1958).

15. Modisette, J. L., and Schryer, D. R., NASA TND-222.

16. Waber, J. T., "Metals for Supersonic Aircraft and Missiles," American Society for Metals, Cleveland (1958).

17. Cordfunke, E. H. P., and Meyer, G., Rec. Tran. Chim. 81, 671 (1962).

18. Wöhler, L., and Witzmann, W., Z. Anorg. Chem. 57, 323 (1908).

19. Cheston, J. C., Pt. Metals Rev. 8:50-54 (April 1964).

20. Fast, J. D., Phillips Technical Review 6, 365 (1941); 7, 73 (1942).

21. Barrer, R. M., Diffusion in and Through Solids, Cambridge University Press (1951).

REFERENCES (Cont'd)

22. Hayes, D., Budworth, D.W., and Roberts, J.D., Trans. Brit. Ceram. Soc. 62, 507 (1963).

23. Moore, D.G., Symposium on Measurement of Thermal Radiation of Solids, Dayton, Ohio (September 1962).

24. Goldwater, D.L., and Danforth, W.E., Phys. Rev. 103, 871 (1956).

25. Smith, A.W., "Actes De Deuxième Congres International De Catalyse," Paris 1960, Editions Tedenip, Paris (1961), P. 1711.

26. Johnson, F.M.G., and Larose, T., J. Am. Chem. Soc. 49, 321 (1927).

27. Dushman, S., Scientific Foundation of Vacuum Technique, John Wiley & Sons, New York (1949) pp. 81-108.

28. Dickinson, C.D., and Nicholas, ASD-TDR-62-205, June (1963), Aeronautical Systems Division, Wright-Patterson Air Force Base, Ohio.

29. Kingery, W.D., Pappis, J., Doty, M.E., and Hill, D.C., J. Am. Ceram. Soc. 42, 393 (1959).

30. Douglass, D.L., Conference on Corrosion of Reactor Materials, AIEA, Salzburg, June (1962) Vol. 2, P. 223.

31. Aronson, S., J. Electrochem. Soc. 108, 312 (1961).

32. Debuigne, J., and Lehr, P., Comp. Rend. 256, 1113 (1963).

33. Cubicciotti, D., J. Am. Chem. Soc. 72, 4138 (1950).

34. Hund, F., Z. Phys. Chem. 199, 142 (1952).

35. Kiukkola, K., and Wagner, C., J. Electrochem. Soc. 104, 379 (1957).

36. Kofstad, P., and Ruzicka, D.V., J. Electrochem. Soc. 110, 181 (1963).

37. McCline, L.A., ASD-TDR-62-204, Part II, May (1963), Aeronautical Systems Division, Wright-Patterson Air Force Base, Ohio.

38. Rodes, W.H., and Carter, R.E., Bull. Am. Ceram. Soc. 41, 283 (1962).

39. Tien, T.Y., J. Appl. Phys. 35, 122 (1964).

40. Mott, N.F., and Gurney, R.W., "Electronic Processes in Ionic Crystals," Clarendon Press, Oxford (1940).

41. Bray, D.T., and Merten, U., J. Electrochem. Soc. 111, 447 (1964).

42. Smeltzer, W.W., and Simnad, M.T., Acta Met. 5, 328 (1957).

REFERENCES (Cont'd)

43. Edwards, H.S., Rosenberg, A.F., and Bittel, J.T., ASD-TDR-63-635 (Contract No. AF 33(657)-8470; General Electric Company) July (1963).

44. Gerds, A.F., and Mallett, M.W., J. Electrochem. Soc. 101, 171 (1954).

45. Foex, M., Compt. Rend. 215, 57 (1942).

46. Holborn, L., Henning, F., and Austin, L., Abh. Phys. Techn. Reichsanstalt 4, No. 1 (1904) 93.

47. Lewis, J.G., Ohlgren, H.A., U.S. Pat 3, 101, 403.

48. Steinberg, M.A., U.S. Pat. 2, 979, 814.

49. Nadler, M.R., Kempter, C.P., J. Phys. Chem. 64, 1468 (1960).

50 Raub, E., Falkenberg, G., Z. Metallkunde 55, 186 (1964).

51. Withers, J.C., and Ritt, P.E., Proc. AES 44, 124 (1957).

52. Campbell, I.E., "Vapor Deposition of High Temperature Coatings" in High Temperatures, A Tool for the Future, Proceedings of a Symposium held in Berkeley, California, June 25-28 (1956).

53. Powell, C.F., Campbell, I.E., Gonser, B.W., "Vapor Plating," John Wiley & Sons, New York (1955).

54. Reerink, E.H., Z. Anorg. Allgem. Chem. 143, 45 (1928).

55. Reerink, E.H., (to N.V. Philips) U.S. Pat. 1, 818, 909, August 11 (1931).

56. Hieber, W., Lagally, H., and Mayr, A., Z. Anorg. Allgem. Chem. 246, 138 (1941).

57. Biltz, W., Z. Anorg. Chem. 89, 160 (1914).

58. Remy. H., Z. Anorg. Chem. 137, 366 (1924).

59. General Atomic, General Dynamics, "The High Temperature Chemistry of Fission Product Elements, Summary Reports GA-4500, August 1, 1962 to July 31, 1963; GA-3398, August 1, 1961 to July 31, 1963; GA-2512, August 1, 1960 to July 31, 1961.

60. Hieber, H., and Lagally, H., Z. Anorg. Allgem. Chem. 245, 321 (1940).

61. Dwight, A. E., and Beck, P.A., "Close-Packed Ordered Structures in Binary AB_3 Alloys of Transition Elements," Trans. of Met. Soc. AIME 215 (976-9) December (1959).

62. ASTM Powder Diffraction File 9-368

63. ASTM Powder Diffraction File 6-0598

64. Private communication, data from M. I. Copeland supplied by L. L. Oden, United States Bureau of Mines, Albany, Oregon.

65. Kroll, W.J., and Schlechtor, A.W., Electrochem. Soc. Trans. 93, 247 (1948).

66. Johnson, P.D., J. Am. Ceram. Soc. 33(5), 168-71 (1950).

67. Komarek, K.L., Coucoulas, A., and Klinger, N., J. Electrochem. Soc. 110, 783 (1963).

68. Muratov, F.Sh., and Novoselova, A.V., Doklady Akad. Nauk SSSR 129, 334-6 (1959).

69. Prescott, C.H., Jr., J. Am. Chem. Soc. 48, 2534 (1926).

70. Kutsev, V.S., Ormont, B.F., and Epelbunm, Doklady Akad. Nauk. SSSR 104, No. 4, 567-70 (1955).

71. Zhelankin, V.I., Kutsev, V.S., and Ormont, B.F., Zhurnal Neorganisheskoi Khimii, Vol. III, No. 5, 1237-1240 (1958).

72. Prescott, C.H., Jr., and Hincke, W.B., J. Am. Chem. Soc. 49, 2744 (1927).

73. Nadler, M.R., and Kempter, C.P., The Review of Scientific Instruments 32, 43 (1961).

74. Chemistry of the Solid State, edited by W.E. Garner, New York Academic Press, Inc., Publisher (1955), p. 305.

75. Zhelankin, V.I., Kutsev, V.S., and Ormont, B.F., Russian Journal of Physical Chemistry 35, 1288 (1961).

76. High-Temperature Technology, Ed., Campbell, I.E., John Wiley & Sons, Inc., New York (1956).

77. Brewer, L., et al., The Thermodynamic Stability of the Refractory Borides, Electrochem. Soc. J. 102:399-406 (1955).

78. Glasser, F.W., Pressure Sintering of Pure (uncemented) Zirconium Diboride at Temperatures above 2500°C, Powder Met. Bult. 6, 51 (1951).

79. Feisel, D.H., "Some Metallurgical Observations of the Transition Metal Borides," Program of the 1962 Fall Meeting of Metallurgical Society of AIME.

80. Popper, P., Special Ceramics Academic Press Inc., New York (1960), Chapter 18, Jackson, J.S., and Palmer, P.E., "Hot Pressing Refractory Hard Materials" p, 318.

81. Wood, A. A. R., A private communication included in following reference.

82. Chown, J., et al. "Refractory Coating on Graphite with some Comments on the Ultimate Oxidation Resistance of Coated Graphite," Part II, British Ceramics Research Association Symposium on Special Ceramics (11 July 1962).

83. Edwards, H. S., Rosenberg, A. F., and Bittel, J. T., ASD-TDR-63-635 (Contract No. AF 33(657)-8470; General Electric Company) July (1963).

84. Nowotny, H., Rudy, E., and Benesovsky, F., "Investigations in the Systems Hafnium-Boron-Carbon and Zirconium-Boron-Carbon," Monatshefte 92:393-402 (1961).

85. Sara, R. V., Private communication (1964), Union Carbide Corporation, Parma Research Center, Parma, Ohio

86. Kaufman, L., and Clougherty, E. V., Investigation of Boride Compounds for Very High Temperature, ManLabs, Inc., p. 356.

87. Lowrie, R., Goldstein, H. W., and Trulson, O. C., Research on Physical and Chemical Principles Affecting High Temperature Materials for Rocket Nozzles, Union Carbide Research Institue, Contract No. DA-30-069-ORD-2787.

APPENDIX A

THEORETICAL CALCULATIONS OF THE RATE OF ABLATION OF IRIDIUM IN AIR AT HYPERSONIC FLIGHT CONDITIONS

Calculations were performed to obtain an order of magnitude value for the required thickness of an iridium coating. In addition, the calculations gave a better definition of the research problem since they helped to clarify those areas where data are incomplete or missing and where experimental work is most urgently required. The vapor pressure of iridium[1, 2] is quite low. The maximum rate of evaporation (e.g., evaporation into a vacuum) was calculated from the vapor pressure data using the Langmuir formula.[3] The results are listed in Table 1 and show that evaporation of iridium will be negligible at temperatures up to at least 2100°C.

TABLE 1

EVAPORATION RATE OF IRIDIUM

Temp.	Vapor Pressure	Evaporation Rate	
°C	mm Hg	g cm^{-2} sec^{-1}	mils/hour
1900	4.8×10^{-6}	8.3×10^{-8}	5.3×10^{-3}
2000	2.2×10^{-5}	3.8×10^{-7}	2.4×10^{-2}
2100	9.3×10^{-5}	1.5×10^{-6}	9.5×10^{-2}
2200	3.5×10^{-4}	5.6×10^{-6}	0.35
2300	1.1×10^{-3}	1.8×10^{-5}	1.14
2400	3.5×10^{-3}	5.4×10^{-5}	3.40

The usefulness of an iridium coating is limited by the oxidation resistance of iridium. Some data on the weight loss of iridium in an atmosphere containing oxygen and/or water vapor are reported in the literature [4, 5, 6] indicating rather low and quite tolerable weight losses. However, closer analysis showed that under the experimental conditions used in the above investigations the rate of weight loss was diffusion controlled. Under hypersonic flight conditions, diffusion is much more rapid than in still or slowly moving air and the rate of weight loss will therefore be greatly increased.

At temperatures above 1200°C, oxidation of iridium is described by the reaction:

$$Ir_{(s)} + {}^{3}/_{2}O_2 \rightarrow IrO_{3(g)} \cdot \qquad (1)$$

The thermodynamics of this reaction have recently been investigated by three independent groups[7, 8, 9] and the results are in good agreement. In

the temperature range 1000° to 1450°C, the equilibrium constant can be expressed as

$$\log_{10} K_p = -2.358 - \frac{900}{T} \tag{2}$$

where

$$K_p = P_{IrO_3}/P_{O_2}^{3/2} \tag{3}$$

(p = atmospheres).

Since the vapor pressure of iridium is very low, Equation (1) is undoubtedly a gas solid reaction. No data on the kinetics of this reaction are available. We, therefore, assumed that in the temperature range 1400° to 2000°C, the rate of reaction is so rapid that the iridium surface is essentially covered with a layer of IrO_3. The rate of weight loss is then determined by the slower of two processes:

(i) the rate of removal of IrO_3 from the surface;

or (ii) the rate of transport (convection, concentration-diffusion and thermal-diffusion) or IrO_3 through the boundary layer.

Certain necessary assumptions and simplifications are helpful at this point:

(a) Iridium trioxide is the only gaseous iridium containing species.

(b) If point (a) is valid, one can assume that Equation (2) for the equilibrium constant can be extrapolated to 2000°C.

(c) Atomic oxygen, produced in the shock wave in front of the leading edge, does not alter the thermodynamic equilibrium expressed by Equation (2). Atomic oxygen recombining on the iridium surface will likely increase the rate of formation of IrO_3[10, 11, 12]. This condition is permissible since we have already assumed that the rate of reaction is so fast that it will not control the over-all rate of weight loss. However, reactions such as $IrO_3 + \overline{O} \rightarrow IrO_2 + O_2 \rightarrow Ir + 2O_2$ are not taken into account.

(d) For numerical calculations from boundary layer theory, the transport properties of IrO_3 are assumed to be the same as the transport properties of the environment (air) at the same temperature. This assumption is the only case for which the complicated equations can be solved, but it is likely to lead to somewhat high values for the weight loss since the diffusion coefficient of IrO_3 differs from that of air by a factor $(M_{air}/M_{IrO_3})^{1/2} \simeq (30/240)^{1/2} = 0.35$. Also, thermal diffusion would tend to drive IrO_3 towards the coolest point, the iridium surface.

(e) Spalling and sputtering are neglected.

The rate of removal of IrO_3 from the surface can be calculated from kinetic gas theory. Langmuir[3] has shown that the rate of evaporation of a substance into its own vapor pressure is given by:

$$\dot{m} = a\,P\left(\frac{M}{2\pi R T}\right)^{1/2} \tag{4}$$

The accommodation coefficient (sticking factor) a is, in the absence of experimental determinations, usually assumed to be equal to one.

For the rate of evaporation into a foreign gas, Scala and Vidale[13] derive from kinetic gas theory:

$$\dot{m}_i = \left[\frac{a\,P\overline{M}}{(2\pi R M_K T_i)^{1/2}}\right] (C_{K_{eq}} - C_{K_i}) , \tag{5}$$

where:

$\dot{m}_i$ = Rate of weight loss

a = Accommodation coefficient

$\overline{M}$ = Mean molecular weight of surrounding gas

M_K = Molecular weight of evaporating species

P = Total pressure

T_i = Surface temperature

$C_{K_{eq}}$ = Equilibrium concentration of evaporating species on the surface

C_{K_i} = Concentration of evaporating species one mean free path away from surface

Since

$$C_K = \left(\frac{P_K M_K}{P\overline{M}}\right) . \tag{6}$$

Equation (5) is reduced to

$$\dot{m}_i = \frac{a(M_K)^{1/2}}{(2\pi R T_i)^{1/2}} (P_{K_{eq}} - P_{K_i}) \tag{7}$$

Equation (7) is identical with the Langmuir formula [Equation (4)] except for $P_{K_{eq}}/(P_{K_{eq}} - P_{K_i})$. This factor depends upon the rate at which the evaporating species is transported from the source and can be evaluated by taking both kinetic and boundary layer theory into account.

The rate of diffusion through the boundary layer depends on altitude (pressure), flight speed, surface temperature, and the geometry of the nose cone or leading edge.[13] Some necessary assumptions regarding transport properties and thermal diffusion have already been mentioned. The problem is finally expressed by a coupled ninth order system of nonlinear differential equations with split boundary conditions. Solutions for a great number of representative flight speeds, altitudes, and wall temperatures have been obtained with the aid of a computer. According to Scala and Vidale,[13] an equation which represents all the data within 15 per cent error may be written as the product of the three factors which depend on temperature, altitude, and flight speed.

$$\frac{\dot{m}_i (R_B)^{1/2}}{C_{K_i}} = \left[1.233 - 6.6667 \times 10^{-5} T_i\right] \times \left[10^{-(4.3243 + 3.9668 \times 10^{-6}\ \mathrm{Alt})}\right] \times \left[V_\infty (0.9576 - 1.201 \times 10^{-6}\ \mathrm{Alt})\right] \quad (8)$$

Where:

T_i = Wall (surface) temperature in °R

Alt = Altitude in feet

V_∞ = Flight speed in feet/sec.

$\dot{m}_i$ = Weight loss in lb/sq. ft. sec.

R_B = Nose cone radius in feet.

Comparing Equation (8) with Equation (5), one may see that the weight loss according to boundary layer theory is proportional to C_{K_i}, whereas the weight loss calculated from kinetic theory is proportional to $(C_{K_{eq}} - C_{K_i})$. Therefore, if the weight losses calculated from the two theories are plotted on the same graph as a function of C_{K_i} (expressed in fractional units of $C_{K_{eq}}$), the intercept of the two straight lines determines the concentration at one mean free path away from the surface, C_{K_i} real.

Calculations were performed for surface temperatures of 1400° and 2000°C, at an altitude of 20,000 meters (66,000 feet), nose cone radius of 30 cm (one foot), and flight speeds of Mach 10 and Mach 20. These appear to be representative and mutually compatible conditions according to Bloom[14] and to Masson and Gazley.[15] The results are listed in Table 2.

TABLE 2

WEIGHT LOSS OF IRIDIUM AT AN ALTITUDE OF 66,000 FEET

Kinetic theory, maximum rate ($C_{K_i} = 0$)

Temp. °C	$C_{K_{eq}}$	Accom. Coeff. α	P_{O_2}(mm Hg)	$\dot{m}_i$[$g_{Ir}\ cm^{-2}\ sec^{-1}$]
1400	2.34×10^{-4}	1	10	2.6×10^{-5}
1400	2.34×10^{-4}	0.5	10	1.3×10^{-5}
2000	3.23×10^{-4}	1	10	3.07×10^{-5}
2000	3.23×10^{-4}	0.5	10	1.54×10^{-5}

Boundary layer theory, maximum rate $C_{K_{eq}} R_B = 1$ ft.

Temp °C	$C_{K_{eq}}$	P_{O_2}(mm Hg)	Flight Speed	$\dot{m}_i$[$g_{Ir}\ cm^{-2}\ sec^{-1}$]
1400	2.34×10^{-4}	10	Mach 10	1.2×10^{-5}
1400	2.34×10^{-4}	10	Mach 20	2.4×10^{-5}
2000	3.23×10^{-4}	10	Mach 10	1.5×10^{-5}
2000	3.23×10^{-4}	10	Mach 20	3.1×10^{-5}

Combined kinetic and boundary layer theory $C_{K_i} = C_{K_{i\ real}}$

Temp. °C	Flight Speed	Accom. Coeff. α	$\dot{m}_i$[$g_{Ir}\ cm^{-2}\ sec^{-1}$]	Ablation Rate (Inches of Iridium per Hour)
1400	Mach 10	1	8.2×10^{-6}	5.2×10^{-4}
1400	Mach 20	1	12.4×10^{-6}	7.8×10^{-4}
1400	Mach 10	0.5	6.2×10^{-6}	3.9×10^{-4}
1400	Mach 20	0.5	8.4×10^{-6}	5.3×10^{-4}
2000	Mach 10	1	10.0×10^{-6}	6.3×10^{-4}
2000	Mach 20	1	15.4×10^{-6}	9.7×10^{-4}
2000	Mach 10	0.5	7.5×10^{-6}	4.7×10^{-4}
2000	Mach 20	0.5	10.0×10^{-6}	6.3×10^{-4}

Under the above conditions and assumptions, the ablation rate of iridium should not exceed 1.1×10^{-3} inches per hour. The ablation rates at other altitudes will differ from the rate at 20,000 meters primarily because of the difference in pressure. Because P_{IrO_3} is proportional to $(P_{O_2})^{3/2}$

[Equation (3)], a tenfold increase (or decrease) in pressure will increase (or decrease) the ablation rate by a factor of $10^{3/2}$ or 31.6. It must be pointed out, however, that at higher pressures the theoretical basis of these calculations becomes increasingly invalid. Therefore, the above relation between ablation rate and pressure should be used for extrapolation towards lower pressures (higher altitudes) only.

The ablation rates calculated here appear tolerable. It is of further interest to discuss those factors which may decrease the ablation rate, but could not be taken into account because the experimental data are lacking. The rate of reaction between iridium and oxygen may not be as fast as assumed, and could become the rate determining step. Kinetic data on the reaction of iridium with molecular and atomic oxygen are therefore urgently needed. Furthermore, the accommodation coefficient α was assumed to be somewhere between 0.5 and 1, which is generally the case; however, for some complicated high temperature evaporation reactions, values of α as low as 10^{-6} have been found.[16-21] Finally, the equilibrium $Ir + {}^3/_2\, O_2 \rightleftharpoons IrO_3$ has only been measured up to 1450°C, and data at higher temperatures are needed. In analogy to IrO_2, which decomposes at 1100°C,[9] IrO_3 will at some higher temperature become thermodynamically unstable. Above this decomposition temperature, there would be no reaction at all between iridium and oxygen.

REFERENCES

Appendix A

1. R. F. Hampson, Jr. and R. F. Salker, J. Res. Natl. Bur. Standards 65A, 289 (1961).

2. M. B. Panish and L. Reif, J. Chem. Phys. 34, 1915 (1961).

3. I. Langmuir, Phys. Rev. 2, 329 (1913).

4. L. Holborn, F. Henning, and L. Austin, Abh. Phys. Techn. Reichsanstalt 4, No. 1, 93 (1904).

5. F. Emich, Monatsh. Chem. 29, 1080 (1908).

6. R. W. Douglas, C. A. Krier, R. I. Jaffee, "High Temperature Properties and Alloying Behavior of the Refractory Platinum Group Metals," AD-265624, August 1961, pp. 130-165.

7. H. Schafer, H. J. Heitland, Z. Anorg. Allg. Chem. 304, 249 (1960).

8. C. B. Alcock, G. W. Hooper, Proc. Roy. Soc. A254, 551 (1960).

9. E.H.P. Cordfunke, G. Meyer, Rec. Trav. Chim. 81, 495 (1962).

10. G. C. Fryburg, J. Chem. Phys. 24, 175 (1956).

11. G. C. Fryburg, H. M. Petrus, J. Chem. Phys. 32, 622 (1960).

12. K. Mitani, Y. Harano, Bull. Chem. Soc. of Japan 33, 276 (1960).

13. S. M. Scala, G. L. Vidale, "Vaporization Processes in the Hypersonic Laminar Boundary Layer," G. E. Technical Information Series No. R-59, SD 323, January 25, 1959.

14. M. H. Bloom, "External Sources of Heat," in High Temperature Effects in Aircraft Structures, N. J. Hoff, ed., Pergamon Press, New York (1958).

15. D. J. Masson, C. Gazley, Jr., Aero Eng. Rev. 15, No. 11, p. 46. (1956).

16. L. Brewer, J. S. Kane, J. Phys. Chem. 59, 105 (1955).

17. R. J. Thorn, G. H. Winslow, J. Chem. Phys. 26, 186 (1957).

18. I. N. Stranski, G. Wolff, Research (London) 4, 15 (1951).

19. J. R. Soulen, P. Sthapitanonda, and J. L. Margrave, J. Phys. Chem. 59, 132 (1955).

REFERENCES (Cont'd.)

20. H. Spingler, Z. Phys. Chem. B52, 90 (1942).

21. M. Hoch, and D. White, "The Vaporization of Boron Nitride and Aluminum Nitride," Ohio State University, Research Foundation, Report No. MCC 1023-RT-214 (1956).

APPENDIX B

PROCEDURES USED IN METALLOGRAPHIC ANALYSIS*

Specimen Mounting

Samples for microscopic examination were diamond-saw cut to show representative cross sections. Those specimens having sufficient rigidity and size were mounted in Lucite powder with a Buehler Speed Press, while others were set up with liquid epoxy.

Specimen Preparation

The oxide specimens were prepared on motorized laps using progressively finer diamond and alumina sizes. During the intermediate stages, lead-tin laps were used to maintain plane surfaces; during the final stages, napless cloth laps were used to maintain plane surfaces. The iridium and rhodium specimens were prepared in a similar manner, however, a short-napped microcloth was used in the final stage to provide a more scratch-free surface. Final polish was accomplished by using a Buehler Whirlimet polishing unit.

Etching procedures were not used in treating the oxide specimens; however, several etching procedures including common acids, sodium hypochlorite, aqua regia at elevated temperature, and d.c. electrolysis were attempted to reveal grain size and structure of the iridium and rhodium specimens. The only successful procedure involved a.c. electroetching. The mounted iridium and rhodium specimens were etched for thirty-five minutes in a 20 per cent aqueous HCl electrolyte at approximately 125 ma.

The following outline describes the polishing sequence for the oxide and metal specimens.

A. ZrO_2, HfO_2, ThO_2

1. Silicon carbide papers, 240-600 grit.
2. No. 15 grade diamond, lead-tin lap.
3. No. 3 grade diamond, nylon cloth.
4. 0.3 micron Linde A, nylon cloth.
5. 0.1 micron Linde B, nylon cloth.

B. Ir, Rh

1. Silicon carbide papers, 240-600 grit.
2. No. 3 grade diamond, lead-tin lap.
3. 0.3 micron Linde A, nylon cloth.
4. 0.1 micron Linde B, microcloth.

Microscopic Examination

Specimens were examined and photographed on a Bausch and Lomb Research metallograph.

* Ruggiero, J.D., staff metallographer for Union Carbide Corporation, Parma Research Center.